Industria Textilă

ISSN 1222–5347
1/2016

Contents

Evaluation of biocompatibility of fibroin-based electrospun nanofibrous mats for medical applications

ŞERİFE ŞAFAK   ŞEBNEM DÜZYER   ESRA KARACA

REZUMAT – ABSTRACT

Evaluarea biocompatibilității nanofibrelor pe bază de fibroină realizate prin electrofilare pentru aplicații medicale

În cadrul acestui studiu, au fost utilizați polimeri de poli(alcool vinilic) și fibroină din mătasea Bombyx Mori. Au fost preparate soluții în amestec, în două proporții diferite, iar parametrii soluției au fost determinați prin măsurarea pH-ului, conductivității și viscozității. Rețelele cu structură nanofibroasă din fibroină de mătase/poli(alcool vinil) au fost produse prin electrofilare. Caracterizarea morfologică a nanofibrelor electrofilate a fost realizată cu ajutorul microscopului electronic cu scanare. Biocompatibilitatea rețelelor din nanofibre de fibroină de mătase/poli(alcool vinil) a fost investigată pe baza testelor de citotoxicitate, sensibilizare și iritare. Ca rezultat, ambele rețele din nanofibre de fibroină din mătase/poli(alcool vinil) au fost evaluate ca materiale noncitotoxice, noniritative și capacitate de răspuns la mediu.

Cuvinte-cheie: electrofilare, nanofibră, fibroină, biocompatibilitate

Evaluation of biocompatibility of fibroin-based electrospun nanofibrous mats for medical applications

In this study, Bombyx Mori silk fibroin and poly(vinyl alcohol) polymers were used. Blend solutions in two different ratios were prepared and solution parameters were determined by pH, conductivity and viscosity measurements. Silk fibroin/ poly(vinyl alcohol) nanofibrous mats were produced by electrospinning process. The morphological characterization of electrospun nanofibers was examined by scanning electron microscope. Biocompatibility of the silk fibroin/poly(vinyl alcohol) nanofibrous mats was investigated by cytotoxicity, sensitization and irritation tests. As a result, both of the silk fibroin/poly(vinyl alcohol) nanofibrous mats were evaluated as noncytotoxic, nonirritative and sensitive materials.

Keywords: electrospinning, nanofiber, silk fibroin, biocompatibility

INTRODUCTION

Fibers with diameters below one micron find many application areas such as protective clothing, cosmetics, filtration, optical applications, ballistic protection and tissue engineering applications (scaffolds, drug delivery and wound dressing). Nanofibers are promising due to their superior properties such as high surface area, high porosity, small pore size and mechanical stability [1].

Tissue engineering is one of the emerging fields of biomedical engineering that applies the principles and methods of biology, medicine, and engineering toward the development of viable substitutes capable of repairing or regenerating the functions of damaged tissue that fails to heal spontaneously. Tissue engineering can be defined as "an interdisciplinary field that applies the principles of engineering and life sciences toward the development of biological substitutes that restore, maintain or improve tissue function". The main aim of the tissue engineering is to mimic the properties of the extracellular matrix (ECM) structure that provides structural and biochemical support to the surrounding cells [2]–[3].

Material selection plays key role in tissue engineering applications. The materials used in those applications should meet several requirements such as mechanical stability, adequate pore size and porosity, biocompatibility and biodegradability [4]. Recently, researchers have used electrospinning method to fabricate artificial nanofibrous tissues to mimic the fibrous structure of ECM [5]–[8].

Silk has been used in biomedical applications as suture materials, drug delivery systems, tissue scaffolds and wound dressings because of its unique properties such as biocompatibility, biodegradability, high strength, toughness and elasticity in the form of powder, fiber, film, gel, sponge, hydrogel or nonwoven mat [9]–[11], [12]–[17]. With arising applications of nanofibers, silk can also be used in medical applications in the form of nanofiber mats [18], [19].

The aim of the work is to investigate the biocompatibility of cross-linked nanofibrous mats produced from silk fibroin/poly(vinyl alcohol) solutions in two different blend ratios for medical applications. Mainly three different biocompatibility tests (cytotoxicity, sensitization and irridation) were performed in order to understand biocompatibility properties of silk fibroin/ poly(vinyl alcohol) nanofibrous mats.

MATERIALS AND METHODS

Materials

Hydrolysis silk fibroin powder (SF) with Mw 500-10.000 g/mol as soluble in water was kindly supplied by Shanghai Soyoung Biotechnology Inc. (China).

Technical poly(vinyl alcohol) (PVA) polymer (BP 7 grade) was purchased from ZAG Chemicals (Turkey). Distilled water was used as the solvent. For the cross-linking process, 37% technical hydrochloride acid (Merck), 50% biological grade glutaraldehyde (EMS), acetone with Mw 58.08 g/mol (Merck), 99.5%, ethyl alcohol (Merck) and phosphate tampon (Euroimmun) were used.

Preparation of electrospinning solutions

In this study water-soluble fibroin powder was used. Due to the low molecular weight of this polymer, viscosity of the fibroin solution was significantly low. In order to provide an efficient electrospinning process, PVA was used as the auxiliary polymer.

SF solution of 25% (w/v) was prepared by dissolving the fibroin powder in distilled water at room temperature for 2 h on magnetic stirrer. PVA powder was dissolved in distilled water by mixing on magnetic stirrer at 80 °C for 8 h. and the PVA solution with concentration of 15% (w/v) was prepared. For the electrospinning solution: SF solution (25%) and PVA solution (15%) were blended in the volume ratio of 1/2 and 1/3 SF/PVA. This blend was stirred at room temperature for 2 h to obtain a homogeneous solution. Electrical conductivity and pH of the electrospinning solutions were measured by Hanna pH and Conductivity Tester. Viscosity measurements of the solutions were performed on Brookfield Viscometer. The properties of the solutions were given in table 1.

Electrospinning

The production of electrospun mats was performed on the electrospinning equipment at Uludag University Textile Engineering Lab. An aluminum plate covered with aluminum foil was used to collect the electrospun mats. The collector was located over against to the spinneret. Voltage, flow rate of solution, and distance between the spinneret and the collector were adjusted for a stable jet formation and kept constant during electrospinning. All the spinning experiments were performed at ambient conditions. The process parameters for electrospinning of the SF/PVA (1/2 and 1/3) solutions were given in table 2.

Cross-linking and sterilization

A cross-linking process was applied on electrospun mats to improve their water resistance for biocompability tests. The SF/PVA electrospun mats were cross-linked by immersing in acetone solution with 1.33 M glutaraldehyde (50%) and 0.25 M hydrochloric acid (37%) at room temperature for 24 h. The cross-linked nanofibrous mats were neutralized in ethyl alcohol (99.5%) for 5 min. The cross-linked and neutralized mats were washed with phosphate tampon solution (1%) three times and then dried at room temperature for 24 h. Cross-linked electrospun SF/ PVA mats were sterilized with ethylene oxide gas for 4 h and aerated for 8 h at Uludag University Medical Faculty prior to biocompability experiments.

Characterization

Carl Zeiss AG-EVO 40 XVP Scanning Electron Microscope (SEM) was used for the analyses of electrospun SF/PVA nanofibrous mats. The average nanofiber diameter and its distribution were determined by measuring 20 random nanofiber diameters based on image analysis software (Image-J) for each nanofibrous mats.

Biocompatibility tests

Biocompatibility of the SF/PVA nanofibrous mats were tested by TUBITAK Marmara Research Center Genetic Engineering and Biotechnology Institute. In order to determine the bicompatibility performance of fibroin-based nanofibrous mats, cytotoxicity, sensitization and irritation tests were performed. The animal experiments for this study were approved by the TÜBİTAK Laboratory Animals Local Ethics Committee (HADYEK) with date Feb 5, 2013 and no. B.14.2. TBT.5.01.13.00-111/20.

All tests were performed with extracts of SF/PVA nanofibrous test samples. Extracts of sterilized SF/PVA nanofibrous mats were prepared by mixing the nanofibrous mats (6 cm^2/ml) into the culture medium – Dulbecco's Modified Eagle's Medium (DMEM/F12) – containing 10% fetal bovin serum and penisilin streptomisin. The test samples were incubated at 37 °C for 72 h.

Cytotoxicity tests were carried out in vitro conditions according to ISO 10993-5:2010. In the tests, L929 mouse fibroblast cell cultures were used. L929 cells were cultured in a 96-well plate at density of 1×10^4 cells/well and afterwards all the plates were incubated in a 5% CO_2 incubator at 37 °C for 24 h. The test sample extracts and the controls were added into the

<div style="float:right">Table 1</div>

THE PROPERTIES OF THE ELECTROSPINNING SOLUTIONS			
Solution	**pH**	**Electrical conductivity (µs/cm)**	**Viscosity (cp)**
15% PVA	6.24	708	1667
25% SF	5.20	9399	2.4
1/2 SF/PVA	5.17	3200	492.8
1/3 SF/PVA	5.23	2650	828.8

<div style="float:right">Table 2</div>

THE PROCESS PARAMETERS OF THE ELECTROSPUN MATS	
Voltage	25 kV
Flow rate of the solution	1.5 ml/h
Tip-to-collector distance	24 cm
Spinneret inner diameter	830 µm
Amount of the solution	50 ml

cell wells and incubated at 37 °C for 24 h with 5% CO_2. Thereafter, WST-1 the cell proliferation reagent (10%, v/v) which is a ready-to-use colorimetric assay for the nonradioactive quantification of cellular proliferation, viability and cytotoxicity were added into the wells and were kept for 3 h. Viability and the proliferation of the cells were determined by the absorbance measurements performed by using a microplate reader at 450 nm. The test results were evaluated by qualitative method as cell reactivity score and by quantitative method as the percentage cell viability. Tests were performed with 3 random samples for each nanofibrous mats and the mean and standard deviation were determined.

During the cell viability evaluation, the test samples were compared with null and with positive and negative controls. As the null controls, incubated culture medium (DMEM-F12) extract (null control 1) and culture medium DMEM-F12 fresh containing serum (null control 2) were used. As the positive control, RAUMEDIC-SIK 8363 tubing in silicone rubber grade was used. The negative control was RAUMEDIC PVC Org Sn.

Sensitization tests in vivo conditions were performed with 15 female albino Guinea pigs weighting 300–500 g according to ISO 10993-10:2010. Ten animals were treated with the test sample and five animals were acted as negative control groups.

The sensitization test consisted of intradermal induction and topical induction phase. For the test material animals, 0.1 ml intradermal injections were applied at the sites A, B and C in figure 1. The blend (1:1) of Freund's Complete Adjuvant (FCA) and physiological saline solution (PS), the test material extract, and the blend solution of FCA/PS and the test material extract were injected on the sites A, B and C, respectively. At the seventh and the fourteenth days after completion of the intradermal injections, the test material extract of 0.3 ml was administered on the sites D1 and D2 at the intrascapular region by topical application, respectively. Topical application sites were covered with sterile gauze patch and all sites were wrapped with an elastic bandage. The negative control animals were treated similarly with FCA and saline solutions. The bandages were removed after 48 h and the reactions on the skin sites of test and control animals were observed. Dermal reactions for
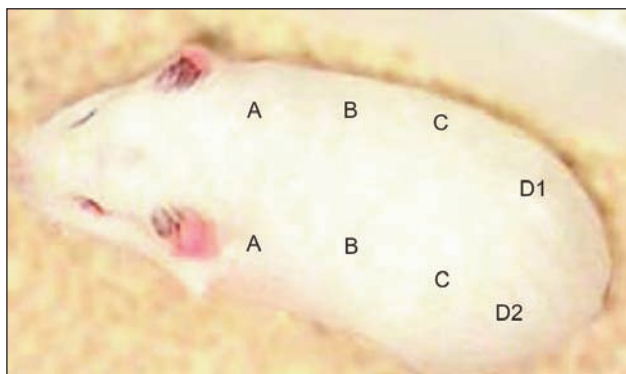
Fig. 1. Location of intradermal injection and topical application sites for the sensitization test

enythema and oedema were evaluated according to the Magnusson and Kligman grading scale in ISO 10993-10:2010.

In the irritation tests performed in vivo conditions according to ISO 10993-10:2010, 3 healthy adult albino female New Zealand rabbits weighing not less than 2 kg were used for each nanofibrous mats.

Initially, extracts of SF/PVA nanofibrous mats were prepared. For positive and negative controls, 90% lactic acid and phosphate buffered saline were used, respectively 0.5 ml of the test extracts and controls were spread on a sterile gauze patches (2.5 × 2.5 cm) and applied on the back side of each rabbit after the hairs in the application areas were shaved. Application areas were covered with an elastic bandage for 4 h. The appearance of each application site was observed and recorded at 1, 24, 48 and 72 h after removal of the patches by using binocular Lopus microscope. The observations on erthema-eschar formation and oedema formation were scored according to the scoring system for skin reaction in ISO 10993-10:2010. The average irritation scores were determined for four observation times and for three animals. For another evaluation of test results, primary irritation index was determined. Primary irritation index was calculated by considering all dermal response scores (erythema-eschar formation and oedema formation) at 24, 48 and 72 h.

RESULTS AND DISCUSSION

Characterization of electrospun SF/PVA nanofibrous mats

In this study electrospinning parameters and ambient conditions were kept constant for both the 1/2 and 1/3 SF/PVA electrospinning solutions. The SEM photographs in figure 2 and 3 showed that the electrospun SF/PVA nanofibrous mats were composed from randomly oriented fibers with various diameters and structures depending on the solution properties. Although uniform and continuous fiber formations were observed, bead formation was seen partly on both of the nanofibrous mats. The morphology and the average fiber diameters of SF/PVA nanofibers were varied with blend ratios of the SF and PVA solutions. The average fiber diameters of the nanofiber mats produced from 1/2 SF/PVA and 1/3 SF/PVA solutions were 310 ± 82 nm and 390 ± 108 nm, respectively. Since 1/3 SF/PVA solution has higher viscosity and lower electrical conductivity compared to 1/2 SF/PVA solution (table 1), the diameters of the fibers produced from 1/3 SF/PVA solution increased. As it was seen from SEM images (figure 2b and 3b) of cross-linked nanofibrous mats, there was no deformation on nanofibrous structure. However the average fiber diameters decreased to 289 ± 78 nm for 1/2 SF/PVA and to 260 ± 104 nm for 1/3 SF/PVA after cross-linking process. In cross-linking process, ethyl alcohol was used for cross-linking of fibroin and neutralization of glutaraldehyde. The decrease in fiber diameters may be explained by the dissolution of PVA, since PVA is partly soluble in ethyl alcohol [20].
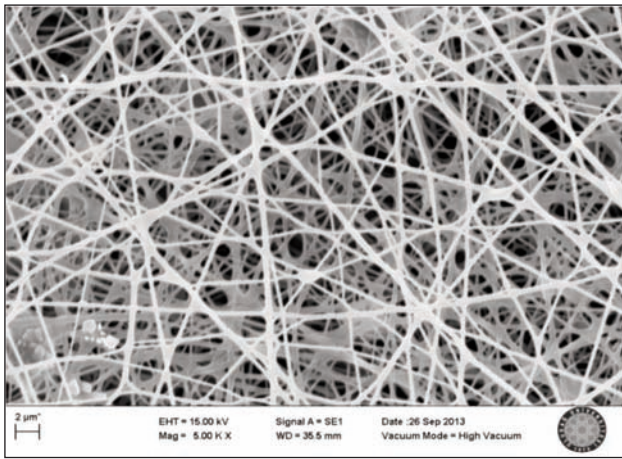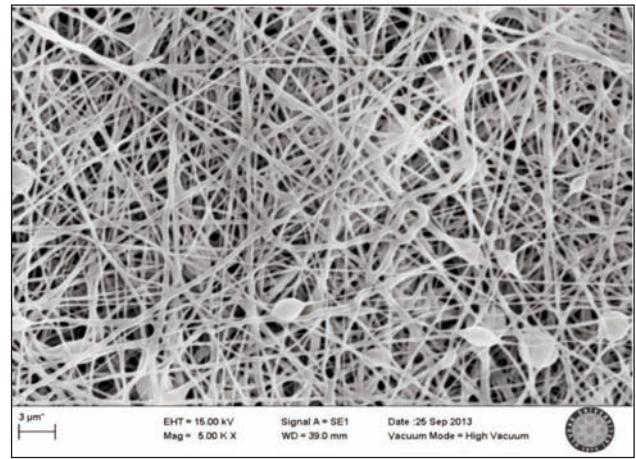
Fig. 2. SEM photographs of 1/2 SF/PVA nanofibrous mats:
a – before cross-linking process, *b* – after cross-linking process
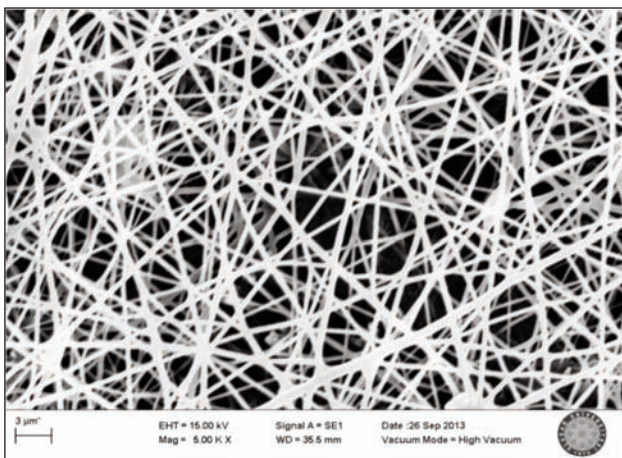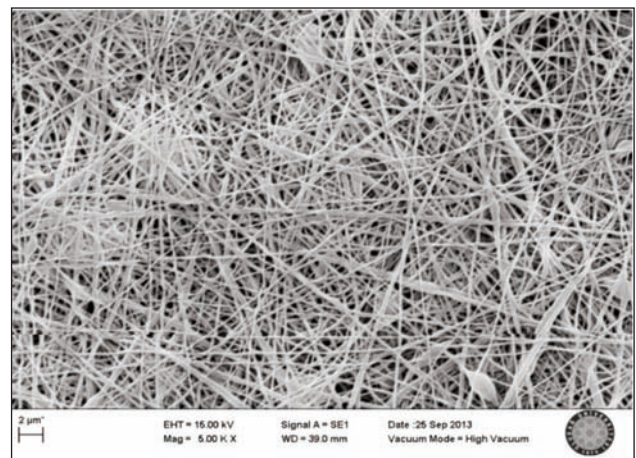
Fig. 3. SEM photographs of 1/3 SF/PVA nanofibrous mats
a – before cross-linking process, *b* – after cross-linking process

Cytotoxicity test results

Cytotoxicity test assesses the biological response of mammalian cells to the materials. The effects of SF/PVA electrospun mat extracts on L929 mouse fibroblast cells were given in table 3 and figure 4.

Table 3

CELL REACTIVITY SCORES OF THE NANOFIBROUS MATS AND THE CONTROLS	
Test samples	**Score**
1/2 SF/PVA nanofibrous mat	1
1/3 SF/PVA nanofibrous mat	0
Null control 1	0
Null control 2	0
Positive control	4
Negative control	0

0: Evident intracytoplasmic granules, no cell lysis, none reactivity
1: No intracytoplasmic granules, cell lysis below 20%, low reactivity
4: Clear and complete destruction of the cell layer, severe reactivity

According to the cell reactivity scores, nanofibrous mat produced from 1/2 SF/PVA solution had low reactivity, while nanofibrous mat produced from 1/3 SF/PVA solution showed no reactivity. 1/2 and 1/3 SF/PVA nanofibrous mats had 88.29% ± 4.55 and 90.37% ± 4.45 average cell viability, respectively.

In terms of both cell reactivity score and cell viability, the effect of 1/2 SF/PVA mat on L929 mouse fibroblast cells was slightly higher than that of the 1/3
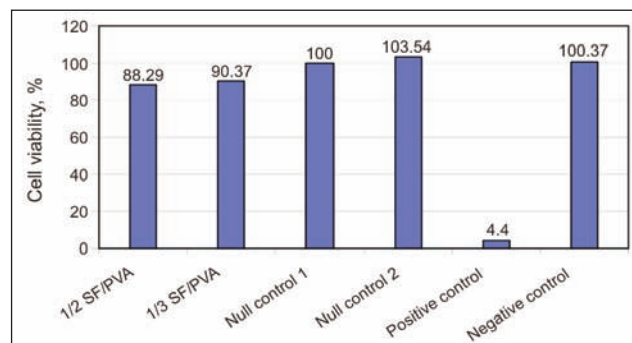
Fig. 4. Percentage cell viability of the nanofibrous mats and the controls

SF/PVA mat. However, no significant cytotoxicity was observed on both of SF/PVA nanofibrous mats.

According to ISO 10993-5:2010, samples with cell viability more than 70% can be considered as noncytotoxic. Therefore, both of the SF/PVA nanofibrous mats were evaluated as noncytotoxic.

Sensitization test results

The average values of sensitization test results for the SF/PVA electrospun mats and the control were given in table 4.

On skins of the animals used for test materials, significant loss of hair, moderate erythema and local allergic reactions have been observed. In control animals no visible change was appeared. According to ISO 10993-10:2010, the grading scales of 1 or greater in the test group generally indicate sensitization. Consequently, both of the SF/PVA nanofibrous mats exhibited skin sensitization effects and were evaluated as sensitive materials.

Irritation test results

The results and the photographs of dermal irritation test for SF/PVA nanofibrous mats and the controls were summarized in table 5 and 6, respectively.

Dermal irritation including oedema was not found in rabbits treated with both of nanofibrous mats. In the group treated with 1/2 SF/PVA nanofibrous mat, one rabbit exhibited very slight erythema (barely perceptible), throughout 72 h after removal of the patches. In the group treated with 1/3 SF/PVA nanofibrous

mat, two rabbit exhibited very slight erythema, 1 h after removal of the patches.

The primary irritation index was 0.17 and 0 for 1/2 SF/PVA nanofibrous mat and 1/3 SF/PVA nanofibrous mat, respectively. According to ISO 10993-10:

Table 4

DERMAL REACTION GRADING SCALES OF THE NANOFIBROUS MATS AND THE CONTROL

Test samples	Grading scale
1/2 SF/PVA nanofibrous mat	2.0
1/3 SF/PVA nanofibrous mat	1.6
Negative control	0.4
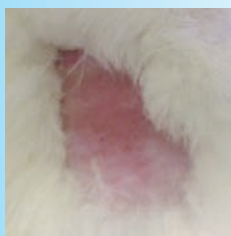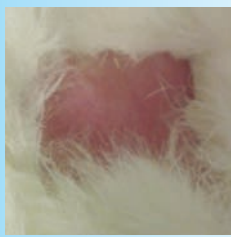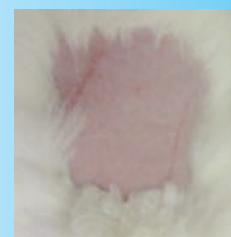
Table 5

THE AVERAGE SCORES AND PRIMARY IRRITATION INDEX OF THE NANOFIBROUS MATS AND THE

Test Samples	Erythema - eschar	Oedema	Total	Primary irritation index
1/2 SF/PVA nanofibrous mat	0.33	0	0.33	0.17
1/3 SF/PVA nanofibrous mat	0.17	0	0.17	0
Positive control	2.71	2.37	5.04	2.47
	0	0	0	0

Table 6

THE PHOTOGRAPHS OF THE DERMAL REACTIONS FORMED ON TEST ANIMALS AFTER REMOVAL OF THE PATCHES

Observation Time	1/2 SF/PVA nanofibrous mat	1/3 SF/PVA nanofibrous mat	Positive control	Negative control
24 h				
48 h				
72 h				

2010, primary irritation index below 0.4 for irritation test is regarded as negligible. Accordingly, it was concluded that both 1/2 and 1/3 SF/PVA nanofibrous mats caused no irritation on the skin.

CONCLUSIONS

In this study, nanofibrous mats were produced from two different blend solutions (Bombyx Mori silk fibroin and poly(vinyl alcohol) by electrospinning with same process parameters and under same ambient conditions.

Afterwards, nanofibrous mats were subjected to a cross-linking process to improve their water resistance for biocompatibility tests.

SEM observations showed that the average fiber diameters decreased from 310 nm to 289 nm for 1/2 SF/PVA and from 390 nm to 260 nm for 1/3 SF/PVA after cross-linking process but no deformation observed on nanofibrous structure.

Biocompatibility of the SF/PVA nanofibrous mats were evaluated by ISO 10993:2010 called "Biological evaluation of medical devices". Cytotoxicity (ISO 10993-5:2010), sensitization, (Guine Pig Max.Test, ISO 10993-10:2010) and irritation/intracutaneous reactivity, (ISO 10993-10:2010) tests were carried out to determine biocompatibility of SF/PVA nanofibrous mats.

In cytotoxicity tests, 1/2 and 1/3 SF/PVA nanofibrous mats showed about 88% and 90% average cell viability, respectively. Both of the SF/PVA nanofibrous mats were evaluated as noncytotoxic.

In sensitization tests, moderate erythema and local allergic reactions have been observed on the skins of the animals that used for test materials. The grading scales were determined higher than 1 for both of the nanofibrous mats. Consequently, both of the SF/PVA nanofibrous mats exhibited skin sensitization effects and were evaluated as sensitive materials.

The results of irritation test for SF/PVA nanofibrous mats revealed that dermal irritation including oedema was not found in rabbits treated with both of nanofibrous mats and calculated primary irritation index regarded as negligible. As a result, it was concluded that both 1/2 and 1/3 SF/PVA nanofibrous mats caused no irritation on the skin.

In conclusion SF/PVA nanofibrous mats could be considered as noncytotoxic, nonirritative and sensitive materials. For further studies, the sensitization of SF/PVA nanofibrous mats should be improved for excellent biocompability.

BIBLIOGRAPHY

[1] Greiner, A., Wendorff, J. H. *Electrospinning: A fascinating method for the preparation of ultrathin fibers*. In: Angewandte Chemie, 2007, vol. 46, issue 30, pp. 5670–5703

[2] Gualandi, C. *Porous polymeric bioresorbable scaffolds for tissue engineering*. PhD Thesis, University of Bologna, Italy, 2011

[3] Langer, R., Vacanti, J. P. *Tissue engineering*. In: Science, 1993, vol. 260, pp. 920–926

[4] Kun, M., Chan, C., Ramakrishna, S. *Textile-based scaffolds for tissue engineering*, In: Rajendran, S. (Ed.), Advanced Textiles for Wound Care, Woodhead Publishing Limited, England, 2009, p. 289

[5] Coskun, G., Karaca, E., Ozyurtlu, M., Ozbek, S., Yermezler, A., Cavusoglu, I. *Histological evaluation of wound healing performance of electrospun poly(vinyl alcohol)/sodium alginate as wound dressing in vivo*. In: Bio-Medical Materials and Engineering, 2014, vol. 24, pp. 1527–1536

[6] Li, W. J., Laurencin, C. T., Caterson, E. J., Tuan, R. S., Ko, F. K. *Electrospun nanofibrous structure: A novel scaffold for tissue engineering*. In: Journal of Biomedical Materials Research, 2002, vol. 60, pp. 613–621

[7] Cernat, I.F., Ciobanu, L., Muresan, R., Abramiuc, D., Stamate, T., Denis, Constantin Vlad, Hanganu, SC S. *Medical efficiency of antibacterial wound dressings*. In: Industria Textila, 2015. vol. 66, pp. 131–135

[8] Pham, Q. P., Sharma, U., Mikos, A.G. *Electrospinning of polymeric nanofibers for tissue engineering applications: A review*. In: Tissue Engineering, 2006, vol. 12, issue 5, pp. 1197–1211

[9] Lammel, A. S., Hu, X., Park, S., Kaplan, D. L., Scheibel, T. R. *Controlling silk fibroin particle features for drug delivery*. In: Biomaterials, 2010, vol. 31, pp. 4583-4591

[10] Mandal, B. B., Kundu, S. C. *Cell proliferation and migration in silk fibroin 3D scaffolds. In:* Biomaterials, 2009, vol. 30, pp. 2956-2965

[11] Martineau, L. And Shek P. N. *Evaluation of a bi-layer wound dressing for burn care II. In vitro and in vivo bactericidal properties*. In: Burns, 2006, vol. 32, pp. 172–179

[12] Dash, R., Acharya, C., Bindu, P. C., Kundu, S. C. *Antioxidant potential of silk protein sericin against hydrogen peroxide-induced oxidative stress in skin fibroblasts*. In: BMB Reports, 2008, vol. 41, issue 3, pp. 236–241

[13] Nogueira, G. M., Weska, R. F., Vieira, W. C., Polakiewicz, B., Rodas, A. C., Higa, O. Z., Beppu, M. M. *A new method to prepare porous silk fibroin membranes suitable for tissue scaffolding applications*. In: Journal of Applied Polymer Science, 2009, vol. 114, issue 1, pp. 617–623

[14] Siri, S., Maensiri, S. *Alternative biomaterials: Natural, non-woven, fibroin-based silk nanofibers of weaver ants (Oecophylla smaragdina)*. In: International Journal of Biological Macromolecules, 2010, vol. 46, issue 5, pp. 529–534

[15] Intavısade, P., Oonkhanond, B. *A study of irradiated silk fibroin–poly vinyl alcohol hydrogel for artificial skin substitutes*. In: Journal of Metals, Materials and Minerals, 2010, vol. 20, issue 3, pp. 119–122

[16] Cilurzo, F., Gennari, C. G., Selmin, F., Marotta, L. A., Minghetti, P., Montanari, L. *An investigation into silk fibroin conformation in composite materials intended for drug delivery*. In: International Journal of Pharmaceutics, 2011, vol. 414, issue 1, pp. 218–224

[17] Altman, G. H., Diaz, F., Jakuba, C., Calabro, T., Horan, L. R., Chen, J., Lu, H., Richmond, J., Kaplan, D. L. *Silk-based biomaterials.* In: Biomaterials, 2003, vol. 24, pp. 401–416

[18] Min, B., Lee, G., Kim, S. H., Nam, Y. S., Lee, T. S. *Electrospinning of silk fibroin nanofibers and its effect on the adhesion and spreading of normal human keratinocytes and fibroblasts in vitro*, In: Biomaterials, 2004, vol. 25, issue 7-8, pp. 1289–1297

[19] Li, C., Vepari, C., Jin, H., Kim, H. J., Kaplan, D. L., *Electrospun silk-BMP-2 scaffolds for bone tissue engineering*, In: Biomaterials, 2006, vol. 27, issue 16, pp. 3115–3124

[20] Joint FAO/WHO Expert Committee on Food Additives. *Compendium of Food Additive Specifications: Addendum 12,* issue 52, World Health Organization, Rome, 2004

Authors:

ŞERİFE ŞAFAK, ŞEBNEM DÜZYER, ESRA KARACA[*]
Uludag University, Faculty of Engineering, Department of Textile Engineering,
Gorukle Campus, Bursa, Turkey

Corresponding author:

Prof. Dr. Esra KARACA
Uludag Univ. Müh. Fak. Tekstil Müh. Böl.
16059 Görükle, Bursa, Turkiye
Tel: +90-224-2942052
Fax: +90-224-2941903
e-mail: ekaraca@uludag.edu.tr
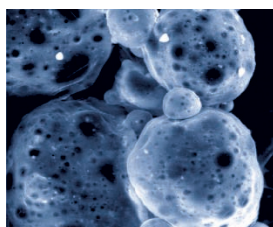
Effect of airway angle of a swirl nozzle on performance of ring-spun yarn

HUA QIU
QIAOLI LUAN
HONGXIA JIANG

YUYE FU
JIHONG LIU

REZUMAT – ABSTRACT

Efectul unghiului de orientare a aerului prin duză cu vârtej asupra performanței firului realizat pe maşina de filat cu inele

La maşina de filat cu inele tradiţională, pilozitatea firelor filate poate fi redusă cu ajutorul unei duze cu vârtej formată din fir şi canale cu aer. În cadrul acestui studiu au fost proiectate şapte duze cu unghiuri diferite de orientare a aerului pentru a optimiza structurile interne ale duzelor cu vârtej. Au fost analizate, de asemenea, efectele unghiului de orientare a aerului prin duzele cu vârtej asupra proprietăţilor firului prin evaluarea indicilor de performanţă ai firului, inclusiv cei pentru pilozitate, forţa de rupere şi neuniformitate. Rezultatele comparaţiei au arătat că toate cele şapte duze cu vârtej au afectat în mod semnificativ calitatea firului realizat pe maşina de filat cu inele. Proprietăţile firului au fost influenţate, în multe moduri, de asemenea, de diferenţa fluxurilor de aer a celor şapte unghiuri de orientare a aerului. Utilizând parametrii similari de filare, duza cu un unghi de orientare a aerului de 40° a produs cel mai bun fir, comparativ cu celelalte duze cu vârtej, din punctul de vedere al pilozităţii de 3 mm şi sub (S3), forţei de rupere şi neuniformităţii firului. Mai exact, S3 a fost redus cu 92,3%, iar calitatea firului s-a îmbunătăţit semnificativ.

Cuvinte-cheie: duză cu vârtej, unghi de orientare a aerului, filare cu inele

Effect of airway angle of a swirl nozzle on performance of ring-spun yarn

In a traditional ring spinning frame, the hairiness of spun yarn can be reduced by a swirl nozzle composed of yarn and air channels. To this end, we designed seven nozzles with different airway angles in this study to optimize the internal structures of swirl nozzles. We also analysed the effects of the airway angle of a swirl nozzle on yarn properties by evaluating the performance indexes of the yarn, including those for hairiness, breaking force, and unevenness. Comparison results showed that all seven swirl nozzles significantly affected the quality of ring yarn. Yarn properties were also influenced by the difference in the air flows of the seven airway angles in various ways. Under similar spinning parameters, the nozzle with an airway angle of 40° produced the best yarn among the other swirl nozzles, with hairiness of 3 mm and above (S3), breaking force, and yarn unevenness. Specifically, S3 was reduced by 92.3% and yarn quality significantly improved.

Keywords: swirl nozzle, airway angle, ring spinning

INTRODUCTION

Ring spinning is still widely applied in spinning mills because of its low cost and adaptability [1]. However, fibers cannot be compacted completely in twisting triangles, thus resulting in hairiness [2]. Furthermore, the fibers are continuously transferred inward and outward along the radial direction of a roving by different centripetal forces under yarn tension. Consequently, the ends of the fibers protrude from the surface of the yarn to generate hairiness [3]. Hairiness generally affects the appearance of yarn and of fabric significantly [4]. In addition, yarn performance depends strongly on its *S3,* a hairiness of 3 mm and above. The tendency for pill formation also increases proportionally with the *S3* level of its constituent yarns [5].

Traditionally, yarn hairiness is reduced to a certain degree by oiling the ring spinning frame and smoothening the yarn guides. Nonetheless, new technologies have been developed to limit hairiness on the surface of spun yarn, including sirospun, sirofil spun, solo spun, and compact spinning [6]–[9].

The intrinsic cause of *S3* and of twisting triangles remains unknown; nonetheless, the methods of reducing yarn *S3* by air jet have been advancing.

For instance, Wang et al. established the novel jet-ringing spinning technique, which incorporated the advantages of ring and air-jet spinning by modifying the conventional ring frame slightly [10]–[12]. The researchers examined the differences between conventional and jet-ring spinning in terms of *S3* reduction, yarn strength, and unevenness. Moreover, they highlighted the mechanism of *S3* reduction within a nozzle and reported that a nozzle can limit *S3* by 39%, although yarn strength and unevenness remain almost unchanged.

Y.C. Zeng and C.W. Yu simulated the air flow and fiber motion in the nozzle of an air-jet spinning machine and examined nozzle parameters with respect to their influences on these variables. The studied parameters include nozzle pressure, jet orifice angle, jet orifice position, and the flexural rigidity of fiber [13]–[14].The simulated results were consistent with the images captured through high-speed

photography. In addition, they investigated the reduction of yarn hairiness by JetRing and JetWind numerically and experimentally [15]. They then explained the effects of nozzle parameters such as nozzle pressure and jet orifice angle on this reduction. The simulation results agreed with those of their experimental study.

Based on Wang's study, Cheng clarified the effects of different spinning parameters on the reduction of yarn hairiness [16]. These parameters include compressed air pressure, the distance between the front roller nip and the nozzle inlet, the level of yarn twist, and spindle speed. This researcher used 100% carded cotton and 100% polyester rovings in the spinning process.

Rengasamy and Patanaik designed another type of nozzle that consisted of a circular yarn duct and four airways. The four airways were tangential to the yarn duct on the same section. These researchers also studied nozzle performance experimentally and through computational fluid dynamics [17]–[18]. When the airway angle was 40°, hairiness is most significantly reduced. However, the fibers are folded and hairiness increased when the airway angle is too large. In addition, they investigated the effects of fiber fineness, pressure, and nozzle parameters (airway angle and diameter of the yarn duct) on hairiness reduction through a series of experiments.

Yarn hairiness can also be limited by the novel swirl nozzle composed of a yarn duct and an airway, which can be mounted on a traditional spinning frame [19]. The rotating air flow inside the swirl nozzle can coil the protruded fibers on the surface of the spun yarn into its body. Furthermore, this method is characterized by its simple structure, convenient operation, and low cost. A previous study also suggested that the swirl nozzle can effectively reduce yarn hairiness and improve the performance of spun yarn [19]. Specifically, the airway angle of this nozzle determines the flow patterns of internal compressed air to limit hairiness. To optimize the internal structure of the swirl nozzle and enhance yarn quality, we therefore designed seven swirl nozzles with different airway angles in the current study to reduce the hairiness of ring-spun yarn. We analyzed the effects of the airway angle of a swirl nozzle on yarn properties by testing the performance of the spun yarn in terms of hairiness, breaking force, and unevenness. We also compared the technique involving the swirl nozzle with conventional ring spinning.

EXPERIMENTAL WORK

Materials and methods

In the experiment, 30 tex Z-twist ring-spun yarns were produced with 100% combed cotton roving (5.22 g/10 m). Figure 1 shows the model of a swirl nozzle, which has three components: (1) air inlet; (2) yarn inlet; and (3) yarn outlet. Yarn channel, air inlet diameter, and length were constant in the seven nozzles designed for this study; however, the slant angles of the inlet varied. The slant angle of the air
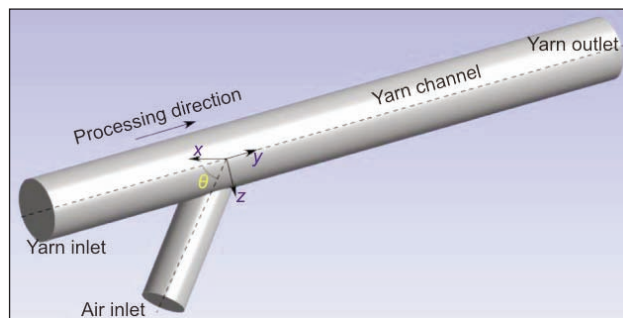
Fig. 1. Model of the swirl nozzle
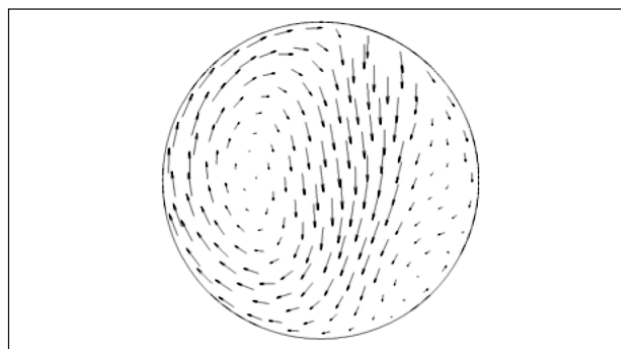
Fig. 2. Direction of the swirling air

inlet is defined as the angle between the axis of the air inlet and that of the yarn channel. Moreover, the air channel wall was tangential to the inner walls of the yarn channel, which generated a swirling air effect. The direction of the swirling effect is shown in figure 2. This effect helps coil protruding fibers into the yarn body. Each nozzle had a constant yarn-channel diameter of 2.0 mm, a channel length of 22 mm, and an air channel diameter of 1.4 mm.

The seven swirl nozzles were divided into three types based on angle: acute (40°, 50°, 60°, 70°, and 80°), obtuse (120°), and right angles (90°). For simplicity, the 30° nozzle indicated a swirl at an axial angle of 30° and so on.

Fixture of nozzles onto the ring frame

The experiments were conducted using the CZJF-5 intelligent multifunction spinning frame, as depicted in figure 3.

The key component of the apparatus is swirl nozzle (2), which is positioned approximately 7.5 cm below delivery roller (1).

Moreover, the gauge pressure of compressed air p ranged from 0.05 MPa to 0.25 MPa. This pressure was regulated by a regulator and filtered before entering the swirl nozzle. The spindle speed was 12000 rpm. The spinning frame was positioned in four ways during each experiment, as presented in figure 4. In position 1, a swirl nozzle was mounted between the front roller and the bobbin. Positions 2 and 3 were left vacant to reduce interference by the air flow jetted from the nozzle (position 1) in yarn formation. In position 4, yarn was manufactured according to the traditional method.
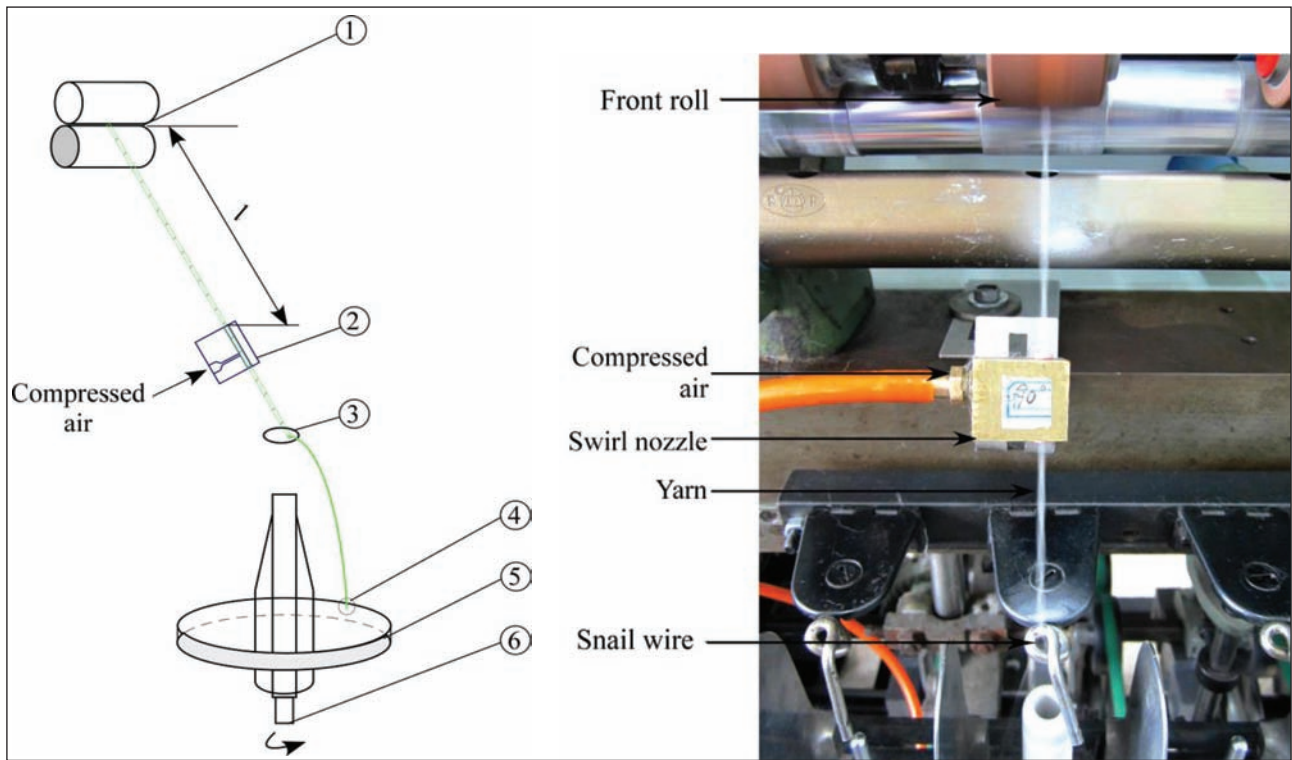
Fig. 3. Installation of the swirl nozzle on a traditional frame
(1) Delivery roller; (2) Swirl nozzle; (3) Lappet; (4) Traveler; (5) Ring; and (6) Spindle
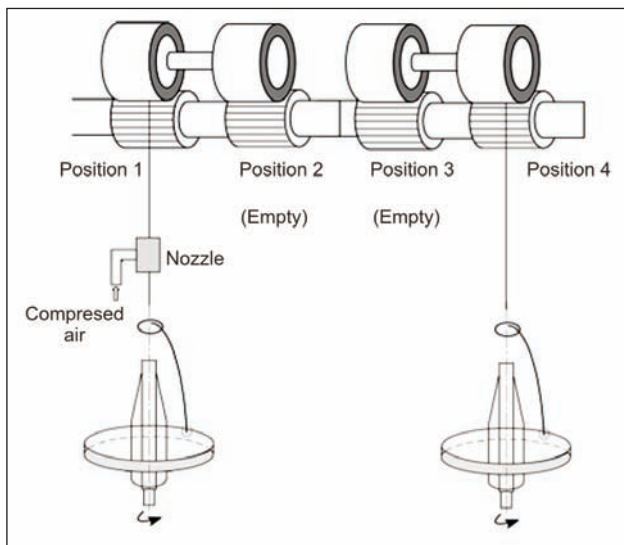
Fig. 4. Schematic diagram of conventional ring spinning versus jet-ring spinning
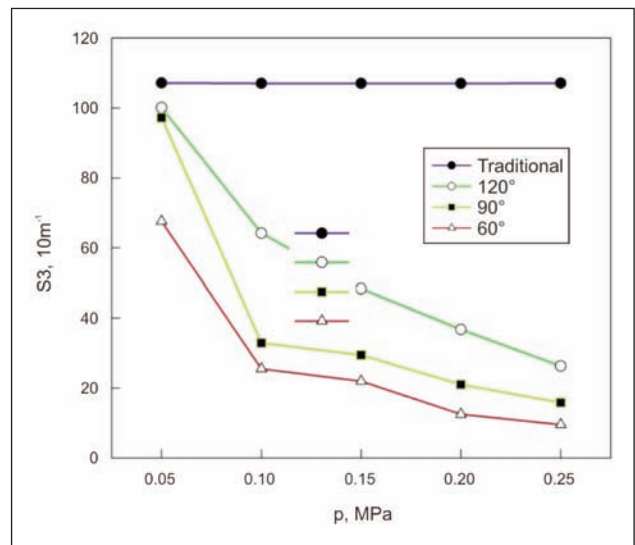
Fig. 5. Relationship between S3 and supplied air pressure

RESULTS AND DISCUSSION

Comparison of the performance levels of the swirl nozzles with acute and obtuse airway angles

Effect of airway angle on the S3 of spun yarn

Figure 4 exhibits the relationship between $S3$ and supplied air pressure p.

The $S3$ of spun yarn can be reduced effectively by the swirl nozzle installed on the traditional ring frame, as shown in figure 5. The effects of swirl nozzles with 90° and 120° airway angles on $S3$ reduction are almost similar when the pressure is 0.05 MPa. However, the effect of the 90° swirl nozzle increases in significance with the increase in p. When the axial angle is between 60° and 120°, the $S3$ of the yarn is lower than that of traditional ring-spun yarn. The significance of this effect also increases with p. Finally, the 60° nozzle reduces yarn $S3$ more effectively than the 90° and 120° nozzles regardless of p level.

Effect of airway angle on breaking force

Figure 6 depicts the relationship between breaking force and supplied air pressure p.

All of the swirl nozzles can enhance the breaking force of yarn when pressure is between 0.05 and 0.12 MPa, as indicated in figure 5. Specifically, the
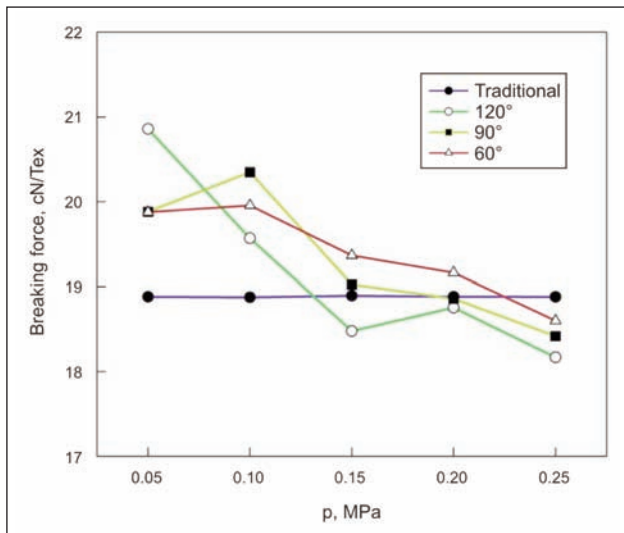
Fig. 6. Relationship between breaking force and supplied air pressure
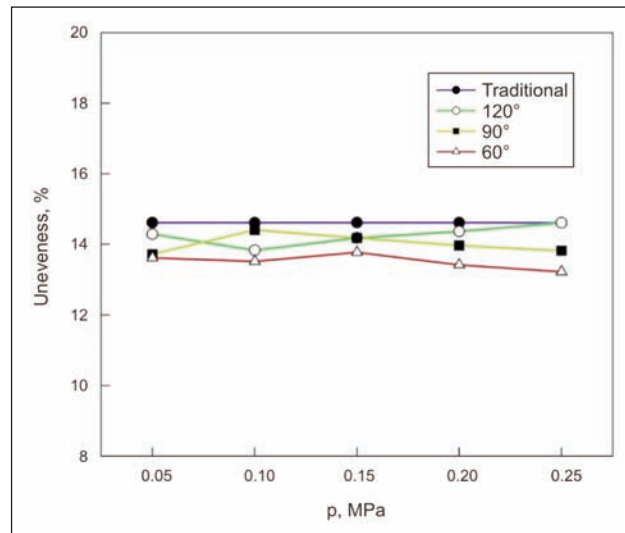
Fig. 7. Relationship between unevenness and supplied air pressure

breaking force of the yarn processed with the 60° and 90° swirl nozzles is greater than that of traditional spun yarn when p increases. Moreover, the breaking force of yarn produced with a swirl nozzle is lower than ordinary ring-spun yarn when p is between 0.23 and 0.25 MPa. When p is between 0.05 and 0.08 MPa, the 90° and 120° nozzles can considerably improve the breaking force of yarn. When p is between 0.13 and 0.25 MPa, the 60° nozzle improves the breaking force of the yarn more effectively than the other two nozzles.

Effect of airway angle on evenness

Figure 7 presents the relationship between unevenness and supplied air pressure.

Swirl nozzles with varied airway angles can improve yarn unevenness. In particular, the effect of the 60° nozzle is significant, as suggested in figure 7. Yarn unevenness is limited by increases in pressure; under a pressure of 0.25 MPa, the maximum reduction ratio is 9.6%.

In conclusion, the swirl nozzle with a 60° airway angle can optimally improve $S3$, breaking force, and yarn unevenness. Furthermore, $S3$ and unevenness decrease when air pressure increases. The change law is relatively uniform. Finally, acute angles are generally better than obtuse ones.

Comparison of the performance levels of the swirl nozzles with acute airway angles

Effect of an acute angle on yarn S3

Figure 8 exhibits the variation in $S3$ following the installation of swirl nozzles with different acute airway angles.

All five swirl nozzles with acute airway angles can effectively lower $S3$ level when air pressure increases, as shown in figure 8. A small airway angle enhances $S3$ reduction when p rises from 0.05 MPa to 0.08 MPa. The maximum reduction rate reaches 91.2% when p is between 0.05 and 0.25 MPa in
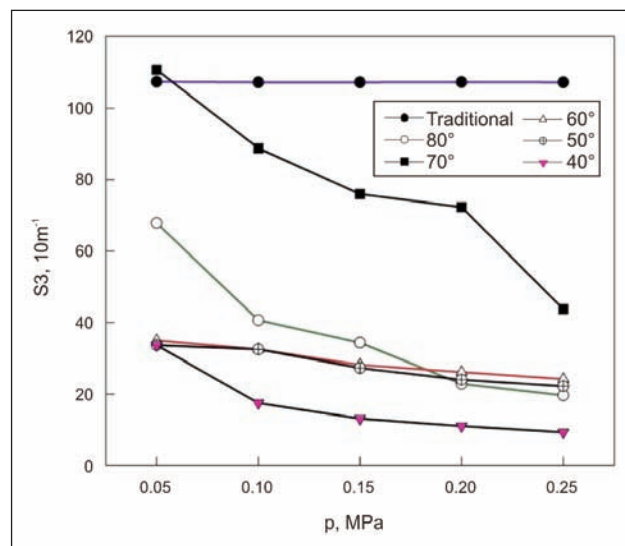
Fig. 8. Variation in S3 following the installation of swirl nozzles with different acute airway angles

40° swirl nozzles under 0.25 MPa of pressure. Yarn quality is thus improved, thereby suggesting that airway angle is important in $S3$ variation.

Effect of an acute angle on breaking force

Figure 9 depicts the variation in breaking force following the installation of swirl nozzles with different acute airway angles.

Swirl nozzles with different acute airway angles can strengthen the breaking force of yarn within a certain pressure range, as indicated in figure 9. This breaking force is strongest under a pressure of 0.05 MPa, but this force declines with the increase in p. The breaking force of the spun yarn processed with swirl nozzles (except for the swirl nozzle with an 80° airway angle) is better than that of conventional ring-spun yarn. Moreover, a small airway angle strengthens the breaking force of yarn in the five swirl nozzles. In particular, the 40° nozzle can significantly improve breaking force by 27.4% under 0.05 MPa
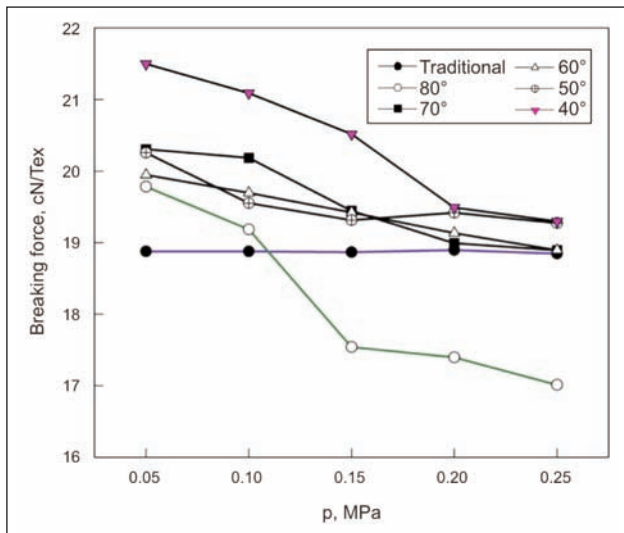
Fig. 9. Variation in breaking force following the installation of swirl nozzles with different acute airway angles
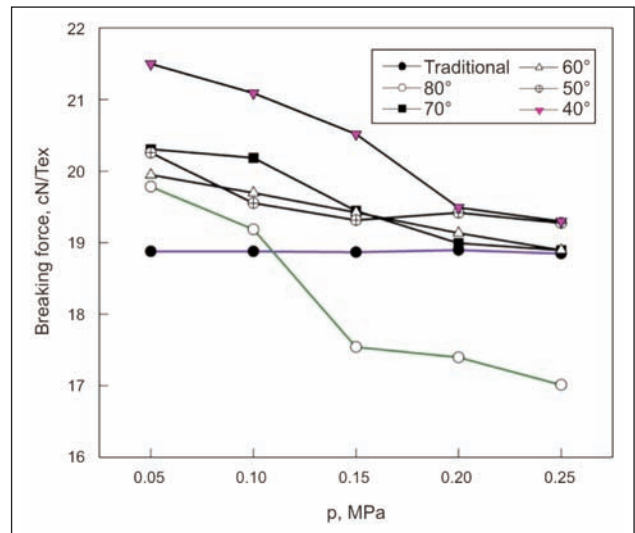
Fig. 10. Variation in unevenness following the installation of swirl nozzles with different acute airway angles

pressure. This enhancement ratio reaches 14.3% when the pressure is 0.25 MPa.

Effect of an acute angle on unevenness

Figure 10 displays the variation in unevenness following the installation of swirl nozzles with different acute airway angles.

Swirl nozzles with different acute airway angles can limit yarn unevenness, as shown in figure 10. Specifically, the unevenness of the yarn produced using the 80° nozzle deteriorates significantly as p rises. In the other four swirl nozzles, unevenness is most strongly reduced at 0.25 MPa; in particular, the 40° nozzle can significantly limit yarn unevenness by a maximum of 10.3%.

Nonetheless, the coefficient of variation (CV%) analysis of yarn evenness cannot generate comprehensive findings. Therefore, we conducted a subsequent experiment under a constant pressure of 0.15 MPa to evaluate this unevenness. Table 1 presents the corresponding comprehensive test results.

Table 1 suggests that yarn CV% can be reduced through the use of swirl nozzles with airway angles of 40°, 50°, 60°, 70°, and 80°. Specifically, the 40° swirl nozzle produces thin positions and neps. Thus, the application of this nozzle is conducive to the next

process, which involves the physical and mechanical properties of yarn and fabric appearance. The 40° swirl nozzle generally performs best among the investigated nozzles. Figure 11 displays the SEM images of the swirl nozzle and of the conventional ring-spun yarns and indicates that the surface of the ring-spun yarn produced with a swirl nozzle is smoother than that of traditionally produced yarn.

In summary, the installation of a swirl nozzle on the ring frame can effectively improve yarn quality. Furthermore, airway angle and air pressure significantly influence yarn performance. Specifically, the following two areas are affected.

Structure of the Swirl Nozzle and the Movement of Internal Air Flow

When compressed air from the airway enters the yarn duct, the airway is tangential to this duct and generates whirling air flow along the tangential plane, which results in a false twist in the yarn (figure 12). The direction of this twist contradicts the original twist direction of the yarn. Moreover, the yarn near the front roller nip is untwisted, and the force of the whirling air flow conductively transfers the untwisting function to the spinning triangle of the roller nip. This function is conducive to *S3* re-arrangement on the

Table 1

COMPREHENSIVE TEST RESULTS OF YARN UNEVENNESS				
Types	Unevenness CV/%	−50%/ thin (Quantity·km^{-1})	+50%thick/ (Quantity·km^{-1})	+200%Nep/ (Quantity·km^{-1})
Traditional ring spinning	14.60	2	3	0
80° nozzle	13.80	2	9	12
70° nozzle	13.81	2	12	3
60° nozzle	13.50	0	9	10
50° nozzle	13.66	1	6	3
40° nozzle	13.45	1	2	3
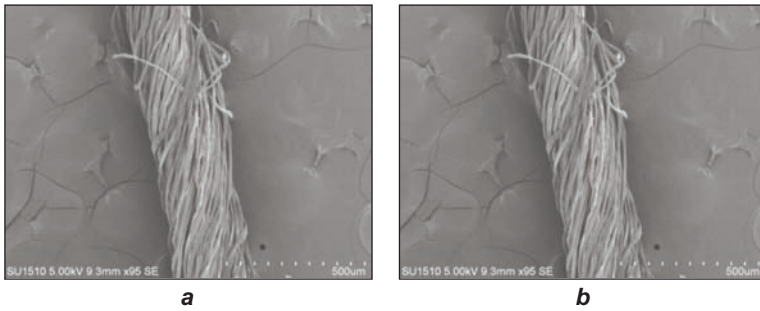
Fig. 11. SEM images of ring-spun yarn produced with a swirl nozzle and traditional spun yarns
a – Spun yarn produced with a swirl nozzle; *b* – Traditionally spun yarn
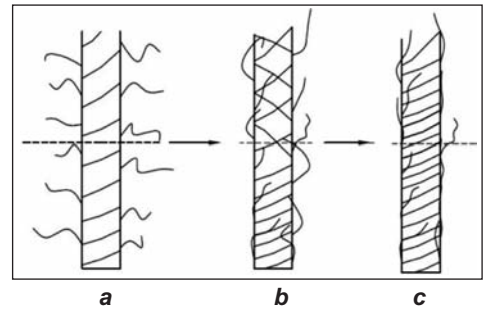
Fig. 12. False twisting process of yarn
a – Before false twisting; *b* – False twisting; *c* – After false twisting

surface of the yarn. Simultaneously, *S3* is incorporated into either the yarn or the untwisted, loose yarn. Once the yarn is disconnected from the point of false twisting, the degree of yarn twist is restored to its original value (before the false twist). Thus, the *S3* is twisted into the yarn body around which it is wrapped. The long hairs on the surface of the yarn are significantly shortened and the short hairs are tightly wound. As a result, yarn strength is enhanced.

Airway angle of a swirl nozzle

Once the air flows into the yarn body, the acting force on the yarn body can be decomposed into axial (F_a), tangential (F_r), and radial forces (F_t) (figure 13) [20]. The tangential force of air flow can carry fibers; the axial force can advance screws; and the radial force applies impact force to the yarn. The whirling air flow generated by the compressed air under the joint action of axial and shearing forces unbends the yarn and winds the hairs around the yarn body. When the airway angle is 90°, the tangential and radial forces of air flow are stronger than the axial force. The impact of air flow force on the holding of the yarn body is great, but the impact on the movement speed toward the front of the jaw is weak. This weakness is not conducive to the unbending of hairs. The axial force of air flow increases and radial force decreases with the reduction in angle; these phenomena are conducive to the transfer of rotary airflow to the twist triangle. Thus, the hairs are straightened and are fully wound around the yarn body. When the airway angle is increased, a recirculation zone is easily formed and the hairs on the yarn body are bent in the process of unbending and coating. Therefore, the process of

Fig. 13. Force analysis of the yarn

Fig. 14. Process of winding hairs around the yarn

straightening and wrapping the hairs is incomplete (figure 14).

CONCLUSIONS

This study developed seven nozzles that can be divided into three types, namely, acute, obtuse, and right angles. These nozzles were used to reduce *S3* and improve the performance of spun yarn. Following analysis and discussion, we drew the following conclusions:

1) The installation of a swirl nozzle on the ring frame can effectively reduce *S3*, increase breaking force, and limit unevenness.

2) The force of the component air flow in the yarn duct varies with airway angle. Therefore, swirl nozzles with different airway angles have varied effects on yarn performance.

3) Under similar spinning parameters, the swirl nozzle with a 40° angle generates yarn with ideal properties, that is, an *S3* of 3 mm and above, breaking force, and yarn unevenness.

BIBLIOGRAPHY

[1] Lawrence C. 2003. *Fundamentals of spun yarn technology*. CRC. p. 257

[2] Haleem N., Wang X. *Recent research and developments on yarn hairiness*, In: Textile Research Journal, 2015, vol. 85, no. 2, pp. 211–224

[3] Huang X., Tao X., Xu B. *A theoretical model of maximum hairiness of staple ring-spun yarns*, In: Textile Research Journal, 2014, pp. 213–221

[4] Zhao Q., Gang Z., Hua S. *Comparison of properties characterization between CHES-F, KES-F and FAST*, In: Industria Textila, 2011, vol. 62. pp. 123–127

[5] Surdu L., Ghituleasa C., Mihai C., Ene A., Radulescu I., Subtirica A., Cioara I. *Comfort properties of multilayer textile materials for clothing*, In: Industria Textila, 2013, vol. 64, no. 2, pp. 75–79

[6] Soltani P., Johari M S. *Effect of using the new solo-siro spun process on structural and mechanical properties of yarns*, In: Fibers and Textiles in Eastern Europe, 2013, vol. 21, no. 3, pp. 51–54

[7] Yang R., Wu W., Wang H. *Effects of solospun roller on properties of cotton/polyester solo-sirofil composite yarn*, In: Journal of Engineered Fibers and Fabrics, 2012, vol. 7, pp. 98–102

[8] Altas S., Kado U G L., Seyin H U. *Comparison of conventional ring, mechanical compact and pneumatic compact yarn spinning systems*, In: Industria Textila, 2012, vol. 7, no. 1, pp. 87–100

[9] Soltani P., Johari M S. *A study on siro-, solo-, compact-, and conventional ring-spun yarns. Part I: Structural and migratory properties of the yarns*, In: Journal of the Textile Institute, 2012, vol. 103, no. 6, pp. 622–628

[10] Wang X., Miao M. *Studies of JetRing spinning. Part 1: Reducing yarn hairiness with the jetring*, In: Textile Research Journal, 1997, vol. 67, no. 4, pp. 253–258

[11] Wang X. *The effect of testing speed on the hairiness of ring-spun and sirospun yarns*, In: Journal of the Textile Institute, 1997, vol. 88, no. 2, pp. 99–106

[12] Wang X., Miao M. *Reducing yarn hairiness with an Air-Jet attachment during winding*, In: Textile Research Journal, 1997, vol. 67, no. 7, pp. 481–485

[13] Zeng Y., Yu C. *Numerical and experimental study on reducing yarn hairiness with the JetRing and JetWind*, In: Textile Research Journal, 2004, vol. 74, no. 3, pp. 222–226

[14] Zeng Y., Yu C. *Numerical simulation of fiber motion in the nozzle of an Air-Jet spinning machine*, In: Textile Research Journal, 2004, vol. 74, no. 2, pp. 117–122

[15] Zeng Y., Yu C. *Numerical simulation of air flow in the nozzle of an air-jet spinning machine*, In: Textile Research Journal, 2003, vol. 73, no. 4, pp. 350–356

[16] Cheng K., Li C. *JetRing Spinning and its Influence on Yarn Hairiness*, In: Textile Research Journal, 2002, vol. 72, no. 12, pp. 1079–1087

[17] Rengasamy R S., Kothari V K., Patnaik A., Bhatia S K. *Hairiness reduction in polyester spun yarns during ring spinning using air nozzles – optimization of nozzle and other parameters*, In: Indian Journal of Fiber and Textile Research, 2006, vol. 31, no. 4, pp. 521–528

[18] Patnaik A., Rengasamy R S., Kothari V K., Ghosh A., Punekar H., Limited F. *Hairiness reduction of yarns by nozzles at ring spinning: Airflow stimulation approach*, In: Apparel Journal of Textile and Apparel Technologe Management, 2005, vol. 4, no. 4, pp. 1–11

[19] Qiu H., Zhang Y., Xu Z., Ge M. *A Novel method to reduce hairiness level of ring spun yarn*, In: Fibers and Polymers, 2012, vol. 13, no. 1, pp. 104–109

[20] Sakthivel J C., Anbumani N. *Effect of yarn twist and loop length on the dimensional characteristics of plain weft knitted fabrics made from spun viscose ring spun yarns*, In: Industria Textila, 2011, vol. 62, no. 6, pp. 296–299

Authors:

HUA QIU
QIAOLI LUAN
HONGXIA JIANG
YUYE FU
JIHONG LIU

Jiangnan University
Faculty of Key Laboratory of Eco-Textiles, Ministry of Education
Wuxi-214000
Jiangsu-CHINA

e-mail: qiuhua@jiangnan.edu.cn, fukui2007@gmail.com, 384377254@qq.com,
523789059@qq.com, liujihongtex@hotmail.com

Corresponding author:

HUA QIU
qiuhua@jiangnan.edu.cn

An investigation into the parameters influencing the abrasion and friction properties of composite yarns containing metal wire

ERHAN KENAN ÇEVEN   HÜSEYİN AYTAŞ

REZUMAT – ABSTRACT

Studiu asupra parametrilor care influențează proprietățile de abraziune și frecare ale firelor compozite cu conținut de fir metalic

Acest studiu se concentrează pe parametrii selectați care influențează proprietățile de abraziune și frecare ale firelor compozite cu conținut de fire metalice. În cadrul studiului experimental, firele compozite conținând fire metalice au fost realizate pe o mașină de răsucit cu fus tubular conform metodei de acoperire. Firele compozite care conțin fire metalice au fost produse prin utilizarea a șapte variante de fire de acoperire cu structuri și materii prime diferite. Acestea au fost: fire de polipropilenă, bumbac, fire cu miez poliester/bumbac, poliester-filament continuu, nailon 6.6-filament continuu, poliester/fire cu miez poliester și fire din fibre tăiate de poliester. Aceste fire au fost acoperite cu fire din oțel inoxidabil (SS) cu două diametre diferite de 50 μm și 100 μm. Testele de performanță selectate pentru aceste fire au fost cele de abraziune și frecare deoarece aceste tipuri de fire sunt vulnerabile la frecare. Testele de abraziune ale firelor compozite conținând fir metalic au fost realizate cu un instrument de testare crockmetru modificat, în timp ce testele de frecare s-au efectuat cu ajutorul unui dispozitiv de măsurare a coeficientului de frecare al firelor. Conform rezultatelor analizelor statistice realizate utilizând valorile experimentale obținute în urma testelor, proprietățile de rezistență la abraziune și de frecare ale firelor compozite au fost afectate de parametrii firelor, cum ar fi tipul firului de acoperire și diametrul firului metalic.

Cuvinte-cheie: fire compozite, fir metalic, oțel inoxidabil, abraziune, frecare

An investigation into the parameters influencing the abrasion and friction properties of composite yarns containing metal wire

This paper is focused on the selected parameters that influence the abrasion and friction properties of composite yarns containing metal wire. In the experimental study, the composite yarns containing metal wire were produced on a hollow spindle twisting machine according to the method of covering. The composite yarns containing metal wire were produced with seven different cover yarns varying in their raw materials and structures. These were: polypropylene, cotton, polyester/cotton core-spun, continuous filament polyester, continuous filament nylon 6.6, polyester/polyester core-spun, and polyester cut fiber yarns. These yarns were cross covered over stainless steel (SS) wires having two different diameters of 50 μm and 100 μm. The performance tests selected for these yarns were abrasion and friction as because these types of yarns are vulnerable to rubbing. Abrasion tests of composite yarns containing metal wire were performed with a modified crockmeter test instrument while the friction tests were carried out by using a yarn friction coefficient measurement device. According to the results of the statistical analyses performed using the experimental values obtained from the tests, abrasion resistance and friction properties of the composite yarns were affected by the yarn parameters like cover yarn type and wire diameter.

Keywords: composite yarns, metal wire, stainless steel, cover yarn, abrasion, friction

INTRODUCTION

In addition to aesthetics, technical considerations are also important in the production of fabrics. Textile products whose primary objective is to meet some technical requirements or functions are called technical textiles. With time technical usage of textiles has been growing. The development of new fibers and new processing technology is widening the areas of application. The forms in which technical textile products are available are thread, tape, woven, knitted, braided, knotted and non-woven fabric. Of all these forms, only non-woven products are made straight from staple fibres or short natural fibres, whereas for the rest the basic raw material is yarn [1]. Composite yarns containing metal wire are used in two main areas. The first usage area is basically for decorative purposes as a fancy yarn, whereas the other usage area is for functional purposes as a technical yarn [2]. Metallic fibres which are used to produce composite yarns are manufactured fibers composed of metal, plastic-coated metal, metal-coated plastic, or a core completely covered by metal. Metal filament thickness varies between 1 and 80 microns. Stainless steel and other metal fibers are used in communication lines such as phone lines and cable television lines. Other uses include tire cord, missile nose cones, work clothing such as protective suits, space suits, and cut resistant gloves for butchers and other people working near bladed or dangerous machinery. Metallic yarns may be in single form of metal filament or in blended form with other fibres. Metallic yarns are woven, braided, and knit into many fashionable fabrics and trims. For additional variety, metallic yarns are twisted with other yarns composed of fibers such as wool, nylon, cotton, and synthetic blends to

Fig. 1. Metal fibre (316 L type monofilament SS wire)

produce yarns which add novelty effects to the end cloth or trim [3].

Besides that, composite yarns with metal fibers are used in fabrics for electromagnetic shielding and for radar waves absorbing and for infrared camouflage purposes. Having excellent permanent conductivity among all of its conductive fibers, metal wire exhibits electrostatic charging or discharging during various industrial processes because of friction, separation or conduction between objects [4]. Therefore, stainless steel fibers are used in carpets. They are dispersed throughout the carpet with other fibers so they are not detected. The presence of the fibers helps to conduct electricity so that the static shock is reduced. Figure 1 shows the image of metal fiber (316 L type monofilament SS wire).

Rankumar et al. determined friction of technical yarns composed of different raw materials and different mixtures (Kevlar, PES, PP, PA 6) produced by friction spinning technology. They stated that PP yarn has the lowest friction coefficient for all the tension values [5]. Svetnickenė and Čiukas examined the friction behavior of technical (SVM, Phenyloin, Nomex) and classic (PA6, PAN, Cotton) yarns used for protective clothing in the knitted fabric form. The highest coefficient of friction value was observed for Cotton and PA 6 while the lowest value was observed for PAN and Nomex yarn. SVM and Phenyloin ranked among the others [6]. Various researchers investigated the electromagnetic shielding effectiveness, far infrared ray emissivity and anion density of fabrics produced with composite yarns [7]–[12]. But the literature survey shows that there is limited research on physical properties of technical yarns containing metal wires. Baykal and Sığnak investigated the performance properties of woven fabrics including metallic yarn [13]. Ramachandran and Vigneswaran manufactured yarns that consisted of copper filament as core and cotton fiber as sheath material in Dref-3 friction spinning system [14]. Perumalraj and Dasadaran produced copper core spun yarns of different counts on Dref friction spinning and modified ring spinning machines and investigated the effects of the process variables on tensile properties of these yarns [15]. Bedeloğlu et al. investigated the effect of roving counts and types of metal wires on hairiness, and tensile properties of composite yarns [16]. Bedeloğlu et al. produced hybrid yarns in modified ring spinning machine by core spinning technique. Physical behavior of complex yarns consisting of cotton yarn and copper and stainless steel wire was evaluated by investigating bending rigidity, tensile and hairiness properties of the samples [17]. Sun et al. investigated the tensile property of stainless-steel composite yarns [18]. However there is no research on abrasion and friction properties of composite yarns containing metal wires. Abrasion resistance and friction behavior in metal-containing composite yarns are important features which affect quality and product performance. Yarn friction is a factor affecting pilling and abrasion resistance, softness, stiffness, yarn hairiness and tenacity properties. This study aims at filling this gap in the literature by contributing to the investigation of the interrelationships and specific influences of composite yarn production parameters like cover yarn type and metal wire diameter on abrasion and friction properties of composite yarns The expected target from this study is to trigger new studies for the determination of the effect of other structural parameters like wire type on the physical properties of composite yarns containing metal wires.

EXPERIMENTAL WORK

Materials

Seven different types of cover yarns varying in their raw materials and structures and two different levels of metal wire diameters were selected in order to determine the influence of yarn structural parameters like cover yarn type and metal wire diameter on abrasion and friction properties of composite yarns. Characteristics of the component yarns selected for the production of composite yarns were:

Cover yarn: polypropylene, cotton, polyester/cotton core-spun, continuous filament polyester, continuous filament nylon 6.6, polyester/polyester core-spun, and polyester cut fiber yarns (yarns varying in their raw materials and structures)

Core yarn: 316 L type SS metal wires varying in diameters: 50 µm (0.05 mm) and 100 µm (0.10 mm)

Fourteen different composite yarns were produced on a hollow spindle twisting machine (S&Z MX model Sapru Machines Pvt.Ltd.) according to the covering method. Yarns varying in their raw materials and structures were cross covered over SS wires having two different diameters of 50 µm and 100 µm. Twist of the first layer was selected as 300 turns/meter (wrapped count: 3 turn/cm) in the S direction and the twist of the second layer was selected as 300 turns/meter (wrapped count: 3 turn/cm) in the Z direction. Wrapped count is defined as the number of turns of wrapped material in per unit length, the unit is turn/cm. Figure 2 illustrates the basic structure of cross covered composite yarns consisting of two covering yarns and one metal core yarn while figure 3 shows the photograph of the hollow spindle twisting machine.

There are many differences in the structure of covered (wrapped) yarns depending on their components, the type of manufacturing system and parameters. Among the methods of producing covered yarns, the hollow spindle technique is a well-known method. As seen from figure 2, a typical covered yarn is composed of straight core, which is wrapped with two covering yarns. The packages with covering yarns are mounted on two hollow spindles of double covering machine. The core yarn goes across the
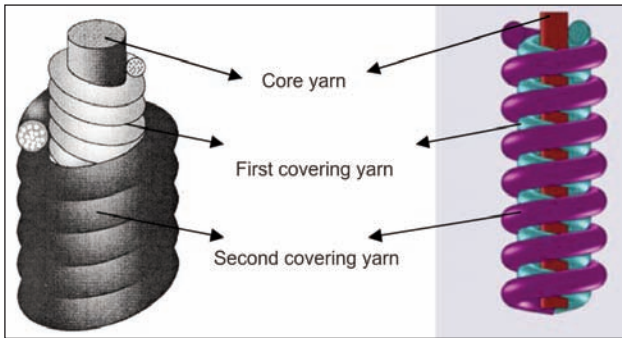
Fig. 2. Illustration of the components of cross covered composite yarn [19], [20]

inside of these spindles. At the initial stage of wrapping process, a semi-manufactured product composed of a core yarn and one covering yarn is made. Finally, this semi-manufactured product is wrapped by second covering yarn. Thus, each covering component has a shape of spiral line. The core yarn has almost no twist during wrapping. Before wrapping, the core is usually stretched [19].

Yarn Coding:

The coding of the composite yarns according to structural parameters is given by:

C_{ab} : (a) cover yarn type   (b) metal wire diameter

for a: 1 stands for polypropylene, 330×2 dtex
       2 stands for cotton, 310×2 dtex
       3 stands for polyester/cotton core-spun, 346× 2 dtex
       4 stands for continuous filament polyester, 295×2 dtex
       5 stands for continuous filament nylon 6.6, 312×2 dtex
       6 stands for polyester/polyester core-spun, 305×2 dtex
       7 stands for polyester cut fiber, 320×2 dtex

for b: 1 stands for 50 µm,
       2 stands for 100 µm

For example, C_{52} means that: the composite yarn is produced by cross covering the 316 L type SS metal wire core having a diameter of 100 µm with two 312×2 dtex continuous filament nylon 6.6 cover yarns. Figure 4 shows the stereomicroscopic images of the C_{11} and C_{32} coded composite yarns.
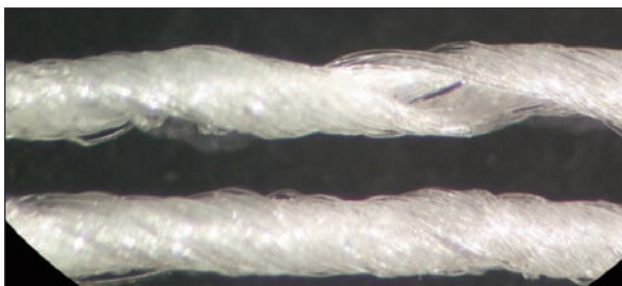
Fig. 3. Photo of the hollow spindle twisting machine (MX model, Sapru Machines Pvt.Ltd)

The codes of the fourteen different composite yarns produced according to the experimental plan are listed in table 1. The linear density values of the composite yarns produced within the scope of the study are given in table 2.

Method

Prior to the abrasion and friction tests, all yarn samples were conditioned for 24 hours in standard atmospheric conditions (at a temperature of 20 ± 2 °C and relative humidity of 65 ± 2%) [21].

Abrasion Test:

A testing device designed by making some modifications to the Crockmeter (James H. Heal & Co. Ltd) was used in order to measure the abrasion resistances of the yarn samples [22]. The test method involved the abrasion of composite yarns by a medium abrasive non-woven scouring pad made from PA and aluminum oxide with dimensions of 5 × 5 cm.

| a | b |

Fig. 4. Stereomicroscopic Images (20×) of the a) C_{11} coded composite yarns (Double layer SS/PP wrapped yarns made with 50 µm SS) and b) C_{32} coded composite yarns (Double layer SS/ PES-Cotton Core-spun wrapped yarns

Table 1		
COMPOSITE YARN CODES	**Metal wire diameter**	
	50 μm	100 μm
Cover yarn type and yarn count expressed in dtex (Nm) — polypropylene, 330×2 (30/2)	$c_{1,1}$	$c_{1,2}$
cotton, 310×2 (32/2)	$c_{2,1}$	$c_{2,2}$
polyester/cotton core-spun, 346×2 (29/2)	$c_{3,1}$	$c_{3,2}$
continuous filament polyester, 295×2 (34/2)	$c_{4,1}$	$c_{4,2}$
continuous filament nylon 6.6, 312×2 (32/2)	$c_{5,1}$	$c_{5,2}$
polyester/polyester core-spun, 305×2 (33/2)	$c_{6,1}$	$c_{6,2}$
polyester cut fiber, 320×2 (31/2)	$c_{7,1}$	$c_{7,2}$

Table 2		
CCOMPOSITE YARN LINEAR DENSITY, DTEX (NM)	**Metal wire diameter**	
	50 μm	100 μm
Cover yarn type and yarn count expressed in dtex (Nm) — polypropylene, 330×2 (30/2)	900 (11)	1402 (7)
cotton, 310×2 (32/2)	824 (12)	1310 (8)
polyester/cotton core-spun, 346×2 (29/2)	943 (11)	1461 (7)
continuous filament polyester, 295×2 (34/2)	802 (12)	1292 (8)
continuous filament nylon 6.6, 312×2 (32/2)	837 (12)	1340 (8)
polyester/polyester core-spun, 305×2 (33/2)	812 (12)	1305 (8)
polyester cut fiber, 320×2 (31/2)	868 (12)	1369 (7)

The composite yarn was wound (ten turns) on a rectangular cardboard with dimensions of 170 × 30 cm. The abrasive pad was moved straight onto the wound composite yarn. Before starting the abrasion tests, primary trials were made in order to determine the abrasion cycle that would be suitable for the yarn samples. According to the results of these trials, mass losses in mg were determined for the abrasion level of 50 cycles. Average values of mass loss ratio (%) were obtained by the proportion of the mass loss of samples after the test levels divided by the initial mass of the samples. Number of repetition for the measurements was three for each yarn type.

Friction Test:

Measurements of the friction coefficient of yarn samples were done according to standard TS 7475 "Determination of The Friction Coefficient of The Yarn to The Solid Material" with Duranax-E.F.I. Yarn Friction Coefficient Measurement Device shown in figure 5 located in the Uludag University, Textile Engineering Department, Physical Testing and Analysis Laboratory.

Eytelwein's law was used for calculating the friction for yarns sliding over a cylindrical guide, which is derived from Coulomb's law for yarns. Coefficient of friction was calculated according to equation (1) and

Fig. 5. Photo of the coefficient of friction measurement device (Duranax-E.F.I.)

equation (2). Test speed was 100 m/min, the average input tension, T_1 was 100 mN and the wrap angle was 3.14 radian (180º). Tests were repeated three times for each yarn sample with a selected contact time of 30 seconds [23].

$$e^{\mu\theta} = \frac{T_2}{T_1} \qquad (1)$$

$$\mu = \frac{\ln \left(\frac{T_2}{T_1}\right)}{\theta} \qquad (2)$$

where:
μ = coefficient of friction,
T_1 = average input tension, mN or gf,
T_2 = average output tension, mN or gf, and
θ = cumulative wrap angle, radians.

Statistical Evaluation:

All statistical procedures were conducted using the SPSS 17.0 Statistical software package. In the study completely randomized two-factor analysis of variance (ANOVA) was used for the determination of the statistical significance of the composite yarn structural parameters as cover yarn type and metal wire diameter on abrasion and friction properties of composite yarns. The means were compared by Student-Newman-Keuls (SNK) tests. The value of significance level (α) selected for all statistical tests in the study is 0.05. The treatment levels were marked in accordance with the mean values, and any levels marked by different letter (a, b, c) showed that they were significantly different.

RESULTS AND DISCUSSION

Abrasion Resistance

The diagram of mass losses of the composite yarns is demonstrated in figure 6.
Abrasion resistances of the composite yarns were evaluated according to mass loss (%) values. When the mass loss values of the composite yarns shown in fig. 6 were inspected, it was observed that, the

minimum mass loss was obtained as 0.80 % from the composite yarn (C_{41} coded yarn) produced with cover yarn of continuous filament polyester and SS metal wire having 50 μm diameter, while the maximum mass loss was obtained as 3.80 % from the composite yarn (C_{22} coded yarn) produced with cover yarn of cotton and SS metal wire having 100 μm diameter. The p-values associated with F-tests for a two-way completely randomized ANOVA and SNK test values for the abrasion resistance test results are presented in table 3 and table 4 respectively.

The results of the of ANOVA test given in table 3 indicated that; there were statistically significant (5% significance level) differences between the mass loss values of the composite yarns having different cover yarn types. Another aspect about the abrasion test results was that there were significant differences between the mass loss values of the composite yarns produced with metal wires having different diameters. The effect of the interaction between cover yarn type and metal wire diameter on mass loss was significant.

The SNK test results given in table 4 revealed that, the composite yarns having different cover yarn types possessed statistically different mass loss values. Mass loss value for the cover yarn type: continuous filament polyester was 0.84 % while that for the cover yarn type: cotton was 3.26 %. According to fig. 6, mass loss values of the composite yarns with cover yarn type of continuous filament polyester were less than those of the composite yarns with cover yarn type of cotton. Cover yarn type difference led to a decrease in mass loss values by 70–77 % depending on the metal wire diameter. As the composite yarn structural parameters like the twist levels of the first and the second layer cover yarns were kept constant in this study, it was obvious that composite yarns' cover yarn type had a great influence on yarns' abrasion behaviors. This situation can be explained as; cover yarn material affects the surface properties of the composite yarn at constant production conditions. The SNK test results given in table 4 revealed that, the composite yarns having metal wires with different diameters possessed statistically different mass loss values. Mass loss value for the metal wire diameter of 50 μm was 1.78 % while that for the metal wire diameter of 100 μm was 2.22 %. According to figure 6, mass loss values of the composite yarns with 100 μm metal wire were more than those of the composite yarns with 50 μm metal wire. Metal wire diameter difference led to an increase in mass loss values by 8–40 % depending on the cover yarn type. From these findings it can be easily concluded that the abrasion resistance of the composite yarns increased meaningfully with the increase in SS metal wire diameter. In this case it must be taken into consideration that, all the composite yarns were produced with constant wrapped count. These results can be interpreted as: the metal wire diameter increase at constant wrapped count leads the cover yarns to slip easier with the abrasive force during the abrasion test. Thus
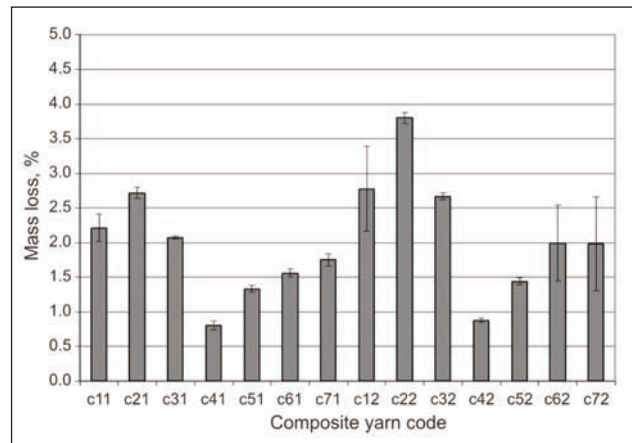
Fig. 6. Mass loss ratios (%) for composite yarns versus yarn codes (error bars indicate the confidence interval of 95 %)

Table 3

UNIVARIATE ANOVA RESULTS FOR MASS LOSS				
	Source	**df**	**F**	**Sig.(p)**
Main effect	Cover yarn type (C)	6	31.588	0.000
	Metal wire diameter (D)	1	58.155	0.000
Interaction	C × D	6	2.863	0.027

Table 4

STUDENT-NEWMAN-KEULS TEST FOR MASS LOSS FABRICS		
Parameter		**Mass loss ratio, %**
Cover yarn type (C)	continuous filament polyester	0.84 a
	continuous filament nylon 6.6	1.39 b
	polyester/polyester core-spun	1.77 c
	polyester cut fiber	1.87 c
	polyester/cotton core-spun	2.37 d
	polypropylene	2.49 d
	cotton	3.26 e
Metal wire diameter (D)	50 μm	1.78 a
	100 μm	2.22 b

NOTE: The different letters next to the counts indicate that they are significantly different from each other at a significance level of 5 %

the resistance to abrasion weakens and the mass loss increases.

Friction Property

The diagram of yarn friction coefficient (μ) values of the composite yarns is demonstrated in figure 7.
As a result of the inspection of the yarn friction coefficient values of the composite yarns shown in figure 7, it was observed that, the minimum friction coefficient was obtained as 0.18 from the composite yarn (C_{41} coded yarn) produced with cover yarn of continuous
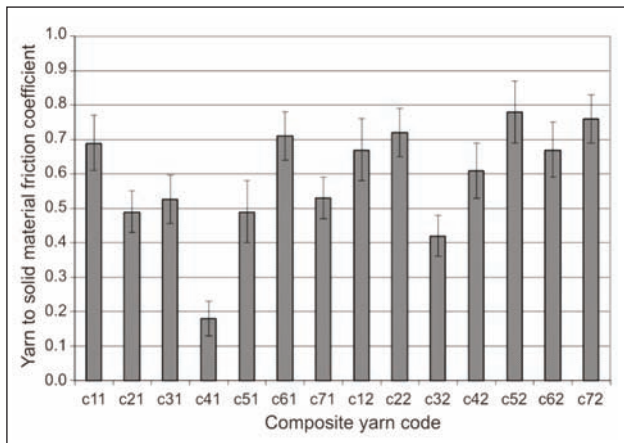
Fig. 7. Yarn friction coefficient (μ) values for composite yarns versus yarn codes (error bars indicate the confidence interval of 95 %)

filament polyester and metal wire having 50 μm diameter, while the maximum friction coefficient was obtained as 0.78 from the composite yarn (C_{52} coded yarn) produced with cover yarn of continuous filament nylon 6.6 and metal wire having 100 μm diameter. The p-values associated with F-tests for a two-way completely randomized ANOVA and SNK test values for the friction test results are presented in table 5 and table 6 respectively.

Table 5

UNIVARIATE ANOVA RESULTS FOR FRICTION COEFFICIENT				
Source		df	F	Sig.(p)
Main effect	Cover yarn type (C)	6	29.061	0.000
	Metal wire diameter (D)	1	85.255	0.000
Interaction	C × D	6	23.391	0.000

Table 6

STUDENT-NEWMAN-KEULS TEST FOR FRICTION COEFFICIENT		Yarn friction coefficient, μ
Parameter		
Cover yarn type (C)	continuous filament polyester	0.395 a
	polyester/cotton core-spun	0.473 b
	cotton	0.605 c
	continuous filament nylon 6.6	0.635 c
	polyester cut fiber	0.645 c
	polypropylene	0.680 c
	polyester/polyester core-spun	0.690 c
Metal wire diameter (D)	50 μm	0.517 a
	100 μm	0.661 b

NOTE: The different letters next to the counts indicate that they are significantly different from each other at a significance level of 5 %

The P values in table 5 indicated that there were statistically significant (5% significance level) differences between the friction coefficient values of the composite yarns having different cover yarn types. Another aspect about the friction test results was that there were significant differences between the friction coefficient values of the composite yarns produced with metal wires having different diameters. The effect of the interaction between cover yarn type and metal wire diameter on friction coefficient was significant.

The SNK test results given in table 6 revealed that, the composite yarns having different cover yarn types possessed statistically different friction coefficient values. The rank for the friction coefficients from the lowest to the highest value was as follows: continuous filament polyester, polyester/cotton core-spun, cotton, continuous filament nylon 6.6, polyester cut fiber, polypropylene, polyester/polyester core-spun. Friction coefficient value for the cover yarn type: continuous filament polyester was 0.395 while that for the cover yarn type: polyester/polyester core-spun was 0.690. The rank was consistent with the data given in a research done by Alagirusamy and Ogale [24]. There was statistically significant difference between the friction coefficients of composite yarns with cover yarn types of continuous filament polyester, polyester/cotton core-spun and cotton. But the friction coefficient values of the composite yarns with cover yarn types of cotton, continuous filament nylon 6.6, polyester cut fiber, polypropylene and polyester/polyester core-spun were statistically same. This situation can be attributed to the fact that; existence of metal wire as a core component in the cross covered composite yarn structure may lead to a remarkable decrease between the friction values of the yarns. According to figure 7, friction coefficient values of the C_{41} coded composite yarns were less than those of the C_{61} coded composite yarns by 74 % while the friction coefficient values of the C_{32} coded composite yarns were less than those of the C_{52} coded composite yarns by 46 %. When the constant twist level for the production is taken into consideration, it is obvious that the difference in the friction coefficients can be attributed to the effect of cover material type to the surface properties of the composite yarns. It is stated in the literature that, the morphology of a yarn like surface roughness affects the frictional properties of the yarns [25].

The SNK test results given in table 6 revealed that, the composite yarns having metal wires with different diameters possessed statistically different friction coefficient values. Friction coefficient value for the metal wire diameter of 50 μm was 0.517 while that for the metal wire diameter of 100 μm was 0.661. According to figure 7, metal wire diameter decrease from 100 μm to 50 μm led to a decrease of maximum 70 % and an increase of maximum 25 % in friction coefficient values depending on the cover yarn type. From these facts it can be easily deduced that the

friction coefficients of the composite yarns increased expressively with the increase in SS metal wire diameter. In this situation, it should be taken into account that all the composite yarns were produced with constant wrapped count. These results can be interpreted as: the metal wire diameter increase at constant wrapped count renders the yarn stiffer thus the average output tension measured at the friction measurement device will increase. It is stated in the literature that; yarn stiffness is influenced by the yarn types and fiber content [25].

CONCLUSIONS

The objective of this study was to investigate the influences of composite yarn production parameters like cover yarn type and metal wire diameter on abrasion and friction properties of composite yarns.

- According to the statistical tests performed on the measurements, the effect of cover yarn type on the abrasion resistance of composite yarns was significant. Mass loss values of the composite yarns with cover yarn type of continuous filament polyester were less than those of the composite yarns with cover yarn type of cotton. This situation was caused by the fact that: cover yarn material affects the surface properties of the composite yarn at constant production conditions.

- Statistical tests revealed that: the composite yarns having metal wires with different diameters possessed statistically different mass loss values. Abrasion resistance of the composite yarns increased meaningfully with the increase in SS metal wire diameter. These results can be interpreted as: the metal wire diameter increase at constant wrapped count led the cover yarns to slip easier with the abrasive force during the abrasion test. Thus the resistance to abrasion weakened and the mass loss increased.

- Statistically significant differences were observed between the coefficient of friction values of the composite yarns produced with cover yarns of different types like continuous filament polyester, polyester/ cotton core-spun and cotton. The morphology of a yarn like surface roughness affects the frictional properties of the yarns. But the friction coefficient values for cotton, continuous filament nylon 6.6, polyester cut fiber, polypropylene and polyester/ polyester core-spun were statistically same. This situation can be attributed to the fact that: existence of metal wire as a core component in the cross covered composite yarn structure may lead to a remarkable decrease between the friction values of the yarns.

- The composite yarns having metal wires with different diameters possessed statistically different friction coefficient values. Friction coefficients of the composite yarns increased expressively with the increase in SS metal wire diameter. This rise is caused by the fact that: the metal wire diameter increase at constant wrapped count rendered the yarn stiffer.

- This study has evidenced that, composite yarn structural parameters like cover yarn type and metal wire diameter affect both the abrasion and friction properties of these yarns.

- Finally, it could be concluded that it will be useful to make further studies on determining the effect of composite yarn parameters on other physical properties of these yarns. The physical properties which should be highlighted are breaking strength and stiffness.

BIBLIOGRAPHY

[1] Alagirusamy R., Das A., *Technical textile yarns*, Woodhead Publishing Series in Textiles No. 101,U.K., 2010, ISBN 1 84569 549 6, pp. 259–260

[2] Örtlek H.G., Çalişkan Ç., Kurban R. *A comparative study on the physical properties of hybrid yarns containing copper wire,* In: Journal of Textiles and Engineer, 2013, vol. 20, pp. 11–20

[3] Gooch, J, W., *Encyclopedic dictionary of polymers,* Springer-Verlag New York, 2011, ISBN 978-1-4419-6246-1, p. 453

[4] Lou, C. W. *Process of complex core spun yarn containing a metal wire*, In: Textile Research Journal, 2005. vol. 75, no. 6, pp. 466–473

[5] Rankumar, S.S., Shastri, L., Tock, R.W., Shelly, D.C., Smith, M.L., Padmanabhan, S. *Experimental study of the frictional properties of friction spun yarns,* In: Journal of Applied Polymer Science, 2003, vol. 88, pp. 2450–2454

[6] Svetnickenė, V., Čiukas, R. *Technical and classical yarns friction properties investigation*, In: Mechanika, 2006, vol. 4, no. 60, pp. 54–58

[7] Bedeloglu, A. *Investigation of electrical, electromagnetic shielding and usage properties of woven fabrics made from different hybrid yarns containing stainless steel wires*, In: Journal of the Textile Institute, 2013, vol. 104, no. 12, pp. 1359–1373

[8] Po-Wen H., An-Pang C., Ching-Wen L., Jia-Horng L. *Electromagnetic shielding effectiveness and functions of stainless steel/bamboo charcoal conductive fabrics*, In: Journal of Industrial Textiles, 2014, vol. 44, no. 3, pp. 477–494

[9] Jia-Horng, L., An-Pang, Chen., Chien-Teng, Hsieh., Ching-Wen, Lin., Chin-Mei, Lin., Ching-Wen Lou. *Physical properties of the functional bamboo charcoal/stainless steel core-sheath yarns and knitted fabrics,* In: Textile Research Journal, 2010, vol. 81, no. 6, pp. 567–573

[10] Ortlek, H.G., Kılıc, G., Okyay, G., Bilgin S. *Electromagnetic shielding characteristics of different fabrics knitted from yarns containing stainless steel wire*, In: Industria Textila, 2011, vol. 62, no. 6, pp. 304–308

[11] Palamutçu, S., Özek, A., Karpuz C., Dağ, N. *Electrically conductive surfaces and their electromagnetic shielding efficiency measurements,* In: Tekstil ve Konfeksiyon, 2010, vol. 3, pp. 199–207

[12] Su, C.I., Chern, J.T. *Effect of stainless steel containing fabrics on electromagnetic shielding effectiveness*, In: Textile Research Journal, 2004, vol. 74, no. 1, pp. 51–549

[13] Baykal, P.D., Sığnak N. *An investigation of performance properties of woven fabrics including metallic yarn*, In: Tekstil ve Konfeksiyon, 2009, vol. 1, pp. 39–44

[14] Ramachandran, T., Vigneswaran, C. *Design and development of copper core conductive fabrics for smart textiles*, In: Journal of Industrial Textiles, 2009, vol. 39, no. 1, pp. 81–93

[15] Perumalraj, R., Dasaradan, B.S. *Tensile properties of copper core yarn*, In: Journal of Reinforced Plastics and Composites, 2010, vol. 29, no. 11, pp. 1688–1701

[16] Bedeloglu, A, Sunter, N., Bozkurt, Y. *Manufacturing and properties of yarns containing metal wires,* In: Materials and Manufacturing Processes, 2011, vol. 26, no. 11, pp. 1378–1382

[17] Bedeloglu, A., Sunter, N., Yildirim, B., Bozkurt, Y. *Bending and tensile properties of cotton/metal wire complex yarns produced for electromagnetic shielding and conductivity applications*, In: Journal of the Textile Institute, 2012, vol. 103, no. 12, pp. 1304–1311

[18] Sun, Y.C. ,Cheng, Z.H., Zhang, Y.M. *Analysis on tensile properties of stainless-steel fiber and yarn quality*, In: Advanced Materials Research, 2011, vol. 309–401, pp. 176–179

[19] Petrulis, D., Petrulyte S. *Effect of manufacturing parameters of covered yarns on the geometry of covering components*, In: Textile Research Journal, 2009, vol. 79, no. 6, pp. 526–533

[20] Örtlek, H.G. *Developing of innovative core-spun yarns for denim fabrics*, in "Proc. UTİB 5th International R&D Brokerage Event", Bursa, Turkey, 2013, pp. 305–306, ISBN: 978-605-5919-05-4

[21] ISO 139:2005. Textiles – *Standard Atmospheres for Conditioning and Testing*

[22] Özdemir, Ö., Çeven, E.K. *Influence of chenille yarn manufacturing parameters on yarn and upholstery fabric abrasion resistance*, In: Textile Research Journal, 2004, vol. 74, no. 6, pp. 515–520

[23] TS 7475. Determination of Coefficient of Friction, Yarn to Solid Material

[24] Alagirusamy, R., Ogale, V. *Development and characterization of GF/PET, GF/Nylon, and GF/PP commingled yarns for thermoplastic composites*, In: Journal of Thermoplastic Composite Materials, 2005, vol. 18, no. 3, pp. 269–285

[25] Ghosh, A., Patanaik A., Anandjiwala, R D., Rengasamy, R. S. *A study on dynamic friction of different spun yarns,* In: Journal of Applied Polymer Science, 2008, vol. 108, pp. 3233–3238

Authors:

ERHAN KENAN ÇEVEN[1]
HÜSEYİN AYTAŞ[2]

[1]Uludag University
Faculty of Engineering
Textile Engineering Department
Görükle Campus,16059-Nilüfer-Bursa-Turkey

[2]Uludag University
Graduate School of Natural and Applied Science
Görükle Campus,16059-Nilüfer-Bursa-Turkey

e-mail: [1]rceven@uludag.edu.tr , [2]haytas89@gmail.com

Corresponding author:

ERHAN KENAN ÇEVEN
rceven@uludag.edu.tr

An investigation on the bagging load of different woven fabrics

R. BEFRU BÜYÜKBAYRAKTAR

REZUMAT – ABSTRACT

Studiu asupra sarcinii de deformare a diverselor tipuri de țesături

În cadrul acestui studiu, a fost investigată tendința de deformare a diferitelor tipuri de țesături. Comportamentul de deformare a țesăturilor a fost evaluat prin investigarea sarcinii de deformare în funcție de caracteristicile țesăturii, cum ar fi: tipul de legătură și parametrii de proiectare. Suplimentar, au fost aplicate diferite proceduri de testare, iar efectul parametrilor de testare a fost analizat statistic. De asemenea, a fost studiată disponibilitatea metodei de analiză a imaginilor. În acest scop, factorul de acoperire a imaginilor țesăturii deformate, precum și a celei nedeformate a fost investigat prin metoda de analiză a imaginilor, cu scopul de a analiza gradul de deformare. Tipul de legătură și parametrii de proiectare influențează geometria țesăturii 3-D și de asemenea sarcina de deformare 3-D a țesăturii. În plus, s-a observat că diametrul mai mare al sferei și timpul de aplicare al sarcinii asupra țesăturii au condus la creșterea deformării.

Cuvinte-cheie: sarcina de deformare, deformare, țesătură, tip de legătură, analiza imaginilor

An investigation on the bagging load of different woven fabrics

In this study, an experimental study was carried out in order to investigate the bagging deformation of different woven fabrics. The bagging behaviour of fabrics was evaluated by investigating the bagging load of fabrics depending on fabric properties such as weave type and settings. Besides different test procedures were applied and the effect of test parameters was discussed statistically. The availability of image analyse method to define the fabric deformation was also studied. For this purpose the cover factor of deformed and un-deformed fabric images was investigated by image analysis method in order to analyses the deformation degree. The weave type and settings are effective in the 3-D fabric geometry and also identified the 3-D bagging load of the fabric. Besides this, it was observed that the bigger sphere diameter and waiting time of the load onto the fabric increased the bagging deformation.

Keywords: bagging load, deformation, woven fabric, weave type, image analysis

INTRODUCTION

The deformation problem of a textile structure has been an important research area for many scientists. Deformation occurs as a result of long-term and repetitive forces during usage and causes changes of structural, mechanical and physical properties of fabric. Therefore, it is important to analyse and estimate the effects of structural properties on the deformation properties of fabric when designing a new product. Bagging is a three dimensional deformation problem defined as a complex biaxial tensile and shearing deformation of the fabric [1]. Especially, it affects the appearance of product at some parts of the body, such as knees and elbows. Recently, experimental and theoretical studies were carried out in order to analyse and predict bagging behaviour of fabric according to structural and mechanical properties. In the experimental studies usually a bagging apparatus attached to the Instron was used in order to simulate the bagging behaviour. This apparatus consisted of a part carried the fabric sample and a sphere applied load on the fabric to a predetermined height with a defined cycle. Zhang et al. evaluated the results of bagging deformation tests by subjective methods and found a linear relationship between subjective rating scores and fabric residual heights

[2]. Residual bagging height was found as a combined impact of bagging fatigue and resistance [3]. The effect of cyclic loading which contained loading and relaxation states was investigated using similar bagging test apparatus [4]. From the experimental study, it was found that the raw material and fabric structure influenced the results. The deformation of 100% wool fabrics was greater than blend ones and the elongation of twill fabric was greater than the plain weave fabric [4]. In the experimental studies, the effect of different test conditions to the deformation behaviour of fabric, such as bagging height, sphere size, test area, relaxation period were also investigated [5]–[8]. Image processing method was used to evaluate the bagging magnitude of tested fabrics by bagging height, volume, shape and fabric surface patterns which were extracted from bagged fabric images [9]. A different test apparatus was developed to investigate the relationship between in-plane tensile properties and bagging behaviour of woven fabric [10]. By this apparatus compression forces at vertical direction and in-plane tensile forces of fabric in warp and weft directions were measured by load cells and the results showed that the bagging behaviour of woven fabrics was related to biaxial tensile properties. An artificial arm test apparatus was improved to simulate the movement of the arm in

dynamic conditions and investigated the bagging deformation of a group of woven fabrics for different deformation cycles and bagging heights [11]. The bagging behaviour of wet and dry fabrics under static and dynamic loading was investigated and the change in the air permeability of fabrics was measured after the deformation tests. The increase of air permeability for wet samples was found higher than dry ones, and it was explained as the pores of textiles was irreversibly opened after wet bagging deformation [12].

In the theoretical part of the studies, the bagging behaviour of the fabric to be evaluated by 'mparameters such as bagging force and residual bagging height was predicted from the mechanical and structural properties of the fabrics. The properties of raw material were found important. Mechanical properties of materials, such as elastic and viscoelastic deformation of fibers, frictional behaviour of fibers and yarns, were taken into account and the bagging behaviour of fabrics having different raw materials was found significantly different related to the visco-elastic behaviour of fibers [13]–[14]. A series of experimental studies was made to analyse the influence of elasticity and viscoelasticity of fibers and inter-fibre friction to the bagging behaviour of fabric and weighting coefficients were obtained. These coefficients were used to simulate the bagging behaviour and the load-time curves of control fabrics were predicted to be close to experimental results [15]. It was noted that the behaviour of the material related to the external forces and elastic properties of the fabric and the Poisson's ratio had an important role on the deformation mechanism

In this study, the bagging behaviour of cotton fabrics having different weave type and weft settings was investigated by bagging deformation tests. The relationship between the bagging load and structural parameters of the fabrics were analysed by statistical methods. Besides the effects of different test parameters, such as sphere size and waiting time, were discussed. In this study, it is also aimed to define the bagging deformation degree of the fabric by image analysis method. It is known that the structural and performance properties of fabrics changes during usage. The images of un-deformed and deformed fabrics were captured. The change in the cover factor of the fabrics were analysed by image analyse methods in order to obtain the deformation degree of the structure from surface images of fabrics.

EXPERIMENTAL WORK

Materials and methods

In this study, tested fabrics consisted of plain, 2/1 twill and 3/1 twill fabrics which were systematically produced with 30 tex cotton yarn in both warp and weft directions and with the same warp setting. On the other hand, these fabrics were woven with three different weft settings for each weave type. Thus, the effect of structural parameters, such as weave type and setting, to the bagging behaviour of the fabric

Table 1

Fabric code	Weave Type	Mass per unit area w (g/m^2)	Warp-Weft Setting (cm^{-1})	Warp-Weft Crimp factors k_1, k_2
A14	Plain	148	36-14	1.053/1.059
A18	Plain	163	36-18	1.057/1.076
A22	Plain	175	36-22	1.070/1.091
B18	2/1 Twill	158	36-18	1.036/1.067
B22	2/1 Twill	171	36-22	1.034/1.075
B26	2/1 Twill	186	36-26	1.076/1.099
C18	3/1 Twill	161	36-18	1.027/1.062
C22	3/1 Twill	186	36-22	1.022/1.142
C26	3/1 Twill	190	36-26	1.040/1.098

STRUCTURAL PROPERTIES OF TESTED FABRICS

could be investigated easily. The structural properties of fabrics were summarized in table 1. In this table, fabric codes A, B, C indicated plain, 2/1 twill, 3/1 twill weaves, and numbers near the capitals indicated weft settings, respectively.

The bagging deformation of the fabric was simulated by bagging test in which a load was applied onto the surface of the fabric along the perpendicular direction. In this study, a bagging testing apparatus integrated to the Instron 4411 was used as seen in fig. 1. The diameters of holes in the testing apparatus were designed being 7 cm. During the test a sphere set up to the moving crosshead of the Instron applied load onto the fabric up to a certain distance with a certain speed. There is no pretension onto the fabric before the test. In this study, the speed of the test was decided being 60 mm/min according to literature. The displacement of the sphere called bagging height was determined by bursting tests. For all fabric types, bursting test was done by using the same bagging test apparatus and load-displacement curves was investigated. A standard bagging height for all fabric samples were decided after some pre-trials was done according to bursting test results. Bursting test was not done according to standards in order to ensure the bagging test conditions. The bursting tests were carried out until the sample was bursted by the spheres having 3 cm and 5 cm sphere diameter with 60 mm/min test speed.

In this study, the effect of test parameters to the bagging behaviour of fabrics was also investigated. For this reason, four different test procedures were planned which reflected the effect
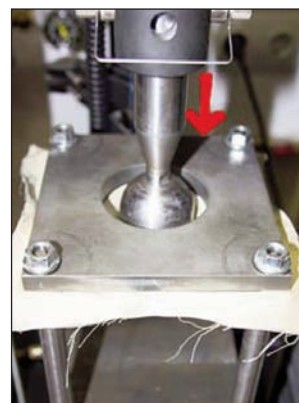
Fig. 1. Bagging test apparatus

THE TEST PARAMETERS OF BAGGING DEFORMATION TESTS		
Test code	Sphere diameter	Time
T1	3 cm	0
T2	5 cm	0
T3	3 cm	3 minute
T4	5 cm	3 minute

of sphere size and waiting time of the sphere onto the fabric after the bagging height was reached. In table 2, bagging test procedures was given. The diameter of the sphere used at T1 and T2 tests were 3 cm and 5 cm, respectively. T1 and T2 tests were ended as soon as the sphere reached the defined bagging height and then the load was noted. This recorded load value was named as bagging load. The bagging behaviour of the fabrics was investigated according to bagging load obtained after the sphere reached to the defined bagging height. On the other hand, T3 and T4 tests were ended after the sphere waited 3 minutes onto the fabrics at the defined bagging height and the bagging load was noted after this period. The effect of cycle and relaxation was not studied in this study.

Fabric images were captured before and after deformation tests in order to observe the change in the structure of the fabric. The cover factor of fabric was determined to define the deformation degree from

Fig. 2. Setup of image analyses system

fabric image. It is easy to get information about the cover factor of fabric by using image analysis method [16]–[17]. In this method the cover factor of the fabric was obtained by the help of light transmission property of fabric. First, fabric image was obtained by using a camera integrated to the computer system as seen in figure 2. The images of deformed fabric samples were captured from the deformed area of sample. In order to ensure a clear image from the surface of 3-D deformed fabric a glass coverslips was placed on to the deformed area. Obtained grey level image was converted to the binary images. Then, the pore regions were cleaned by opening and cleaning process in order to clean the fiber ends. And finally, the cover factor of each sample was calculated from the ratio of black pixels to the whole pixels of the final binary image. In figure 3, the steps of image analysis were summarized. For each fabric and each test procedure five fabric images were processed.

All tests were performed at standard atmospheric conditions. Bagging tests were repeated for 10 times for each fabric type. The bursting load and bagging load were discussed according to test type and fabric parameters by statistical methods and Minitab 14 was used as a statistical software.

RESULTS

Bursting test results

The displacement of the sphere at the bagging deformation tests was determined according to bursting test. All fabric types were tested and a smaller value than minimum bursting displacement of these fabrics was selected as bagging height, in order to prevent the bursting of any fabric sample. In figure 4, load-displacement curve of a bursting test with 3 diameters of sphere was given for A14 fabric as an example. The mean, minimum and maximum values of bursting load and displacement results of all tested fabrics were given in table 3. The minimum bursting height was found being 20.39 mm with 3 cm diameter sphere. The displacement of the sphere was decided as being 18 mm for bagging test. This displacement of sphere was a reliable value for all fabric types during bagging test because the higher values caused bursting of some samples. On the other hand, the residual deformation of tested fabrics was small at the lower ones (for instance 12 mm) because
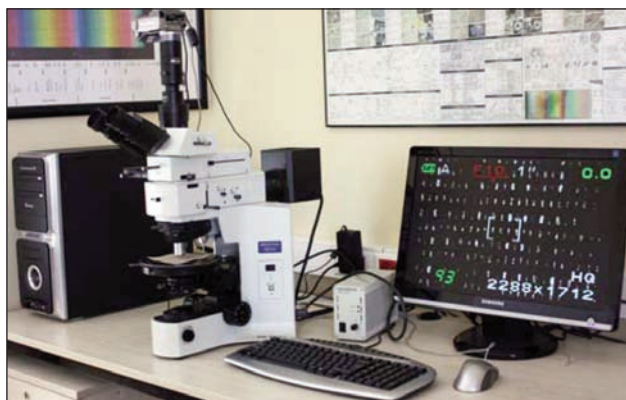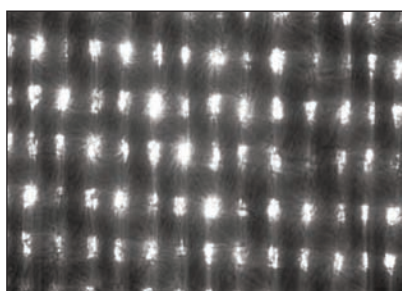
Fig. 3. Steps of image analysis
a – Grey level image, b – Binary image, c – Final binary image after opening and closing operations
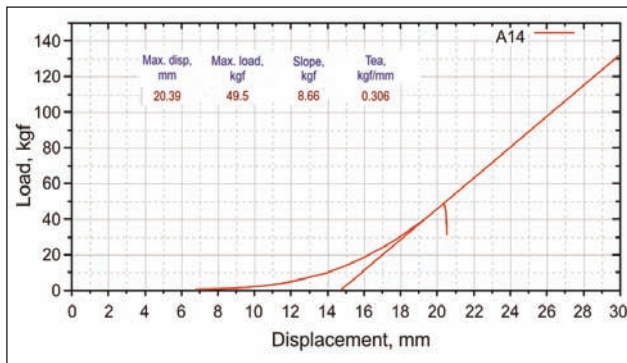
Fig. 4. A load-displacement curve of bursting test for A14 fabric

of being at the elastic region of the load-displacement curve.

The mean value of bursting load and height were increased with the increase of setting at all tested fabrics. When the bursting load and height of test results were investigated, generally the differences between the fabrics having close setting values were not found significant at the 95% confidence level. The effect of different weave types was investigated and it was observed that the mean value of bursting load and displacement of 3/1 twill weave was minimum at 18 cm^{-1} and 22 cm^{-1} weft settings, although the differences between the bursting load of different weave types was not found significant. At 26 cm^{-1} weft setting the bursting load and displacement of the 2/1 twill weave was found higher than 3/1 twill weave and the differences were found significant at the 95% confidence level.

Table 3

SUMMARIZED BURSTING TEST RESULTS FOR ALL TESTED FABRICS				
	5 cm sphere		3 cm sphere	
Value	Displacement (mm)	Load (kgf/ mm)	Displacement (mm)	Load (kgf/ mm)
Mean	22.53	115.6	23.38	73.82
Minimum	20.77	88.2	20.39	49.50
Maximum	24.04	136.3	24.90	86.80

Bursting loads of the fabrics tested with the bigger sphere were higher in all fabric types. Bigger sphere having 5 cm diameter had a larger contact area with the fabric surface than 3 cm one during the bursting test. The ratio between the bursting load of fabric tested with 5 cm sphere and 3 cm one were found 1.6 according to the results of all fabrics. This ratio was similar to the ratio of contact surface area of 5 cm and 3 cm diameter of spheres at bursting time which was found as 1.6. It could be said that the increase rate of the load was related and approximately the same with the increase rate of contact area between the sphere and fabric surface.

Bagging test results

The mean value of bagging loads of tested fabrics was given in table 4 according to different test procedures. The bagging load results of each test were discussed in terms of fabric properties and test parameters by using ANOVA test.

The relationship between the bagging loads of fabrics having different settings was analysed statistically depending on weave type. In figure 5, the bagging load results of each bagging test procedure were shown for different weave types having different weft settings. The differences between the bagging loads of plain fabrics having different weft settings were found significant at each bagging test. The differences between the bagging loads of B22 and B26 fabrics were not significant at the 95% confidence level for T1 and T2 tests. On the other hand, the differences between the bagging loads of all 2/1 twill fabrics having different settings was found significant according to T3 test. The differences between the bagging load of B26 fabric and others were found significant for T4 test. For 3/1 twill fabrics, only the differences between the bagging load of C26 fabric and others were found significant at 95% confidence level for T1 test. However, the differences between the bagging loads of 3/1 twill fabrics having different weft settings was not found significant for T2, T3 and T4 tests.

Table 4

MEAN BAGGING LOAD VALUES OF TESTED FABRICS				
Fabric Code	T1 Load (kgf/mm)	T2 Load (kgf/mm)	T3 Load (kgf/mm)	T4 Load (kgf/mm)
A14	32.28	47.23	24.12	34.94
A18	25.91	39.58	19.95	30.36
A22	23.46	34.88	17.61	25.91
B18	29.96	58.70	30.02	43.17
B22	33.04	51.99	26.70	41.54
B26	28.87	48.91	24.06	38.98
C18	37.20	54.25	26.89	39.24
C22	37.22	55.89	26.48	40.24
C26	34.09	55.29	26.58	36.76

As seen in figure 5, the increase of the setting decreased the mean value of bagging load at the determined bagging height for each weave type. This situation was valid for all bagging tests. This result was related to the fabric geometry. Increased setting caused the increase of yarn crimp. First, the crimp of the yarns was opened during the bagging test. Therefore, the bagging load at the defined displacement was measured lower at higher settings. On the other hand, it was observed that the increase of crimp factor caused the increase of bursting load and displacement. The correlation coefficients between the crimp factor of plain fabrics having different settings
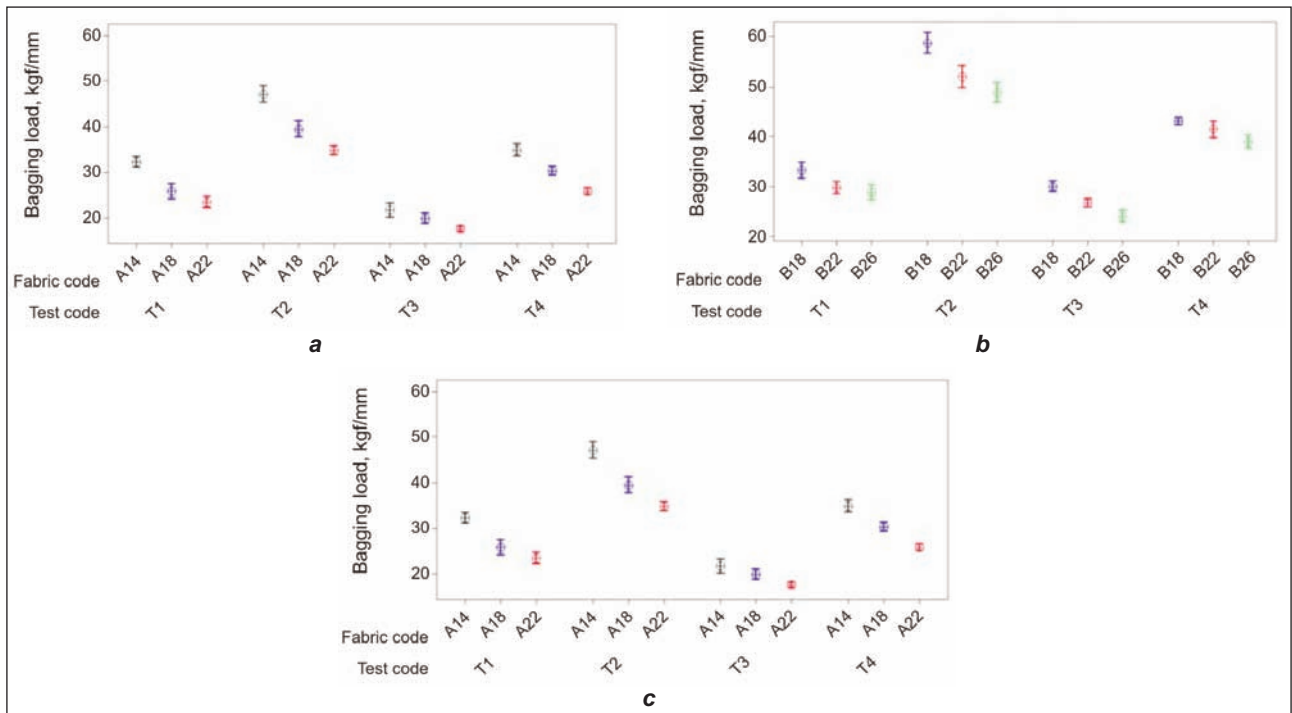
Fig. 5. Bagging load results according to weft settings and test type
a – Plain weave, *b* – 2/1 twill weave and *c* – 3/1 twill weave

and the bagging load were calculated –0.95, –0.98, –0.97, –1 for T1, T2, T3 and T4 tests, respectively. For 2/1 twill fabrics, the correlation coefficients between the crimp factor and the bagging load were calculated –0.64, –0.79, –0.87, –0.97 for T1, T2, T3, T4 tests, respectively.

For 3/1 twill fabrics, the correlation coefficients between the crimp factor and the bagging load were

found higher only for T2 and T4 test and they were –0.93, –0.99, respectively.

The effect of weave type was examined and the mean value of bagging load was found lower in plain fabrics. The differences between the bagging load of plain weave and twill weaves were found significant at 95% confidence level for all bagging tests, as seen in figure 6. For T1 test, the difference between the
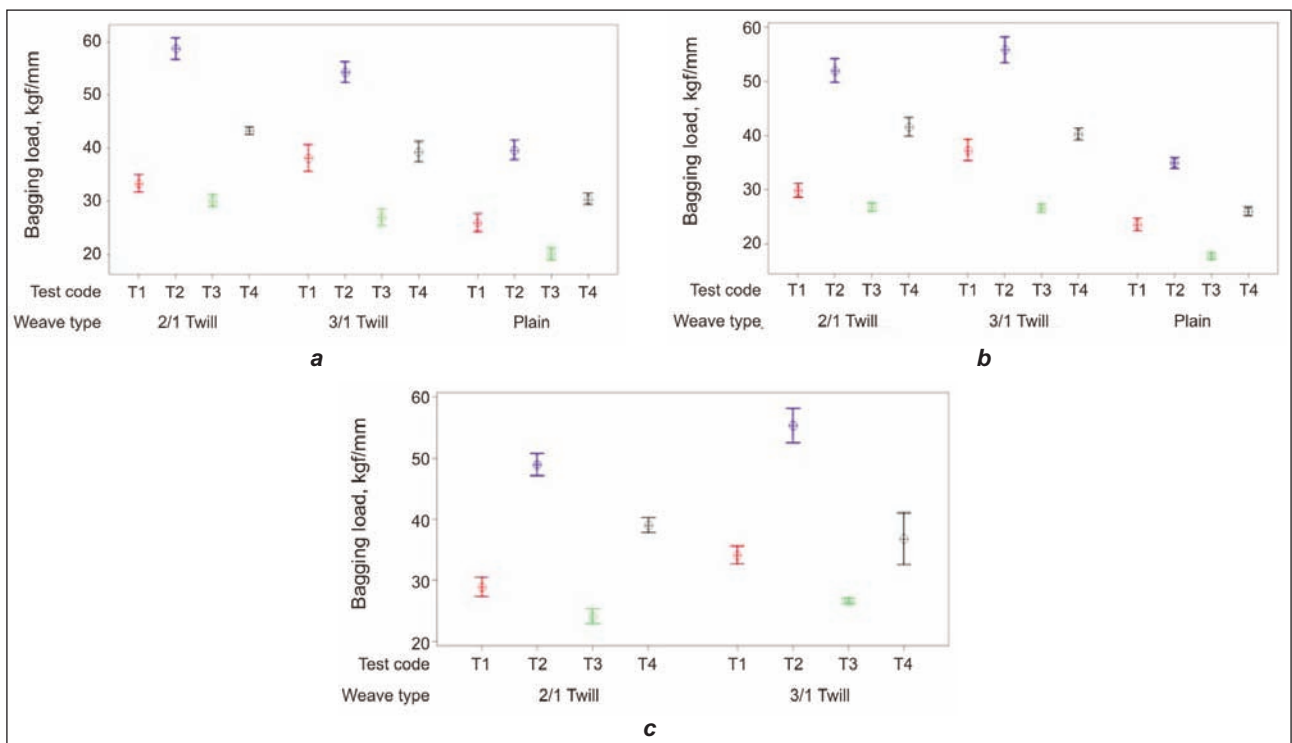
Fig. 6. Bagging load results according to weave type and test type
a – 18 cm^{-1} weft setting, *b* – 22 cm^{-1} weft setting and *c* – 26 cm^{-1} weft setting

bagging load of B18 and C18, and B22 and C22 was not found significant, but there was significant difference between B26 and C26. The difference between the bagging loads of all weave types was found significant for T2 test. For T3 test, the differences between bagging loads of different weave types were found significant at 18 cm^{-1} and 26 cm^{-1} weft setting, however the difference between 2/1 twill and 3/1 twill weave having 22 cm^{-1} weft setting (B22 and C22) was not found significant. For T4 test, the difference between different weave types was found significant at 18 cm^{-1} and 22 cm^{-1} weft settings, although there was no significant difference between the bagging loads of B26 and C26 fabrics.

Weave type was found as an important parameter in the deformation behaviour of the fabrics according to test results. This situation proved the influence of the fabric geometry. The intersections of the yarns form the 3-dimentional (3-D) fabric geometry depending on weave type and this geometry determines the behaviour of the fabric. Plain weave consists of repeated intersection regions and these intersecting increase the crimp of the yarn when compared with other weave types having same structural properties. During the bagging test, first the crimps of the yarns open, and then the yarns start to elongate until break. Therefore, the bagging load of the plain weave was lower than other weave types at defined bagging height. Fabric geometry caused higher crimp factor and this creates lower bagging load. Conversely, increased floating region in the weave unit caused the decrease of yarn crimp. Generally, the bagging load of 3/1 twill weave was measured higher than other weaves having same settings, because it has long floating regions than plain and 2/1 twill weave and the crimp of the yarns were lower. In addition, the bursting load of the 3/1 twill weave was found lower than other weave types depending on the fabric geometry. At 18 cm^{-1} weft setting, the correlation coefficient between the crimp factors of different weave types and bagging loads were calculated being 0.92, 0.87, 0.83, and 0.83, for T1, T2, T3 and

T4 tests, respectively. Additionally, the correlation coefficients were also calculated high at 22 cm^{-1} and 26 cm^{-1} weft settings. The correlation coefficient between the crimp factor of different weave types and bagging loads were found significant at all settings.

In this study, the effects of test parameters were also discussed. The relationship between tests could be observed in figure 6. The differences between the bagging load of T1 and T2 and the differences between the bagging load of T3 and T4 were found significant at 95% confidence level, according to sphere diameter. The average increase rate of bagging load between T2 and T1 tests was calculated as 37%. The average increase rate between T4 and T3 was calculated as 33%. The bigger sphere caused the increase of bagging load because the contact area between the bigger sphere and fabric increased during the test.

The sphere was waited 3 minutes onto the fabric after reached determined bagging height at T3 and T4 tests. The bagging load onto the fabric was measured at 0, 15, 30, 60, 90, 120, 150 and 180 seconds during the test. It was observed that the bagging load decreased during this waiting period as seen in figure 7. The decrease ratio of the load is higher at the beginning and then it starts to slow down. The differences between the first bagging load (at 0th second) and last bagging load (at 180th second) were found significant at 95% confidence level, for each sphere. The fabric structure got used of new condition and reformed under the load during the waiting period.

Image analysis results

The mean cover factor (CF) values of un-deformed and deformed fabrics obtained from images were given in table 5. At the beginning of the study, the open space of fabric samples was expected to be increased and contrarily the CF was expected to be decreased after bagging deformation tests. However, this situation was not observed for all deformation tests. This may be the result of variation along the fabric structure. According to image analysis results,
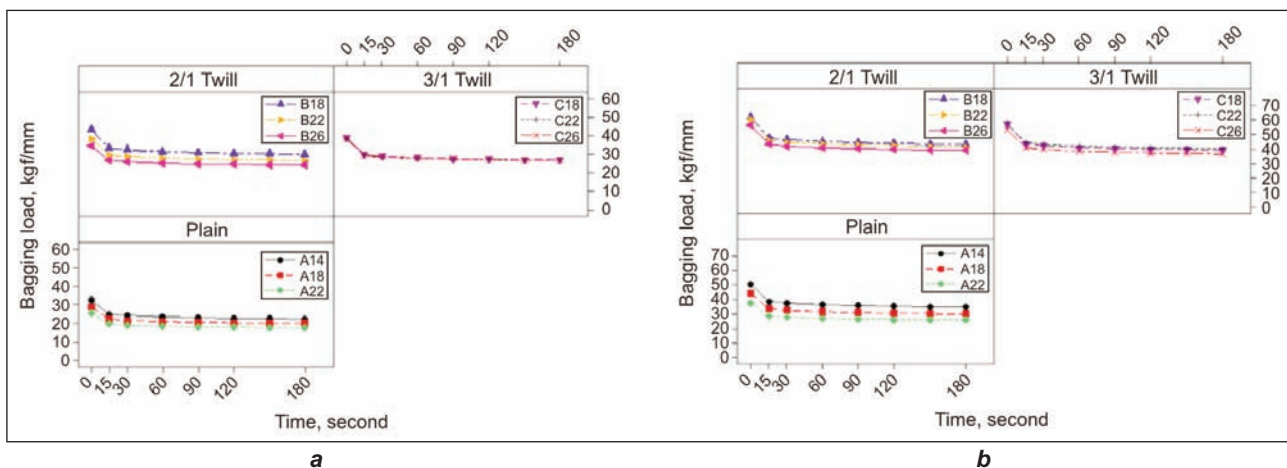
Fig. 7. The decrease of load during waiting time for each fabric
a – T3 test, *b* – T4 test

Table 5

	IMAGE COVER FACTOR (CF) BEFORE AND AFTER DEFORMATION TESTS				
Fabric Code	**CF Un-deformed (%)**	**CF-T1 (%)**	**CF-T2 (%)**	**CF-T3 (%)**	**CF-T4 (%)**
A14	80.79	77.38	82.20	75.99	82.03
A18	89.93	87.49	89.96	85.31	85.00
A22	90.23	88.45	90.87	89.87	89.29
B18	85.48	82.73	83.63	81.58	82.88
B22	89.46	87.36	89.94	87.78	86.52
B26	91.49	89.30	91.93	91.20	89.95
C18	84.52	84.92	82.95	79.94	81.93
C22	88.70	85.89	90.04	84.93	86.18
C26	91.41	88.44	93.88	90.60	88.69

the cover factor of all fabrics were decreased with T1 and T3 tests having 3 cm diameter of sphere, but the differences between non-deformed samples were not found significant for all fabric types. On the other hand, the CF of fabrics (except B18 and C18) increased and the difference between non-deformed samples was not found significant at 95% confidence level after T2 test having 5 cm diameter of sphere. The waiting time was generally caused the decrease of CF, this means waiting time caused the increase of open spaces and the deformation degree of fabrics. The change in the 3-D structure of deformed fabrics could not be observed clearly by image analysis system. It is known that the variation of yarn diameter and pore size along the fabrics affected the cover factor results of fabric samples and after deformation test these properties changed. The sphere applies load onto the fabric during the bagging test. This pressure causes the change at open spaces and also the flattening ratio of yarns. The compression of yarns could increase surface area of yarns, also the cover factor of fabric. But the differences of cover factor between un-deformed and deformed images were not found significant because of variation in fabric structure. Two dimensional (2-D) surface images of fabrics were investigated by this method. However bagging deformation of the fabric is a 3-D behaviour and the change in the fabric structure occurred in 3-D. Consequently, it was found that image analysis method is not sufficient alone to observe the bagging deformation degree. From the previous studies, air permeability test which is a 3-D performance property of fabric was found an effective method to analyse the bagging deformation degree.

CONCLUSION

In this study, bagging tests were applied to a group of systematically produced fabrics and the effects of structural properties of fabrics and test parameters to the bagging load were discussed. Besides, fabric porosities before and after bagging tests were determined by image analyses method in order to analyse the change (deformation degree) occurred in the fabric structure. Deformation degrees were investigated according to structural properties and test parameters. It was observed that fabrics having different settings and weave types showed different bagging loads. The differences between the bagging loads of fabrics having same settings and different weave types proved the influence of the fabric geometry. Bigger sphere diameter increased the bagging load as a result of increasing the contact area between the sphere and fabric. The bagging load of fabric decreased during the waiting period, however, the deformation degree. The bagging deformation behaviour of the fabric is related to 3-D properties of the structure. Therefore, the image analysis results which reflected 2-D properties of fabric were not an effective method to investigate the deformation degree of fabrics. In further studies, it was aimed to estimate the bagging load depending on the structural properties and deformation conditions.

BIBLIOGRAPHY

[1] Kawabata S., Niwa M., Kawai H. *The finite-deformation theory of plain-weave fabrics part I: The biaxial-deformation theory,* In: Journal of the Textile Institute, 1973, vol. 64, no.1, pp. 21–46

[2] Zhang X., Li Y., Yeung K.W. *Fabric bagging, part I: Subjective perception and psychophysical mechanism,* In: Textile Research Journal, 1999, vol. 69, no. 7, pp. 511–518

[3] Zhang X., Li Y., Yeung K.W. *Fabric bagging, part II: objective evaluation and physical mechanism*, In: Textile Research Journal, 1999, vol. 69, no. 9, pp. 598-606

[4] Kısılak D. *A new method of evaluating spherical fabric deformation*, In: Textile Research Journal, 1999, vol. 69, no. 12, pp. 908–913

[5] Sengoz N.G. *Bagging in Textiles*, In: Textile Progress, 2004, vol. 36, pp. 1–64

[6] Büyükbayraktar R.B. *The relationship between the bagging deformation and air permeability performance*, In: Industria Textila, 2014, vol. 65, no. 1, pp. 10–16

[7] Amirbayat J. *An improved analysis of bagging of textile fabrics. Part I: Theoretical*, In: International Journal of Clothing Science and Technology, 2006, vol. 18, no. 5, pp. 303–307

[8] Amirbayat J., Namiranian B. *An improved analysis of bagging of textile fabrics. Part II: Experimental work,* In: International Journal of Clothing Science and Technology, 2006, vol.18, no. 5, pp. 308-313

[9] Yeung K.W., Li Y., Zhang X., Yao M. *Evaluating and predicting fabric bagging with image processing*, In: Textile Research Journal, 2002, vol. 72, no. 8, pp. 693–700

[10] Abghari R., Najar S.S., Haghpanahi M., Latifi M. *Contributions of in-plane fabric tensile properties in woven fabric bagging behaviour using a new developed test method,* In: International J of Clothing Science and Technology, 2004, vol. 16, no. 5, pp. 419–433

[11] Sülar V. *A new testing instrument with artificial arm to simulated fabrics bagging by human elbow*, In: Industria Textila, 2011, vol. 62, no. 5, pp. 259–264

[12] Juodnukyte D., Daukantiene V., Gutauskas M. *Investigating the implications of static and dynamic loading in high-performance fabrics for outdoor clothing*, In: International Journal of Clothing Science and Technology, 2008, vol. 20, no. 1, pp. 7–14

[13] Zhang X., Li Y., Yeung K.W., Yao,M. *Mathematical simulation of fabric bagging*, In: Textile Research Journal, 2000, vol. 70, no. 1, pp. 18–28

[14] Zhang X., Li Y., Yeung K.W., Yao M. *Viscoelastic behavior of fibers during woven fabric bagging*, In: Textile Research Journal, 2000, vol. 70, no. 9, pp. 751–913

[15] Zhang X., Li Y., Yeung K.W., Yao M. *Relative contributions of elasticity and viscoelasticity of fibers and inter-fibre friction in bagging of woven wool fabrics,* In: Journal of the Textile Institute, vol. 91, no. 4, pp. 577–589

[16] Turan R.B., Okur A. *Investigation of pore parameters of woven fabrics by theoretical and image analysis methods*, In: Journal of the Textile Institute, 2012, vol. 103, no. 8, pp. 875–884.

[17] Çay A., Vassiliadis S., Rangoussi M., Tarakçıoğlu I. *On the use of image processing techniques for the estimation of the porosity of textile fabrics,* In: International Journal of Signal Processing, 2004, vol. 1, no. 1, pp. 51–54

Author:

R. BEFRU BÜYÜKBAYRAKTAR

Dokuz Eylul University
Faculty of Engineering, Department of Textile Engineering

Buca-35397
Izmir-TURKEY
e-mail: befru.buyukbayraktar@deu.edu.tr

Corresponding author:

R. BEFRU BÜYÜKBAYRAKTAR
befru.buyukbayraktar@deu.edu.tr

Designing a textile gripping device for tensile testing machine

RAŞIT ARSOY   İBRAHIM ÜÇGÜL

REZUMAT – ABSTRACT

Proiectarea unui dispozitiv textil de fixare pentru aparatul de testare a rezistenței la rupere

Rezistența textilelor laminate depinde de mulți factori. Aparatele de testare a rezistenței la rupere au ca scop evaluarea modului în care un material reacționează la alte tipuri de forte. Pentru acest studiu a fost proiectat și realizat un dispozitiv de fixare a epruvetelor, pentru testarea rezistenței materialelor laminate. Pentru a demonstra eficiența și precizia acestui dispozitiv, au fost efectuate teste comparative utilizând un dinamometru de testare a rezistenței la rupere "Lloyd LR5K Plus". Atât faza de proiectare, cât și rezultatele obținute sunt prezentate în lucrare. Rezultatele obținute au arătat că prin intermediul utilizării dispozitivului de fixare, a fost descoperită o structură mai simplă, cu tensiune distribuită uniform și care nu deteriorează materialul textil în punctele de fixare ferma, în timpul testării.

Cuvinte-cheie: dispozitiv de testare a rezistenței la rupere, țesături laminate, frecare

Designing a textile gripping device for tensile testing machine

The strength of bonded textile seams to depend upon many factors. Tensile test machines are employed to predict how a material will react under other types of forces. As part of this thesis a device has been designed and manufactured, a gripping device for testing the strength of the bonded materials. To prove the efficiency and accuracy of the device, comparative tests employing the "Lloyd LR5K Plus" tensile test machine were conducted and both the design phase and the results obtained are presented in this paper. The results obtained showed that through the use of the gripping device, a more simple structure, with evenly distributed stress and which does not damage the textile material at the firmly gripped points during testing, has been discovered.

Keywords: tensile device, adhesives, laminated fabrics, friction

INTRODUCTION

One of the important works in garment production is the bonding processes. The external appearance and the surface quality of the manufactured products, such as garments and textile materials are important. The adhesion of the bonded materials can be measured, but cannot be measured in absolute terms. For this purpose, the tests applied cannot fully explain the physical strength in adhesion, but these tests may indicate relative adhesion performance, which has been described [1]. In some methods, the gravitational force between the surfaces can be measured, but the physical strength of the bonds of adhesion are not fully explained [2].

Adherence to the surface of textile materials is an issue that is quite complex and difficult to understand. Due to the ease of operation and economic demands the cross-cut test is performed in some industrial areas [3, 4]. The strength of the textile bonded seam depends upon a large number of factors (material, structure, bonding parameters and methods etc.) which makes impossible the implementation of this test in the course of garment manufacturing [5]. With the principles of known technology as TS EN 24624 (Paints and varnishes-tensile test, 1996) and ASTM D 4541 (Standard test method for pull-off strength of coatings using portable adhesion testers) different devices are used in accordance with these standards [6, 7]. During testing with these devices the stresses are unevenly distributed and there is damage to both ends of the samples at the firmly gripped points.

Both theoretical and experimental research of the produced grip structure to measure the adhesion strength of the bonded seam in the study was discussed to resolve these afore mentioned deficiencies.

EXPERIMENTAL WORK

Materials and method

Tensile testing device for textile bonded seams

In order to eliminate the shortcomings of the existing tensile testing machines the tensile testing device for textile bonded seams was designed and manufactured as an easy to operate tensile device.

The designed tester has an electro-mechanical structure. The gripping device is driven by a speed controlled electric motor or manually. In the project planning and device designing CAD software were employed. The production and test issues of the construction at the design stage have been corrected.

The device techniques assembly drawn is given in figure 1.

Its technical indicators: tensile strength – 400 N, change the location of the moving grip – 200 mm, dimensions 132 × 300 × 1000 mm, weight – 20 kg, precision – ± 2%.

The tensile device's grip is one of the important parts. The desired properties of the grips at the beginning of
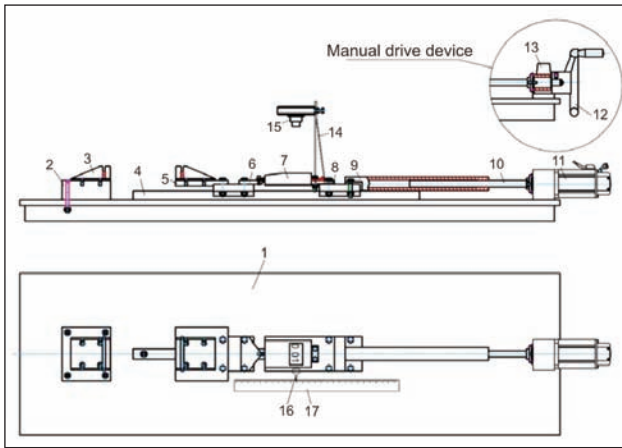
Fig. 1. Technical drawing of tensile tester of textile bonded seams: *1* – body; *2* – fixed holding device; *3* – fixed grip; *4* – linear ball bearings; *5* – mobile grip; *6* – connecting member; *7* – electronic weighing; *8* – weighing coupling element; *9* and *10* – special screw-nut connection; *11* – speed controlled electric motor; *12* – wheel; *13* – bed; *14* – the support; *15* – camera; *16* – pointer; *17* – ruler

Fig. 2. General view of the tensile testing device

the process are maintaining the stability, independence of tensile strength, material non-destruction and simplicity of use.

During the experiment, non-uniform pressure across the width of the sample at the standard grips was observed. In the delamination experiments the evenly distribute stresses, composed in the fabrics adhesive bond, which influence the test results cannot be ignored. The structure analysis of the grips construction revealed that the main reasons for evenly distributed stresses were the following:

– The value of the pressing force applied to the grips must be much above the performed pulling force supposed to break the fabric. This will cause deformation and a reduction of the strength of the samples that are in contact with the grip section;

– To provide a simple and efficient method to clamp test samples, most grips are fitted with serrated ground or diamond cut and wave action. In these cases the sample cannot tighten across the width of the sample and this causes the separation of

the fibres during the tensile process in the inner part of the grips.

– During the placement of a sample on the grips the tension cannot properly distributed, as the result values are smaller than the actual tensile strength.

To eliminate such problems, theoretical and construction research helped in the course of designing an extremely simple and handy self-holding fabric grip. The technological scheme of the grip is given in figure 3, *a*. Fixed (1) and movable (2) clamping devices, grips comprising two rollers (3 and 4) made of steel placed on the slide-way. The fabric (5) passed through the rollers is shown in figure 3, *b*.

The principle of the grip is as follows: when rightward movement is transmitted to the moving grip (2), the free end of the fabric under the effect of frictional force causes the compression of the upper rollers (3) onto the lower roller (4) and consequently compacts itself. Increasing the fabric tensile force evenly affecting and increasing the compression force and ensures reliable fastening of the fabric.

To minimize the friction and to prevent errors in the calculations of the movable grip it is installed on a special linear bearing.

Investigation of the grip mechanism

The samples to be tested are compressed by placing one end on a fixed grip and the other attached to the movable grip. From the following equation the minimum value of the compression force can be found [8]:
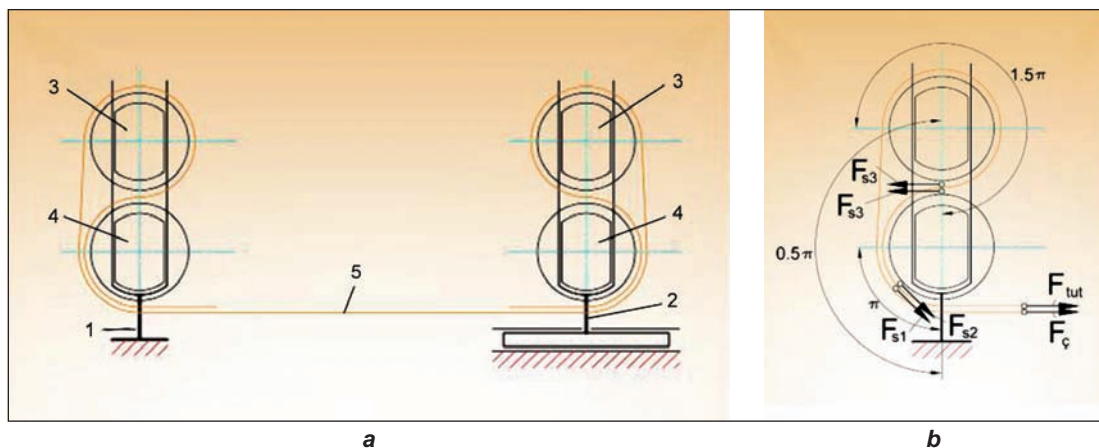
Fig. 3. *a* – the grips technological scheme; *b* – the fabric's path through the rollers

$$F_{min.comp.} > F_{ten.str.} / \mu \qquad (1)$$

In equation: $F_{min.comp.}$ is the minimum value of the compressive force; $F_{ten.str.}$ – the tensile strength of the sample; μ – the friction coefficient between the sample and the gripping element.

From the influence of tensile force ($F_{ten.}$) to keep intact the gripping of the fabric in the desired conditions is possible if (figure 3, b):

$$F_{grip} < F_{s1} + F_{s2} + 2F_{s3} \qquad (2)$$

In the equation: F_{grip} is a force occurring between the fabric and the roller surface as a result of the presence of the tensile $F_{ten.}$ force and affecting the free end of the fabric. When this force is applied to the free end of the fabric, the system comes into equilibrium and the influence of the tensile $F_{ten.}$ force is the reset movement of the fabric; F_{s1}, F_{s2} and F_{s3} – the friction force occurring through the normal forces in the contact areas of the rollers and fabrics overlapped one above another from the influence of the compression force.

F_{grip} force found from figure 4 considering the Euler equation [8]:

$$F_{grip} = F_{ten.} / e^{[f_1(\alpha_2+\alpha_3)+f_2\alpha_1]} =$$

$$= F_{ten.} / e^{(0.2*2.5\pi + 0.3*\pi/2)} = 0.13\,F_{\varsigma} \qquad (3)$$

In the equation: f_1 is the coefficient of the friction between the fabric and roller. Between the fabric and the steel $f_{1min} = 0.2$ [9]; f_2 – the coefficient of the friction occurring between the fabric and fabric. Between the fabric and fabric $f_{2min} = 0.3$ [9]; α_1, α_2, α_3 – the grip angles.

From figure 3, b:

$$\alpha_1 + \alpha_2 + \alpha_3 = \pi/2 + \pi + \pi/2 + \pi = 3\pi$$

The additional friction force occurring between the fabrics from the influence of the upper fabric forces that covers the lower roller F_{s1} under $\pi/2$ angle.

$$F_{s1} = f_2 = \sqrt{F_{ten.}^2 + (F_{ten.} / e^{f_2\pi/2})^2} =$$

$$= 0.3\sqrt{F_{ten.}^2 + (F_{ten.} / e^{0.3\pi/2})^2} = 0.354\,F_{ten.} \qquad (4)$$

The additional friction force occurring between the fabric and the roller from the influence of the upper fabric forces that covers the lower roller F_{s2} under $\pi/2$ angle.

$$F_{s2} = f_1 = \sqrt{F_{ten.}^2 + (F_{ten.} / e^{f_2\pi/2})^2} = 0.236\,F_{ten.} \qquad (5)$$

The additional friction force occurring by $F_{ten.}/e^{f_2\pi/2}$ force compression of the rollers one-to one in the F_{s3} area

$$F_{s3} = f_1 F_{ten.} / e^{f_2\pi/2} = 0,125\,F_{ten.} \qquad (6)$$

from the equation (2) – (6)

$$F_{grip} = 0.13\,F_{ten.} << F_{s1} + F_{s2} + 2F_{s3} = 0.715\,F_{ten.}$$

The total friction forces for holding the free end of the fabric is 5.5 times more than is the necessary minimum force and it causes the sturdy gripping of the fabric.

The grips design and construction has been produced based upon the obtained theoretical results. Technical drawing of the grips assembly is shown in figure 4, the general view is given in figure 5.

The holder consists of the body (2) and of two cylindrical clamping (1) elements. The holder is connected to the body and movable skid which is fixed with four bolts.

In order to demonstrate the principle of operation, materials with a low coefficient of friction other than the fabrics were tested. In these experiments, steel foil samples were prepared and placed in the grips to tensile in dry and oily circumstances. Results showed the grip had kept intact the steel foil.

EXPERIMENTAL

With the aim of establishing the operability and technical parameters, the device was subjected to comparative test trials. For comparison, the LR5K Plus tensile testing machine which is commonly employed in textile laboratories, was utilised.

During the tests, 20 mm width samples prepared from plain weave cotton fabric were employed. The number of test samples subjected to bonding 5 pieces, were made for each material according to the standards. To better reflect the reality of these results the number of times the tests were conducted was 10.

Tensile tests

The samples were placed in the designed tester device and the resulting diagrams were obtained as shown in figure 6, a and in figure 6, b for

Fig. 5. The overall appearance of the image of the holder assembly
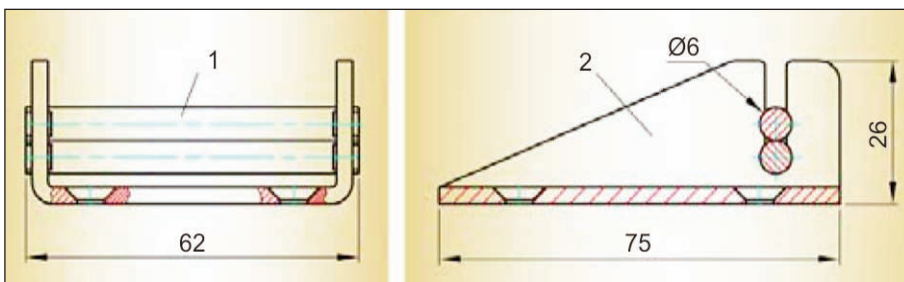
Fig. 4. Scheme of the grip assembly
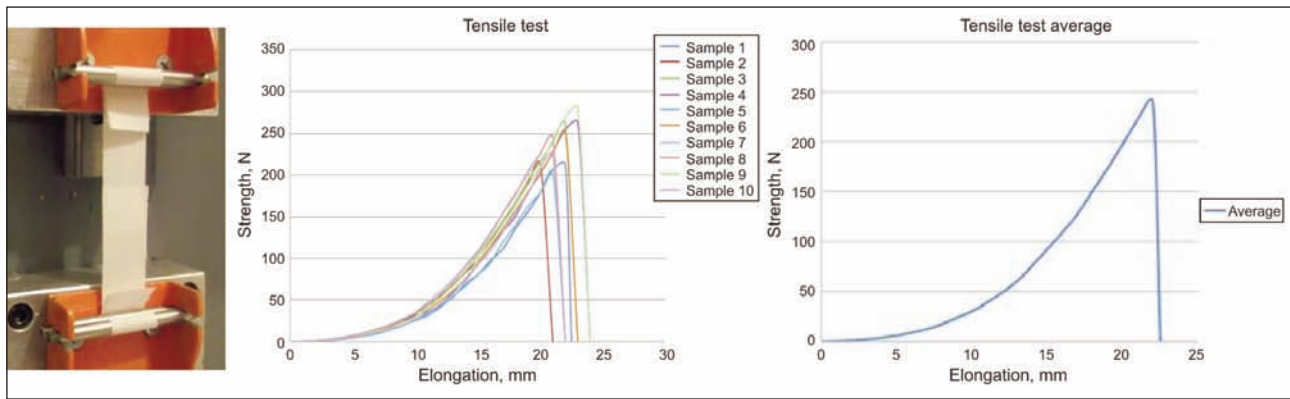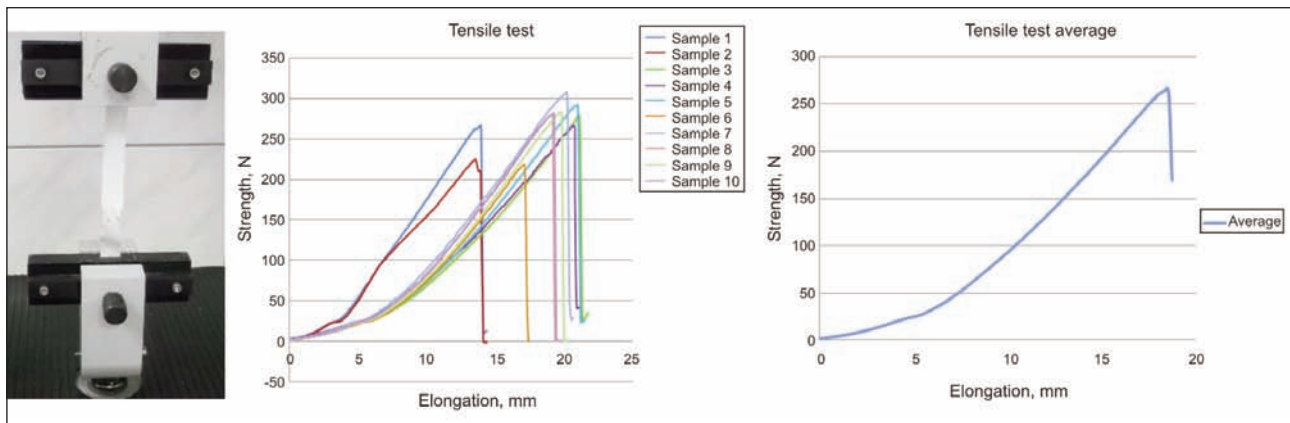
Fig. 6. *a* – Tensile tests on the designed device; *b* – Tensile test on the LR5K Plus tester

the LR5K Plus tester. The test results were drawn as diagrams in NEXYGEN Plus Data Analysis Software and MS Excel 2007. The vertical axis given in the diagrams are the force values (N), while the horizontal axis shows the distance values (mm).

Visual analysis of these diagrams shows that the average values are almost the same. The LR5K Plus tester test values indicate greater distribution than the designed device. So the difference between the maximum and minimum tensile values (218/309) is 91N, the difference between the maximum and minimum elongation at break (13.5/21.1) is 7.6 mm. In the designed device, difference between the maximum and minimum tensile values (205/282) is 77N, the difference between the maximum and minimum elongation at break (20/23) is 3mm. The analysis performed indicates that the clamping unit causes this distribution.

Small deviations from the average value are derived from the different length of the binding.

Delamination tests

Samples were placed in the designed tester device and the resulting diagrams were obtained as shown in figure 7, a and in figure 7, b for the LR5K Plus tester. The delamination average value curves of the test are recorded in figure 7, c.

The test results were drawn as diagrams in NEXY-GEN Plus Data Analysis Software and MS Excel 2007. The vertical axis given in the diagrams records the force values (N), while the horizontal axis records the distance values (mm).

Analysis of these diagrams shows the average values are almost the same. Small deviations from the average value are derived from the different lengths of the binding.

The evaluation of these tests shows that the designed device can be used instead of the LR5K Plus tester for both tensile and delamination stresses.

RESULTS AND CONCLUSIONS

In this work, a simple and non-destructive tensile testing device was designed and manufactured to measure the adhesive strength of bonded fabrics. The efficiency and the accuracy of the device was verified with comparison of the data by the data produced by a universal tensile testing machine LR5K+ (Lloyd, UK) in Suleyman Demirel University, Faculty of Engineering, Department of Mechanical Engineering.

The equipment grips are important part of a tensile testing equipment. The analysis in this work has shown obvious drawbacks of the conventional gripping devices used for determination of fabric mechanical properties. These drawbacks are because of the force applied to the grip the fabric must be more than pulling force applied to break the fabric; the grips surfaces with patterns of fitted with serrated ground or diamond cut and wave action to clamp test samples;
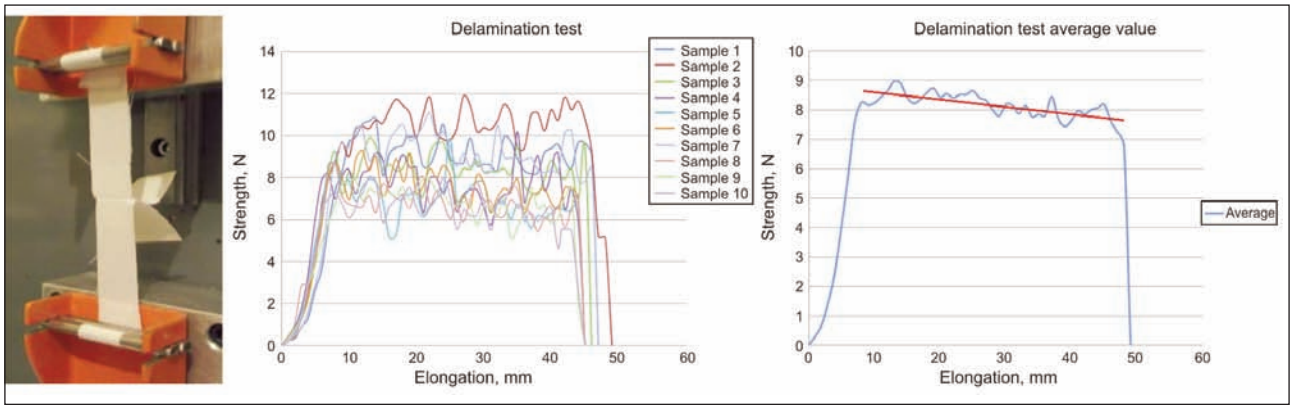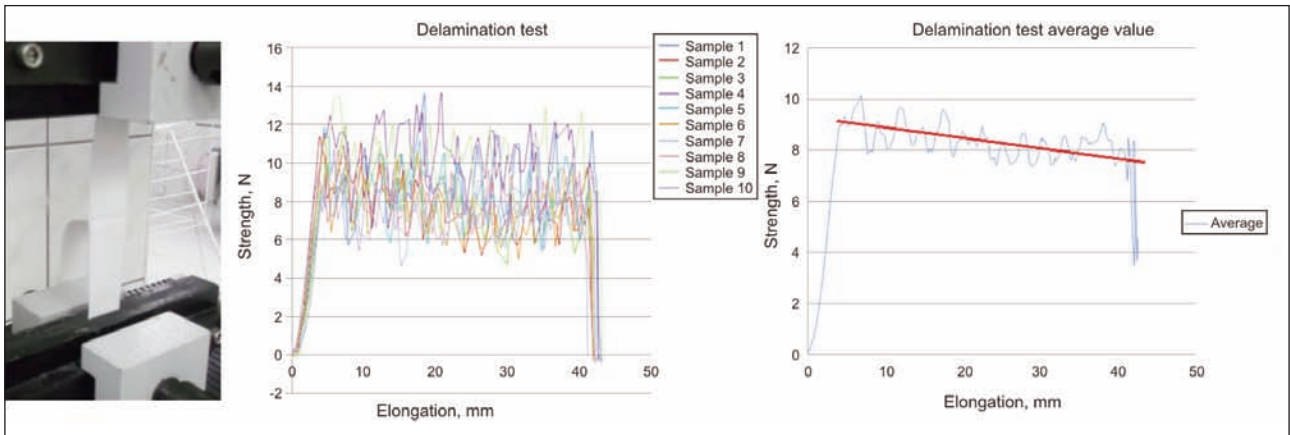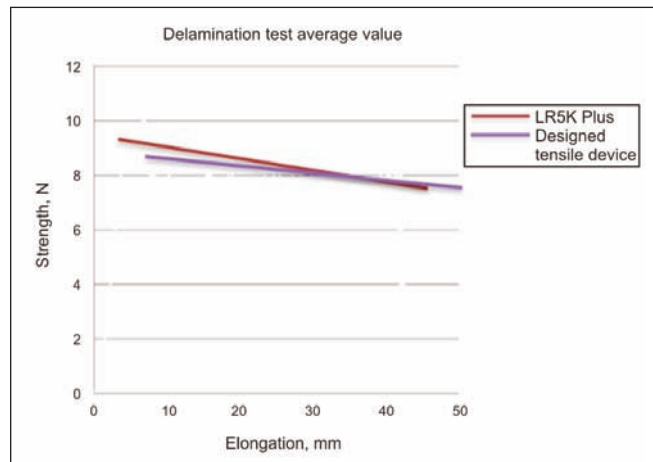
Fig. 7. *a* – Delamination tests on the designed device; *b* – Delamination test on the LR5K Plus tester;
c – The average value curves of the delamination test

the tension which cannot be properly distributed because of the placement of test sample on the grips. All the above factors cause deformation and a reduction of the strength of the samples that are in contact with the grip section, the separation of the fibers during the tensile process in the inner part of the grips and as result affect the actual tensile strength.

We designed a gripping device to eliminate the described disadvantages. This gripping device had properties such as simple and convenient production and functionality of use by self-clamping ability. Unlike all known devices it is non-destructive for the fabric structure and it allows clamping any type of fabric.

The efficiency of the gripping device was evaluated by comparison of conventional gripping devices. The study of mechanical factors showed that fabric having lowest coefficient of friction had 5.5 times gripping strength than fabric strength. In addition to fabric tests, steel foil samples with a low coefficient of friction were prepared and placed in the grips under dry and oily circumstances. Results showed the grip was remained intact with the steel foil for both circumstances.

The gripping device can be easily mounted on all types of tensile test machines. This gripping device has potential to be improved by modifications in geometry. Addition of an automation process to this testing grip can let researchers to benefit from automated withdrawal and optimized testing speeds.

This application of these grips to current tensile equipment will decrease the costs of testing equipment in the textile industry, students and researchers will benefit from this work by studying the gripping systems and improving their knowledge in about new techniques and results.

BIBLIOGRAPHY

[1] Nelson, G. L. Adhesion, *Paint and coating testing manual*. Chapter 44, ASTM Special Technical Publication, 513-523, Philadelphia, P.A.,1995.

[2] Mittal, K. L. *Commentary, Adhesion measurement of films and coatings*. VSP, 1-13, Utrecht, The Netherlands, 1995.

[3] ASTM D 3359. *Standard test methods for measuring adhesion by tape test*. American Society for Testing and Materials, 1997.

[4] TS.6884. *Ahşap mobilya yüzeyleri-vernik veya boya katmanlarının yapışma mukavemetinin tayini*, T.S.E., Ankara, 1989.

[5] Koç, E., Yürek, O.D. *Predicting the tensile strength of polyester/viscose blended open-end rotor spun yarns using the artificial neural network* and statistical models. Industria Textila, vol. 62, nr. 2, 2011.

[6] TS EN 24624. *Boya ve Vernikler-Çekme Deneyi*. TSE, Ankara, 1996.

[7] ASTM D 4541. *Standard test method for pull-off strength of coatings using portable adhesion testers*. American Society for Testing and Materials, 1995.

[8] Artobolevski, I. I. *Theory of machines and mechanisms*. 4th edition, revised and enlarged. Moscow: Nauka, 1988. 640 p.

[9] Kragelskiy, I.V., Vinogradova I.E. *Friction coefficients*. Reference Guide, M.: Mashgiz, 1962. 220 p.

Authors:

RAŞIT ARSOY[1]
IBRAHIM ÜÇGÜL[2]

Suleyman Demirel University
[1, 2]Faculty of Engineering, Department of Textile Engineering

Çünür-32260
Isparta-TURKEY
e-mail: d0940124006@stud.sdu.edu.tr, ibrahimucgul@sdu.edu.tr

Corresponding author:

RAŞIT ARSOY
d0940124006@stud.sdu.edu.tr
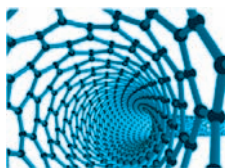
Research on biodegradable wool on sheepskin processing and eco-labeling

CARMEN GAIDAU
MIHAELA NICULESCU
A. GEORGIANA VESA
CLARA RADULESCU

STEFANA JURCOANE
PETRUTA CORNEA
FLORENTINA ISRAEL-ROMING
L. FLORENTINA PASCU

REZUMAT – ABSTRACT

Cercetări privind realizarea şi eco-etichetarea articolelor din blană ovine biodegradabile

Biodegradabilitatea articolelor de piele naturala reprezintă o caracteristică a produselor cu valoare adăugată ridicată care respecta mediul şi după încheierea ciclului de viață. Evaluarea biodegradabilitatii articolelor de piele şi blană este în fază de cercetare, metodele practicate durează cel puţin 45 de zile şi se bazează pe evaluarea dezintegrării în contact cu compostul, în mediul natural. Necesitatea dezvoltării unei metode rapide de evaluare a biodegradabilitatii articolelor de piele şi blană rezidă din marea varietate de sortimente care trebuie analizate individual. În acest sens, dezoltarea unor preparate enzimatice specifice reprezintă un pas inovativ în direcţia analizării biodegradabilitatii articolelor de îmbrăcăminte din blană naturală. Prelucrarea blănurilor de ovine pentru realizarea unui material biodegradabil reprezintă o opţiune intermediară pentru realizarea unui material durabil prin tăbăcire şi în acelaşi timp uşor degradabil după ieşirea din uz, în condiţii de mediu natural sau simulate. Lucrarea prezintă metoda propusă pentru analiza biodegradabilităţii blănurilor naturale, tehnologia de prelucrare şi prototipul de articol de îmbrăcăminte din blană naturală realizat în condiţii industriale. Propunerea unei etichete ecologice privind biodegradabilitatea articolului de blană realizat reprezintă un demers în promovarea produselor naturale, cu valoare adăugată.

Cuvinte-cheie: biodegradabilitate, blană ovină, enzime specifice, îmbrăcăminte biodegradabilă.

Research on biodegradable wool on sheepskin processing and eco-labeling

Biodegradability of natural fur items is a characteristic of high value-added products in compliance with the environment after the end of its life cycle. Biodegradability evaluation of leather and fur items is still in the research phase, the practiced methods last for at least 45 days and are based on assessing disintegration in contact with the compost in a natural environment. The necessity of developing a quick method of analyzing biodegradability of leather and fur items comes out of the wide variety of assortments to be evaluated individually. In this regard, developing specific enzymatic preparations is an innovative step in the direction of analyzing biodegradability of clothing items made of natural fur. Sheepskin processing to create a biodegradable material is an intermediary option for developing a sustainable material by tanning and at the same time, easily biodegradable after decommissioning in natural or simulated environmental conditions. The paper presents the proposed method for biodegradability analyzing of natural furs, the technology for developing biodegradable furs and the prototype natural fur item under industrial conditions. Proposing an eco-label for biodegradability of the developed fur item is an approach aiming to promote high value-added natural products.

Keywords: biodegradability, wool on sheepskins, specific enzymes, biodegradable garments

INTRODUCTION

Leather biodegradability

Assessing biodegradability of natural fur products is a first step in the direction of proposing, in the future, a scheme for voluntary eco-labeling of natural fur products with advanced biodegradability, based on the producers' and other interested parties' affidavit, taking into account the possibility of exploiting the protein component of products, at the end of their life cycle. Within this scheme, the main segment is elaborating a method of accelerated biodegradation and biodegradability assessment.

According to scientific research the average time required for degradation of woolen cloth waste (keratin) is approximately 1 year and shoe leather (collagen) degrades over 40–50 years.

The recent discussions regarding the need for supporting through EU legislation the labeling of natural leather authenticity of leather goods, garment and upholstery represent another tool for consumer education and protection. The development of a method for biodegradability assessment of natural leathers and fur skins represents an important instrument for leather goods labeling and consumer perception improving in connection to sustainable environmental protection as compared to synthetic materials with less durability and non-biodegradability.

The definition of polymers biodegradability and assessment was delimited from the other meanings as a process which best simulates the disposal pathway, keeps the accumulation under control, generates as end products CO_2, water, minerals, intermediate biomass which includes hemic materials and

the polymers biodegradation safety or the use of end products must be friendly [1].

Even though there are enough standards for polymer biodegradability testing many works need to be done to understand the mechanism of biodegradation. The lack of methods for the survey of intermediate materials generated by biodegradation is the most important blocked progress in biodegradability assessment. The biodegradability assessment of wet-white, vegetable or chromium tanned leathers by composting for 150 days of leathers tanned with different organic phosphates, vegetable tannin and chromium salts showed a rate of degradation between 6% and 80% depending on crosslinking strength [2]. The influence of leather manufacturing technology and consequently of the leather composition on biodegradability is stressed in different studies and attest the need for every kind of leather evaluation. The first tannery who claims to be the most ecological and certified for the first time a biodegradable product is Dutch Hulshof with Piuro product, a fully organic product able to be decomposed under natural composting conditions in 28 days. Literature data presents various methods of biodegradation of tanned leather, which do not exceed values of 68–84% for chromium salt-free leather and of 20–23% for leather tanned with chromium salts [3, 4]. More recently, standard EN ISO 7827:2013 estimates that a material is quickly biodegradable if a 60% release of the theoretical amount of O_2 (ThOD) occurs in 10 of the 28 days of incubation.

The efforts to adapt the methods for plastics biodegradability assessment to leathers were already reported and consist in measurement of CO_2 released by biomass biodegradation [3, 5, 6]. Even under these conditions the test is time-consuming and needs a step forward in microorganism selection and rapid assessment of biodegradability of leathers. The first step in biodegradability assessment is the evaluation of structural changes of materials under the composting conditions and understanding the mechanism of biodegradation initiation.

Wool on sheepskins are complex materials composed of keratin and collagen, two proteins with different reactivity, and literature does not report any study regarding the biodegradability of sheepskins. Even the processing of wool on sheepskin must comply with fashion trends and chemical materials are very complex (from syntans to finishing binders), the main components are collagen and keratin, biodegradable materials. In comparison to synthetic leathers and fur skins, wrongly called "ecological", natural wool on sheepskin are more durable and less pollutant materials.

Eco-labeling fur items

Eco-labels are complementary tools, associated to the traditional environmental policy and to other basic marketing tools, by means of which the consumer is educated regarding environmental protection and the option of ecologic products or products having a low environmental impact.

The result of a long international experience, appropriate eco-labeling, associated with procedure verification and certification, leads to an increase in requests for recyclable products or for products based on sustainable development principles.

According to Romanian legislation (Government Decision no. 189/2002), eco-label is defined as "a graphic symbol or a short textual description of the product applied to the product or found in a brochure or in an informative document accompanying the product, and offers information on no more than three environmental impacts generated by that product". Eco-label is awarded on demand to groups of products that meet the following conditions: high potential for environmental protection that determine the choice made by the buyer; competitive advantages for consumer goods manufacturers and/or service providers or there is a high demand or a final use certified by the sales volume.

Most eco-labels are based on life cycle assessment (LCA) of a product, feature by means of which the consumer is informed about the impact the product has on the environment, in various stages of its production and use. Equally important is the information on the induced impact at the end of the product's life cycle, when it is categorized as waste (figure 1).

Fig. 1. The life cycle of natural furs from raw material to end of use

The eco-labeling scheme grants an eco-label to products considered less harmful for the environment than others in the same group of products. Eco-labeling is a voluntary method of certifying environmental performance, practiced worldwide.

According to the classification proposed by the International Standardization Organization (ISO), there are three types of eco-labeling schemes:

- Type I: voluntary schemes, based on multiple criteria, taking into account the products' life cycle. They require certification by a third party.
- Type II: voluntary schemes, based on an affidavit of manufacturers and other interested parties.
- Type III: voluntary schemes presenting quantified information on the product, based on independent verification and using real indexes.

There is no eco-labeling scheme regarding biodegradation of leather products; there are, however, eco-labeling schemes regarding harmlessness of products for consumers. These products are found in the info sheet which provides general information on the eco-label for textiles based on GD no. 177/2004 establishing eco-label granting criteria for the group

of textile products, which transposes the European eco-label for textiles at national level, as a result of the Commission's Decision no. 371/2002/EC establishing European eco-label granting criteria for textile products [7].

Eco-label granting criteria provided for textile products aim at reducing water pollution associated with the production process and promotion of textile products with low environmental impact, absolutely applicable to leather products and, therefore, fur products. The specific ecological criteria are common and refer to: limiting toxic waste; reducing air pollution; reducing water pollution during production and limiting the use of chemicals in the manufacturing process.

Although data on natural fur biodegradation tests were not identified in the literature, it is known that many types of fur are processed without chromium salts (mink, chinchilla fine fur etc.) to ensure a low specific weight. The possibility that these types be completely biodegradable is much higher compared to the kinds of furs and leathers tanned with chromium salts.

This paper presents a biodegradability assessment scheme for fur items, in which an essential step is the proposed method for assessing biodegradability of natural furs. Verification of the biodegradability labeling scheme proposed was performed in industrial conditions through development and implementation of technologies for biodegradable furs and items and verification of their biodegradability. Proposal for an eco-label on biodegradability of fur items is an approach to promoting natural value-added products.

EXPERIMENTAL PART

Elaborating the technical flowchart for eco-labeling fur items

To access future procedures that lead to eco-labeling of fur items, the present study initiated a technical flowchart (figure 2) for fur biodegradability assessment, based on a method of accelerated biodegradation associated with the exploitation of useful components at the end of life cycle of natural furs.

We specify that the limit of 70% biodegradability for biodegradable fur items is consistent with the literature and the recently developed standards for biodegradability testing of organic chemical materials (ISO 7827:2010) and with pure collagen biodegradability tests which have led to a biodegradation level of 70%. Since fur is composed of collagen and keratin (a more hydrophobic and chemically more inert protein), the imposed limit is comparable to that for natural leather, suggesting the possibility of applying the method in this case as well, which leads to an extension of the application.

Developing biodegradable furs

In order to develop prototypes of biodegradable clothing, sheepskins were processed using a tanning and retanning technology without chromium salts, according to the technological flowchart shown in figure 3, compared with traditional technology.
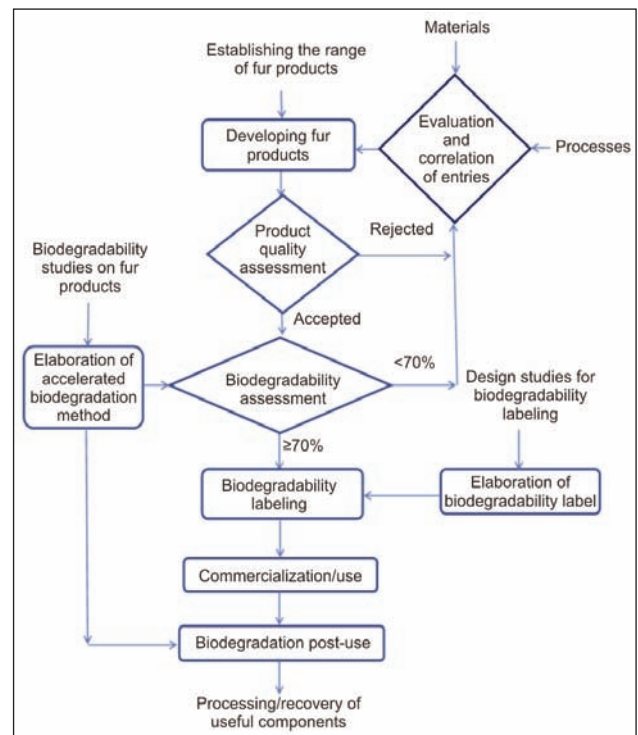
Fig. 2. Flowchart for biodegradability assessment of natural furs for eco-labeling
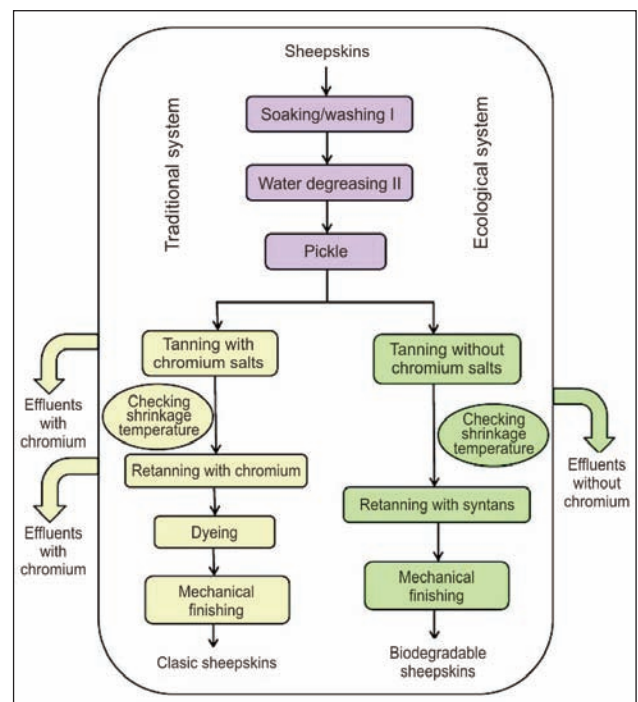
Fig. 3. Technological flow chart for biodegradable fur development

Elaborating the method of accelerated biodegradation

In this study, a method of accelerated biodegradation of furs was developed using an enzymatic preparation obtained by selection, isolation, identification and cultivation in a specific environment of two strains with collagenase and keratolytic activity [8, 9].

The two selected strains were from the BIOTEHGEN collection (*Bacillus licheniformis* ATCC 14580) marked

BN1 and another from a natural environment, identified using *BIOLOG – Microbial Identification system* as *Bacillus amyloliquefaciens,* marked BN7, with collagenase and keratinase activity. Bacterial strains (Bl and BN7) were cultivated in minimal medium, where the source of carbon and nitrogen was represented only by natural fur samples, at 30–32°C in stirring conditions (140 rpm). The composition of the culture medium (g/L) was: NaCl 1 g; $CaCl_2$ 0.05 g; KH_2PO_4 0.7 g; sucrose 3 g; $MgSO_4$ 0.9 g; K_2HPO_4 2.38 g. A pre-inoculum on feathers was used. Enzymatic preparations were stabilized by lyophilization and were conditioned on clay substrate. Collagenase and keratinase activity was examined after lyophilization and after immobilization on clay substrate.

Biodegradability of natural fur was assessed by incubating fur samples in the presence of specific bacterial preparations for the fur substrate in the spirometer (figure 4) and by daily recording the biochemical oxygen demand for 20 days.

Testing medium:

Incubation is performed in the dark or diffuse light, in brown dishes, at a constant temperature of 35°C ± 2°C, with magnetic stirring.

Materials:
- Lyophilized enzymatic preparation immobilized on clay substrate, with collagenase activity of 23 U/g and keratinase activity of 3.06 U/g.
- Natural fur with humidity determined according to SR EN ISO 4686-2006.
- Sterilized distilled water.

Work method:
- In the sterilized recipients of the WTW – OxiTop device (figure 4) 0.6 g natural fur is added, over which 2 g immobilized lyophilized enzymatic preparation is poured, dissolved in distilled water and filled up to 1000 mL distilled water, sterilized and heated at temperature of 30°C.

Fig. 4. WTW – OxiTop to assess biodegradability of natural furs

- Minimum 2 test samples and minimum 2 control samples identical to the test samples, without enzymatic preparation, are prepared and introduced in the WTW – OxiTop device equipped with stirrer and placed in an incubator at the temperature of 35°C ± 2°C.

- Biochemical oxygen demand (BOD) is automatically measured in the 0–700 mg/L range starting from moment 0 and every day for 4 days. Measurement continues up to 20 days for validation of results.
- The biodegradability degree is calculated as follows:

$$B\% = (x\ mgO_2/L : 360\ mgO_2/L) \times 100$$

where:

x is the amount of O_2/L released as a result of fur sample biodegradation;

360 is the theoretical amount of O_2 required for total decomposition of 0.6 g natural fur with 11% humidity in CO_2 (ThOD).

RESULTS AND DISCUSSIONS

Biodegradable furs

Furs made in this research study, following the technological flowchart of making biodegradable fur, have physical and mechanical properties according to the designed model, falling into the limit values required for manufacturing (table 1).

Biodegradability assessment

Specific enzymatic preparations for biodegradation of natural furs

Analyses of collagenase and keratinase activity of enzymatic preparations grown on specific medium after lyophilization (figure 5) and after immobilization on clay substrate (figure 6) are presented in table 2 and show a good enzymatic activity.
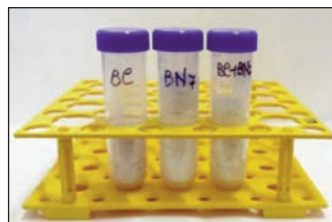
Fig. 5. Lyophilized enzymatic preparations
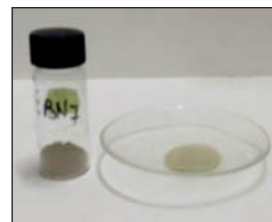
Fig. 6. Lyophilized and immobilized enzymatic preparation

Testing biodegradability of natural furs

We tested the biodegradability properties of the fur prototype made with standardized enzymatic preparation with collagenase and keratinase activity obtained by combining the two bacterial strains (Bl and BN7). The substrate on which the preparation was deposited consisted of a prototype fur and a synthetic fur (PE/PA). The test validation was done with the fur prototype that was kept in medium without inoculum. Initial verification of substrates' biodegradability was achieved by quantitative analysis of amino acids released at different time intervals. Figure 7 shows the biodegradation of prototype fur after 4 days of incubation, more evident after 8–15 days of incubation compared with synthetic fur and fur without inoculum.

The upward trend in the amount of amino acids released within 15 days shows the evolution of biodegradation processes.

Table 1

PHYSICAL-MECHANICAL AND CHEMICAL CHARACTERISTICS OF THE BIODEGRADABLE FUR PROTOTYPE			
No.	Characteristics, UM	Values	Test method standard
1	Appearance	According to the sample	SR EN ISO 4686 - 2006
2	Color	According to the sample	SR EN ISO 4048 - 2008
3	Volatile matter, % – dermis – wool	 max. 15 max. 12	SR EN ISO 4047 - 2002
4	Extractible substances, % – dermis – wool	 max. 15 max. 2	SR EN ISO 4098 - 2006
5	Total ash, %	max. 5	SR EN ISO 4045 - 2008
6	pH of aqueous extract, pH units	min. 3.5	SR EN ISO 3376 - 2012
7	Shrinkage temperature, °C	min. 60	SR EN ISO 3377 - 2012
8	Tensile strength and percent elongation – elongation at 30 N load, % – tensile elongation at break, % – grain cracking tensile load, N – tensile load, N – tear tensile load of the dermis, N – tear tensile load of the stitch, N	longitudinal / transverse max. 18 / max. 26 max. 125 / max. 135 min. 40 / min.30 min. 100 / min. 70 min.15 min.20	SR 5045 - 2008

Table 2

ENZYMATIC ACTIVITY (EA) OF LYOPHILIZED AND IMMOBILIZED PREPARATIONS				
	EA LYOPHILIZED ENZYMATIC PREPARATIONS, (U/g)		EA LYOPHILIZED AND IMMOBILIZED PREPARATIONS, (U/g)	
Sample	Collagenase	Keratinase	Collagenase	Keratinase
BI	25.45	5.38	15.42	3.06
BN7	27.29	4.25	23.00	2.14
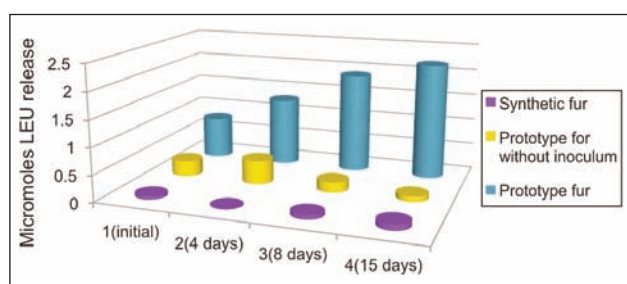
Fig. 7. Amount of amino acids released from the prototype biodegradable fur sample compared to synthetic fur and prototype fur without inoculum

Fig. 8. BOD for synthetic fur without inoculum, Ms
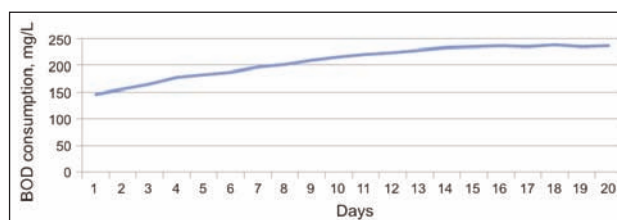
Fig. 9. BOD for sheepskin prototype without inoculum, Mvalu

Biodegradability was quantified by recording biochemical oxygen demand (table 3 and figures 8–11) for: synthetic fur control sample, incubated without enzymatic preparation (marked Ms); biodegradable fur prototype control sample, incubated without enzymatic preparation (marked Mvalu); synthetic fur incubated with enzymatic preparation (marked Ps) and the biodegradable fur prototype incubated with enzymatic preparation (marked Pvalu).

Calculation of biodegradability for the created prototype furs indicates 92% biodegradability, which represents a total biodegradation after 4 days of incubation with the specific enzymatic preparation, compared with synthetic fur, which is basically non-biodegradable.

Table 3			

BIOCHEMICAL OXYGEN DEMAND FOR BIODEGRADABLE FURS (Pvalu)			
Days	**BOD, mg/L**		
	Ms	**Ms**	**Ms**	**Ms**

Days	Ms	Ms	Ms	Ms
1	154	145	130	142
2	161	155	139	148
3	164	165	142	173
4	168	177	143	332
5	168	183	141	440
6	167	187	140	468
7	174	197	143	520
8	175	201	142	557
9	181	210	144	584
10	183	216	144	600
11	186	220	145	616
12	187	223	145	631
13	187	228	145	642
14	191	233	148	654
15	191	235	148	660
16	191	236	148	665
17	189	235	149	667
18	159	238	152	672
19	186	234	149	669

Fig. 10. BOD for synthetic fur with inoculum, Ps
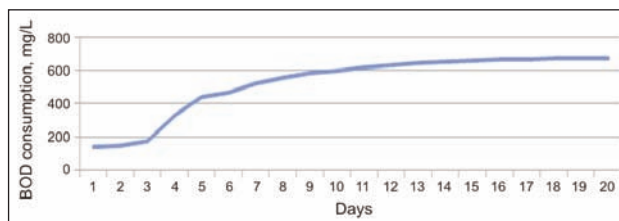
Fig. 11. BOD for sheepskin prototype with inoculum, Pvalu

The developed method allows rapid assessment of natural fur biodegradability compared to existing methods that require a long time, even up to 6 months. The results obtained by the Spiro metric method are consistent with determinations of amino acid released in the biodegradation medium (figure 7). Demonstrating biodegradability of fur items after the end of their life cycle allows them to be considered secondary resources of protein, carriers of a bio-energy potential and the development of specific processes for the extraction of collagen components from the dermis to exploit them. Previous studies have validated that collagen extracts have properties that recommend them for applications in agriculture and other industries [10].

Creating eco-labeled biodegradable sheepskin fur coats

It should be noted that usually, furs are processed with smaller amounts of chromium salts, their shrinkage temperature (the main indicator for the degree of tanning) is at least 20 degrees lower than in cattle hides for shoe uppers. The biodegradable fur prototype (figure 12, a) was processed without using chromium salts and dyes.

The research aimed to develop a method underpinning the assessment of biodegradability for the created furs and a fur assortment from which a model was manufactured under industrial conditions (figure 12, b), a niche product, for which a logo was created, specific for the property of biodegradability (figure 12, c). The biodegradability label will be a means to educate both consumers and producers for the development, consumption and disposal of products that do not affect the future health of the environment.

CONCLUSIONS

This paper proposes a system for biodegradability assessment of natural furs, constituting the basis for labeling natural fur items that can be recycled at the

Fig. 12. Biodegradable furs (a), biodegradable fur coat prototype (b) and label (c)

end of their life cycle. The main steps of biodegradability assessment scheme have been completed successfully by developing a method for analyzing the accelerated biodegradability of natural furs and developing the biodegradable fur prototype resistant to industrial manufacturing conditions. The specific enzymatic preparations for biodegradation of natural fur are original and allow short-time assessment of biodegradability of natural furs. Labeling the biodegradability of natural fur is a means of correctly informing the consumers of natural products, which do not pollute the environment at the end of their life cycle.

BIBLIOGRAPHY

[1] Van der Zee, M., *Analytical methods for monitoring biodegradation processes of environmentally degradable polymers in Handbook of biodegradable polymers: synthesis, characterization and applications*, First Edition. Edited by Andreas Lendlein, Adam Sisson, Published by Wiley-VCH Verlag GmbH & Co. KGaA, 2011

[2] Qiang, T., Wang, X., Ren, Y., Ren, L., *Study on biodegradation of several chrome-free goat garment leathers*, XXXI IULTCS Congress, 2011, Valencia (Spain), September 27th–30th, Paper B15

[3] Bertazzo, M., Poveda, D., Albert, A., Segarra-Orero, V., Roig, M., Garrote, N. C., Lopez M. I., Martínez-Sanchez, M. A., *System for biodegradability evaluation on leather used in the footwear industry*, XXXI IULTCS Congress, 2011, Valencia (Spain) – September 27th–30th, Paper E50

[4] Stefan, D.S., et al., *Identifying microorganisms able to perform biodegradation of leather industry waste*, Molecular Crystals and Liquid Crystals, 2012, vol. 556, pp. 301–308

[5] Calise, A., *Biodegradabilita dei materiali cuoiosi: Sviluppo di un metodo in impianto pilota di compostaggio e valutazione tramite analisi ecotossicologiche del compost ottenutto*, CPMC, 2011, vol. 6, no. 212, pp. 373–380

[6] Lombardi, S., *Smaltimento dei prodotti cuoiosi: Indagine sui principali microrganismi aerobi coinvolti nella loro transformazione e valutazione degli effetti tossici derivanti*, CPMC, 2013, vol. 89, pp. 63–75

[7] Gaidau, C., Jurcoane, S., Cornea, P., Israel-Roming, F., Dinu, L., Radulescu, C., Niculescu, M., Vesa, G., *New method for biodegradability of collagen and keratin based material assessment*, 5th Conference on Advanced Materials and Systems, ICAMS 2014, Bucharest, 23–25 October, pp. 255–260

[8] Luta, G., Balan, D., Gherghina, E., Simion, V., Matei, F., Jurcoane, S., *Concentration and immobilization of a proteolytic complex*, Scientific Bulletin. Series F. Biotechnologies, Vol. XVIII, 2014, pp. 169–173

[9] Israel-Roming, F., Cornea, P., Gherghina, E., Luta, G., Balan, D., *Bacterial proteolytic enzymes tested on keratin and collagen based material*, Scientific Bulletin. Series F. Biotechnologies, Vol. XVIII, 2014, pp. 174–177

[10] Gaidau, C., Niculescu, M., Stepan, E., Taloi, D., Filipescu, L., *Additives and advanced biomaterials obtained from leather industry by-products*, Rev. Chim.-Bucharest, 2009, vol. 60, no. 5, pp. 501–507

Authors:

CARMEN GAIDAU[1], MIHAELA NICULESCU[1], ANDREEA GEORGIANA VESA[2]
CLARA RADULESCU[3], STEFANA JURCOANE[4], PETRUTA CORNEA[4]
FLORENTINA ISRAEL-ROMING[4], LUOANA FLORENTINA PASCU[5]

[1]R&D National Institute for Textile and Leather (INCDTP),
Leather and Footwear Research Institute (ICPI) Division,
93, Ion Minulescu street, Bucharest, 031215, Romania
[2]A&A VESA Ltd, Sebis, Romania
[3]R&D National Institute for Textile and Leather (INCDTP)
16, Lucretiu Patrascanu street, Bucharest, 030508, Romania
[4]University of Agronomical Sciences and Veterinary Medicine of Bucharest,
Faculty of Biotechnology, Microbial Biotechnological Center-BIOTEHGEN
59, Marasti, street, Bucharest, 011464, Romania
[5]R&D National Institute for Industrial Ecology – ECOIND
71-73, Drumul Podu Dambovitei street, Bucharest, 060652, Romania
e-mail: carmen_gaidau@hotmail.com; mihaelaniculescu59@yahoo.com;
jstefana@yahoo.com; clara.radulescu@certex.ro

Corresponding authors:

CARMEN GAIDAU
carmen_gaidau@hotmail.com
MIHAELA NICULESCU
mihaelaniculescu59@yahoo.com

Nettle biofibre bleaching with ozonation

MUTLU KURBAN
OZAN AVINC

ARZU YAVAS
HÜSEYIN AKSEL EREN

REZUMAT – ABSTRACT

Albirea biofibrei din urzică prin ozonizare

Urzica este o cultură industrială care poate fi utilizată ca hrană, furaj și materie primă în scopuri diferite în industria produselor cosmetice, medicină, industrie, agricultură biodinamică și textile. Utilizarea fibrei de urzică asigură o producție de textile biodegradabile, din surse regenerabile, durabile și ecologice care necesită consum redus de energie. Cu toate acestea, culoarea naturală a fibrei de urzică este bej, crem, sau maro deschis. A fost studiată albirea țesăturilor din 100% fibră naturală de urzică, prin ozonizare. Au fost, de asemenea, investigate ozonizarea în prezența activării omogenizatorului ultrasonic, albirea convențională cu diverși agenți de albire, albirea cu o enzima lacază și aplicațiile lor secvențiale cu ozonizare (albire convențională, ozonizare, urmată de albire cu enzima lacază și ozonizare). Valorile pentru gradul de alb, rezistența la tracțiune, hidrofilia și consumul chimic de oxigen (COD) au fost determinate și comparate. Albirea cu ozon a condus la o pierdere mai mică a rezistenței în comparație cu albirea pe bază de peroxid de hidrogen. Formarea unei mai mari cantități de oxiceluloză a condus la pierderea mai mare a rezistenței, în cazul albirii cu peroxid de hidrogen în comparație cu albirea cu ozon. Albirea cu ozon a țesăturilor din fibră de urzică ar putea fi folosită ca o alternativă viabilă la albirea cu peroxid de hidrogen datorită eficienței sale, a aplicării unei temperaturi mai mici, a timpului de aplicare scurt și a caracterului mai puțin dăunător pentru mediu.

Cuvinte-cheie: fibră de urzică, albire, grad de alb, ozon, ozonizare, peroxid de hidrogen

Nettle biofibre bleaching with ozonation

The nettle plant is an industrial crop, different parts of which can be used as food, fodder, and as a raw material for different product purposes in cosmetics, medicine, industry, biodynamic agriculture, and textiles. Nettle fibre usage provides bio-degradable, renewable, sustainable, and eco-friendly textile production and requires low energy consumption during production. However, the natural colour of nettle fibre is beige, cream, or light-brown. In this study, bleaching of 100% natural nettle fibre fabric with ozonation was explored. Apart from ozonation alone, ozonation in the presence of ultrasonic homogeniser activation, conventional bleaching with various bleaching agents, bleaching with a laccase enzyme, and their sequential applications with ozonation (conventional bleaching, then ozonation, followed by laccase enzyme bleaching, and then ozonation) were also investigated. Whiteness, tensile strength, hydrophilicity, and chemical oxygen demand (COD) values were determined and compared. Ozone bleaching led to less strength loss in comparison to hydrogen peroxide bleaching. Higher oxycellulose formation resulted in higher strength loss in the case of peroxide bleaching in comparison to ozone bleaching. Ozone bleaching for nettle fibre fabrics could be used as a viable alternative to hydrogen peroxide bleaching due to its effectiveness, lower application temperature, lower application time, and less environmentally harmful nature.

Keywords: Nettle fiber, bleaching, whiteness, ozone, ozonation, hydrogen peroxide

INTRODUCTION

The nettle plant (figure 1), a member of the *Urticaceae* family, is an important industrial crop; different parts of nettle plant fibre can be used as food, fodder, and as raw material for different product purposes in cosmetics, medicine, industry, and biodynamic agriculture [1]. Therefore, nettle plant fibre has found a wide scope of usage, such as in pharmaceuticals, cosmetics, dyes, fibre production, food, and fertiliser, since ancient times [2, 3]. The nettle plant can be grown on unproductive marginal lands, which is an important advantage for nettle fibre production. Furthermore, after fibre has been extracted from the stalk of the nettle plant, the debris can be used as provender and also be used in pharmaceutical manufacturing [2, 3, 4]. The cost of nettle production is less than that of cotton production. This is a very good advantage over cotton. Once the nettle is planted, nettle fibre production can be sustained for the next 10 consecutive years and nettle fibre shines out due to its breathability, easy care, lower wrinkle occurrence, antistatic, UV transmittance, silky appearance, and anti-allergenic properties. What is more, nettle fibre fabric is very resistant against impacts. Overall, nettle fibre usage provides bio-degradable, renewable and eco-friendly textile production and requires low energy consumption during production [5]. Nettle fibre (*Urtica dioica* L.) is a cellulosic fibre which contains approximately, on average, 9% hemicellulose, and 4% lignin 86% cellulose [6, 7]. Nettle fibre is primarily composed of cellulose and the cellulose content of nettle fibre is the closest to that of cotton fibre among all other bast fibres [8]. Recent studies have shown that cotton fibre can be replaced by nettle fibre in

Fig. 1. Nettle plant (*Urtica dioica*) nettle fiber yarns and t-shirt made from

many applications because of its suitable textile performance [9]. Nettle fabric's superior moisture absorption properties and the fact that it is soft to handle means that it has a comfortable feeling for the wearer [10]. Nettle fibre is found in many different textile usages, such as shirts, t-shirts (figure 1), jackets, denim fabrics, table linens, carpets, bedding, etc. [11]. Organically produced nettle fibres are in demand in the green textile industry and exhibit a potential which is economically promising [1].

The natural colour of nettle fibre is beige, cream, or light brown, as can be seen in figure 1. The exact nature of colouring matter in the textile fibres is generally not known, and presumably changes for different fibre types and origins [12]. For example, the natural colour of cotton, which is a yellowish and brownish discolouration, may be related to the flavone pigments of the cotton flower [13]. Even if the fabric is dyed, these naturally occurring colouring matters may affect the tone and brightness of the shade obtained when dyeing, especially for lighter shades [14]. What is more, climate, soil, drought, and frost may also result in different degrees of yellowness [13]. Colour may also come from dust, dirt, insects, harvesting, and/or processing equipment in the form of oils and greases [13]. These impurities, which mask the natural whiteness of the fibres, may absorb light in fibres giving them a creamy, yellowish, or dull appearance [12]. With the help of bleaching agents, white fabrics can be produce through decolouration of the impurities by destroying the colouring matter on the fibre – of course, with a minimum degradation of the fibre itself [13]. It is known that bleaching agents either oxidise or reduce the colouring matter, which is then washed out leaving a permanent whiteness [13]. Indeed, bleaching is routinely carried out on cellulosic fabrics to whiten textile materials in industry. Due to these reasons, it is usually necessary to bleach nettle fibre fabrics in order to improve their whiteness. Conventional processes for bleaching textiles most often entail hydrogen peroxide. The conventional bleaching of cellulosic fabrics, such as cotton fabrics, is done with hydrogen peroxide in the presence of caustic soda at high temperatures, usually at the boil [15–22]. However, this treatment has to be carried out at this elevated temperature, with a high associated energy cost, and is fairly aggressive, often causing significant deterioration in the mechanical properties of the fibre as well as damage to the

fibre surface. These considerations prompted our investigation of ozonation as a milder alternative to harsher (and less environmentally friendly) treatments such as those based on hydrogen peroxide. Ozonation is known as an eco-friendly technique. Ozone (O_3) has a relatively high oxidation potential (2.07 V) compared with that of the more conventional oxidants, such as hydrogen peroxide, used on textiles (1.77 V). The effectiveness of ozone treatments on textiles and in related industries has already been demonstrated [23–28], and several recent publications, in particular [29, 30], report its successful application in the processing of fabrics based on polyester and polyester/ cotton blends. The major advantages of ozonation identified in the studies referred to above were in terms of energy and time savings, as the procedure is performed at room temperature and appears to require only short durations of exposure to achieve effective treatment. There is also a significant reduction in environmental load due to the avoidance of harsh chemicals.

In this study, the effectiveness of the ozonation process in neutral distilled water at room temperature as a bleaching process for 100% nettle fibre fabrics is investigated. There are very limited studies on nettle fibre, and it is especially hard to find any scientific studies on the textile wet processing of nettle fibre fabrics. In this paper, we report the initial results obtained using a promising alternative bleaching procedure based on ozone for nettle fibre fabrics. In addition to being a milder treatment, the ozonation method is applied at ambient temperature, thus lowering energy consumption. There is a modest cost associated with generating the ozone; but the sole reagent, oxygen, is freely available from the atmosphere, and the energy input to the conversion process is entirely electrical. This implies that the sustainability of the ozonation method could be expected to improve progressively as the adoption of renewable energy sources becomes increasingly commonplace. Moreover, the help of ultrasound technology during ozonation has been explored for bleaching to investigate the effect of ultrasound on the whiteness property of nettle fibre fabrics. In addition, conventional bleaching agents such as sodium percarbonate, sodium perborate, hydrogen peroxide, peracetic acid, sodium borohydride, and a laccase enzyme were chosen as control bleaching processes for comparison. Furthermore, their sequential applications with ozonation (conventional bleaching then ozonation and laccase enzyme bleaching then ozonation) were also investigated. Whiteness, tensile strength, hydrophilicity, oxycellulose formation, and chemical oxygen demand (COD) values were determined and compared.

EXPERIMENTAL

Materials

Twill-woven 100% nettle fibre fabric (295 g/m^2) was obtained from Octans Fabrics (South Korea). Different bleaching agents (sodium percarbonate,

sodium perborate, hydrogen peroxide (50%), peracetic acid, and sodium borohydride), a laccase enzyme (Novalite II S enzyme, Alfa Kimya, Istanbul, Turkey), and ozone (O_3) were used for nettle bleaching.

Bleaching

Nettle fibre fabrics were bleached with different process types. Ozonation, ozonation in the presence of an ultrasonic homogeniser (UH), a combination of the conventional bleaching and ozonation process, and finally a combination of laccase enzyme and ozonation processes were carried out.

Bleaching via ozonation (Ozone Application Procedure)

The equipment used to produce the ozone was an Opal OS1 model O_3 generator, using the corona discharge method (fig. 2, C), (Opal Ltd., Ankara, Turkey) which can supply 3 g/h of O_3 from a feed of high-purity (99.5%) oxygen. The ozone treatments were performed at room temperature in a glass reactor containing 100 mL of distilled water into which the nettle fabric samples were immersed. The reactor, which had a closed cylindrical with a total volume of 130 mL and a diameter of 29 mm, was connected via polytetrafluoroethylene (PTFE) tubing to the ozone generator, and its base was fitted with a diffuser to produce a stream of fine O_3 bubbles (figure 2, A). The nettle fabric samples were ozonated as above for durations of 15, 30, 45, 60, 90, and 120 minutes in order to determine the optimum bleaching time via ozonation. The O_3 concentration was measured according to the standard iodometric method (Standard Method 2350E, APHA). To facilitate this, outlet O_3 from the O_3 generator was directed to gas washing bottles filled with a 2% w/w potassium iodide (KI) solution. A concentration of 6.5 ± 0.4 mg/min was measured at a 600 mL/min O_3 gas flow rate.

Bleaching via ozonation with Ultrasonic Homogeniser (UH) (use of ultrasound technology)

The help of ultrasound technology during ozonation is explored for bleaching to investigate the effect of ultrasound on the whiteness property of nettle fibre fabrics. Therefore, a UH (Bandelin Sonopuls HD2200 (20 kHz, probe type: VS70, 13 mm in diameter, 200 W HF-power)) was used in this study. Ozonation g was combined with this ultrasonic homogeniser (ozonation + UH) for bleaching. The experimental set-up is presented in figure 2, B. The glass reactor contains the ozone diffuser, UH probe (immersed 1 cm into the bleaching solution), and bleaching solution (figure 2, B).

Bleaching combinations

Conventional bleaching with various bleaching agents, bleaching with laccase enzyme, and their sequential applications with ozonation (conventional bleaching then ozonation, and laccase enzyme bleaching then
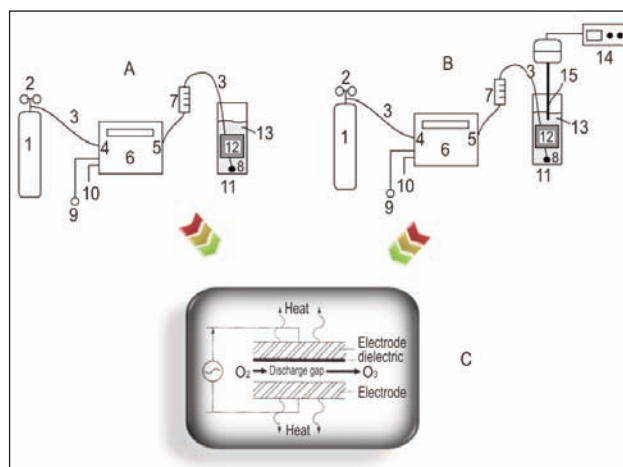
Fig. 2. Experimental set-up for the ozonation experiments (A) Ozonation only, (B) Ozonation + UH (Ultrasonic Homogenizer) [1. Oxygen tube, 2. Oxygen pressure regulator, 3. Teflon tubing, 4. Oxygen inlet to the generator, 5. Ozone/Oxygen outlet from the generator, 6. Ozone generator, 7. Gas-flow scale, 8. Diffuser, 9. Cooling water inlet, 10. Cooling water outlet, 11. Glass reactor, 12. Nettle Fabric, 13. Water, 14. UH (Ultrasonic homogenizer), 15. Probe of UH], (C) Corona-discharge ozone generator (6. Ozone generator) (schematic) [27]
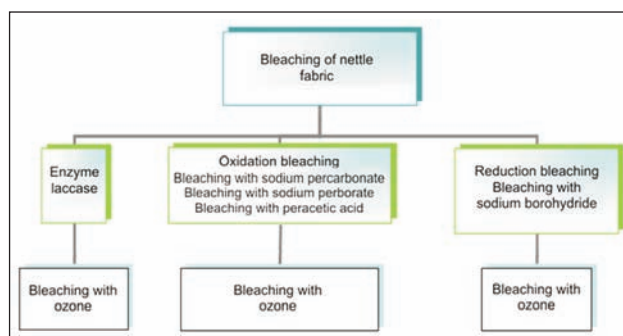
Fig. 3. Sequential bleaching application types and their two steps

ozonation) were investigated. Sequential bleaching types can be seen in figure 3.

Conventional bleaching and their sequential combination with ozonation

Bleaching is achieved chemically using oxidising or reducing agents [31]. Therefore, conventional bleaching of nettle fibre fabric was carried out with different oxidative (sodium percarbonate, sodium perborate, hydrogen peroxide, peracetic acid) and reductive bleaching (sodium borohydride) agents.

Based on the preliminary studies, the application conditions of each bleaching agent which resulted in the best whiteness properties in the nettle fabrics were determined and selected (table 1). All conventional bleaching processes were carried out for nettle fabrics using Ataç Lab Dye HT model IR sample dyeing machine via the exhaustion process. After these conventional bleaching processes, ozonation was also applied to conventionally bleached nettle fibre fabric samples as the second step of the sequential process.

APPLICATION CONDITIONS OF CONVENTIONAL BLEACHING AGENTS AND LACCASE ENZYME FOR NETTLE BLEACHING						
Application conditions	Peracetic acid	Sodium borohydride	Sodium percarbonate	Sodium perborate	Hydrogen peroxide	Laccase enzyme
Concentration	20 ml/l	15 g/l	6 g/l	6 g/l	30 ml/l	%1
pH	7	9	10,5–11	9	10,5–11	4,5–5,5
Temperature (°C)	70	70	70	70	95	65
Time (minutes)	60	90	60	90	90	20

Bleaching with a laccase enzyme and its sequential combination with ozonation

Enzyme bleaching with laccase and its sequential combination with ozonation was also examined. Bleaching with a laccase enzyme was carried out with an ATAC Lab Dye HT model IR sample dyeing machine via the exhaustion process. Optimum application conditions of the laccase enzyme (Novalite II S) were chosen according to the producers' recommendation (table 1). After bleaching with the laccase, ozonation was also applied to the nettle fabric as the second step of the sequential process.

Whiteness determination

Following bleaching treatment, the whiteness (measured along the Stensby scale) of the nettle fabrics was determined using a Datacolor 600 spectrophotometer. Each sample was measured from four different areas, twice on each side of the fabric for consistency, and the average value was calculated.

Hydrophilicity determination

The effectiveness of different bleaching processes on the hydrophilicity character of the nettle fabrics was detected through a sinking (submersion) test according to the TS EN ISO 139 test standard. The length of the fabric specimens was 1 cm and they were equal in weight. The samples were allowed to free fall 10 cm above the water container. The times of the submersion (in seconds) to reach the bottom of the container were reported as hydrophilicity. The determination of the sinking test was carried out under standard laboratory conditions (20 ± 2 °C; 65 ± 2 % relative humidity).

Tensile strength

Fabric tensile strength testing was carried out in accordance with ISO 13934, using a Tinius Olsen H10K tensile strength tester under standard laboratory conditions (20 ± 2 C; 65 ± 2% relative humidity). The tensile strength results of nettle fibre fabrics were reported in Newtons (N).

Chemical Oxygen Demand (COD) evaluation

The COD values of the bleaching solutions were measured according to the standard titrimetric method (Standard Methods 5220C, APHA). The average COD values of the three repeated experiments were reported in mg/unit.

Oxycellulose determination with methylene blue

Bleaching processes with oxidising agents must be carefully controlled. Cellulose can be damaged by oxidation during bleaching, in the form of damage to the fibrous material during the removal of colouring matter from the fibres [12]. This is because the oxidation of cellulose produces carbonyl and carboxyl groups in the cellulose, in turn leading to higher amounts of the carboxyl group in the fibre, which can be easily dyed by cationic dyes [12]. Therefore, oxycellulose formation will be apparent in the fibre. This possible damage can be detected by the methylene blue cationic dye. Damaged cellulosic fibre can be dyeable with a dye concentration of 0.1% methylene blue cationic dye in 60–100°C for 5 minutes or in cold water for 20 minutes [32]. Therefore, the greige and bleached cellulosic nettle fibre fabrics were dyed with methylene blue cationic dye in the same manner. The bluer the fabric, the more oxycellulose formation and therefore more damage due to oxidative agents.

RESULTS AND DISCUSSIONS

Data obtained from the assessments of fabric whiteness appear in figures 4, 5, and 6, while the results of the hydrophilicity tests, tensile strength measurements, oxycellulose determination, and COD evaluation appear in table 2, figures 7–8, and table 3, respectively.

Ozonation for nettle bleaching

The whiteness degrees of the nettle fabrics after ozonation with different times are shown in figure 4. The whiteness degree of the greige fabric was 62.97. Ozonation led to an increase in the whiteness level of nettle bast fibre. For example, even after 15 minutes of ozonation, the whiteness degree of the nettle fibre fabric was improved by 4.8% (figure 4). The whiteness improvement was 8.9% after 30 minutes of ozonation. It can be seen from figure 4 that after 30 minutes of ozonation there was very little whiteness improvement. For example, it can be seen from figure 4 that the whiteness degree difference between 30 minutes of ozonation (68.59 Stensby units) and 45 minutes of ozonation (69.23 Stensby units) was less than 1 Stensby unit. It is known that cellulose macromolecules oxidise and turn into oxycellulose during bleaching with oxidative bleaching agents. Hydroxyl
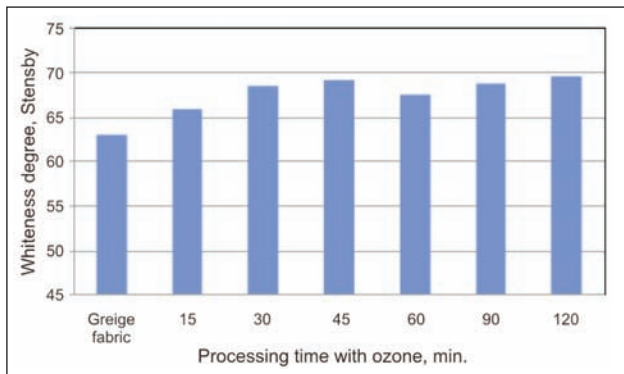
Fig. 4. Effect of ozonation time on whiteness degree of nettle fiber fabrics
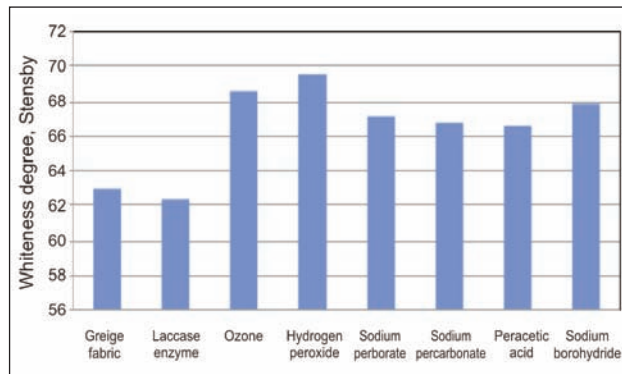

Fig. 5. Whiteness values of nettle fiber after various one-step bleaching processes

groups of glucose turn into carboxyl or aldehyde groups during bleaching. One should not forget that increasing treatment time for bleaching in order to achieve higher whiteness degrees may lead to extended oxidation of the fibre, which ultimately causes strength losses. Considering the increase of the whiteness degree against ozonation time, 30 minutes of ozonation for nettle bleaching can be selected as the optimum ozonation time, leading to 8.9% whiteness improvement. Henceforth, 30 minutes of ozonation will be used for further evaluation.

Bleaching through ozonation with an Ultrasonic Homogeniser (UH)

Following the ozonation trials, 30 minutes of ozonation was selected as the optimum ozonation. Therefore, for even comparison, 30 minutes of ozone bleaching was combined with an ultrasound source (UH) to investigate the effect of ultrasound on the whiteness property of the nettle fibre fabrics. Ultrasound is defined in relation to human hearing and is acoustic (sound) energy in the form of waves that have a frequency above the hearing range of humans.

As indicated earlier, ozonation alone for 30 minutes resulted in a whiteness of 68.59 Stensby units for nettle fibre fabrics (figure 4). Ozonation + UH resulted in a slightly higher whiteness value of 69.24 Stensby units. Therefore, ozonation alone and ozonation + UH led to an 8.9% and 10% improvement, respectively, in the whiteness property of the 100% nettle fibre fabric. It seems that the effect of the ozone was only slightly intensified with the help of ultrasonic energy, which was created by a UH probe. It is known that high-power ultrasound produces cavitation, which facilitates particle disintegration or reactions. In this case, the effect of the ozonation is slightly strengthened by the ultrasound energy. He *et al.* indicated three factors to explain the enhanced effect of the ultrasound support; the mechanical action of ultrasound enhancing the dissolution of ozone and the generation of additional •OH, the improved the mass transfer of ozone by ultrasound leading to more ozone entering the liquid phase and the turbulence of the aqueous solution to enable more substances to migrate into the bulk of the solution [33].

Conventional and laccase enzyme bleaching in comparison to ozone bleaching

The whiteness degrees of nettle fibre fabric after respective bleaching with conventional bleaching agents, laccase enzyme and 30 minutes ozonation are shown in figure 5.

As can be seen from figure 5, the laccase enzyme did not lead to an improvement in the whiteness value of the nettle fibre. The ozone and the other bleaching agents studied caused a development in the whiteness level of the nettle fibre. As mentioned above, 30 minutes of ozonation led to an 8.9% whiteness improvement in the nettle fibre to 68.59 Stensby units. Bleaching with sodium percarbonate, sodium perborate, hydrogen peroxide, peracetic acid, and sodium borohydride resulted in a 6.1%, 6.7%, 10.5%, 5.8%, and 7.0% whiteness improvement in the nettle fibres, respectively (figure 5). The highest improvement in the whiteness value was achieved with the peroxide and ozone bleaching processes. This suggests that ozone bleaching could be effective at much shorter treatment times than is normally needed for hydrogen peroxide while having, potentially, substantial cost savings.

Sequential combination bleaching processes: conventional bleaching then ozonation

After the conventional bleaching processes and laccase bleaching process, 30 minutes of ozonation was also applied to nettle fibres as the second step of the sequential process (figure 3). The whiteness values of the nettle fibre fabrics after the different two-step bleaching processes (conventional bleaching then ozonation and laccase enzyme bleaching then ozonation) are exhibited in figure 6.

Although 30 minutes of ozonation after laccase enzyme bleaching resulted in a 7.7% whiteness improvement in the nettle fibre, the obtained whiteness level was below all other two-step bleaching types (figure 6). Ozonation as a second step in the bleaching process after conventional bleaching processes led to a slight improvement in the whiteness values of the bleached nettle fibre. However, these whiteness increases were not that impressive, with maximum rise of 2 Stensby units (figure 6). It is very
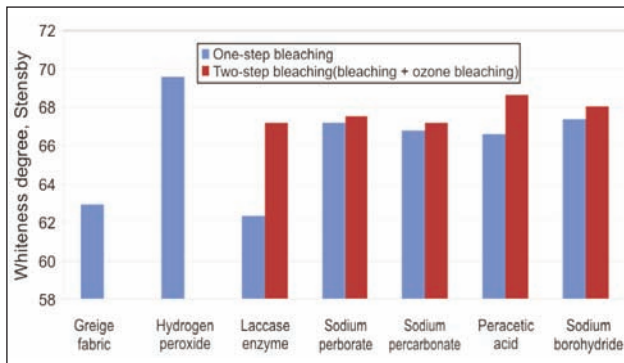
Fig. 6. Whiteness values of nettle fiber after various
two-step bleaching processes

clear that the whiteness degrees after all sequential applications (conventional bleaching processes then ozonation) could not even reach the whiteness degree achieved through the hydrogen peroxide bleaching process alone (figure 6). Therefore, one-step bleaching processes can be preferred over two-step bleaching processes which have ozonation as a second process type, due to less process complexity, less processing time, and lower cost to achieve comparable whiteness values. After all these process types were tested, 30 minutes of ozonation and the hydrogen peroxide bleaching process resulted in the best whiteness results in the nettle fibre fabrics. On the one hand, 90 minutes of a conventional hydrogen peroxide bleaching process at 95°C resulted in a whiteness value of 69.58 Stensby units; on the other hand, a comparably close whiteness value of 68.59 Stensby units can be obtained via ozonation but just with 30 minutes of application at room temperature. Obviously whiteness determination is the first priority for a bleaching process. However, apart from the whiteness property, hydrophilicity levels of bleached fabrics as well as possible strength loss after the bleaching process should be investigated for comparison. Therefore, the effects of 30 minutes of ozonation and hydrogen peroxide bleaching processes have been compared with regard to the above issues along with the chemical oxygen demands of bleaching effluents.

Hydrophilicity change after ozonation and peroxide bleaching

The hydrophilicity results (in seconds) of greige fabric and ozonated and hydrogen peroxide bleached

nettle fibre fabrics are given in table 2. The hydrophilicity value of greige nettle fabric was 5.63 seconds for submersion (table 2). Therefore, the greige fabric was already hydrophilic at the beginning before any bleaching application. The lower the sub-mersion time is, the more hydrophilic the fabric is. As can be seen in table 2, the hydrogen peroxide bleaching process slightly improved the hydrophilicity property of the nettle fibre fabrics, leading to a lower submersion time of 3.71 seconds. However, the ozonation bleaching process did not cause a significant improvement in the hydrophilicity. This difference probably occurred due to the differences in the treatment bath compositions and temperatures. Hydrogen peroxide bleach was performed at 95°C with caustic soda, which may create more suitable environment for removing impurities present on the fibre due to high temperature accompanied severe chemicals, hence, resulting in better hydrophilicity.

Tensile strength change after ozonation and peroxide bleaching

The bleaching process results in more or less chemical damage on the fibre depending on the bleaching type and its conditions. Achieving a high degree of whiteness alone is not enough for cellulosic fibres. Indeed, the best way of processing them is to achieve a high whiteness levels without causing too much damage to the fibre. The tensile strength of nettle fibre fabrics after ozonation and peroxide bleaching is given in figure 7. It can clearly be seen that, as expected, both bleaching processes resulted in strength loss. Ozone bleaching led to less strength
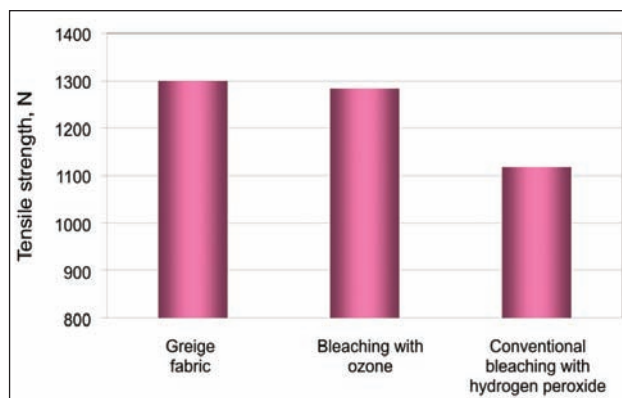
Fig. 7. Whiteness values of nettle fiber fabric after
ozonation and bleaching processes

Table 2

HYDROPHILICITY LEVELS OF BLEACHED NETTLE FIBER FABRICS		
(H_2O_2 bleaching process: 30 ml/l H_2O_2, 1,5 g/l NaOH at 95 °C and pH 10,5–11 for 90 minutes; Ozone bleaching process: 600 mL/min ozone at 25°C (room temperature) and pH 7 for 30 minutes)		
Bleaching type	**Whiteness degree (Stensby)**	**Hydrophilicity-sinking time (sec.)**
Greige fabric (Before bleaching)	62,97	5,63
Bleaching with Ozone (30 minutes)	68,59	5,60
Bleaching with Hydrogen Peroxide	69,58	3,71

Fig. 8. Bleached nettle fiber fabrics dyed with methylene blue cationic dye (***H₂O₂ bleaching process:*** 30 ml/l H₂O₂, 1,5 g/l NaOH at 95 °C and *p*H 10,5–11 for 90 minutes; ***Ozone bleaching process:*** 600 mL/min ozone at 25°C (room temperature) and *p*H 7 for 30 minutes)

CHEMICAL OXYGEN DEMAND (COD) VALUES OF RESPECTIVE BLEACHING BATHS (*H₂O₂ bleaching process:* 30 ml/l H₂O₂, 1,5 g/l NaOH at 95 °C and *p*H 10,5–11 for 90 minutes; *Ozone bleaching process:* 600 mL/min ozone at 25 °C (room temperature) and *p*H 7 for 30 minutes)	
Process Type	**COD (mg/l)**
Ozone bleaching	< 300
Hydrogen peroxide bleaching	1152

loss in comparison to hydrogen peroxide bleaching. Conventional hydrogen peroxide bleaching using 30 ml/l H₂O₂, 1.5 g/l NaOH at 95 °C and *p*H 10.5–11 for 90 minutes and ozone bleaching using 6.5 ± 0.4 mg/min ozone at 25°C (room temperature) and *p*H 7 for 30 minutes resulted in 14% strength loss and 1.3% strength loss, respectively (figure 7). The shorter processing time at the less aggressive *p*H and temperature conditions in the case of the ozonation process is most probably responsible for the lower strength loss.

Oxycellulose evaluation

When cellulosic fibre experiences damage due to oxidative substances, oxycellulose formation appears in the fibre. These fibres damaged with oxycellulose formations can be dyed with methylene blue cationic dye. Greige and bleached fabrics which were dyed with methylene blue cationic dye are shown on figure 8. The bluer the fabric, the more oxycellulose formation and therefore more damage due to oxidative agents there is. It is important to mention that undamaged cellulosic fibres are stained during this test [32, 34]. Indeed, greige cellulosic fibres such as cotton, flax, hemp, and regenerated cellulosic fibres are stained with methylene blue cationic dye [35]. This is exactly in line with the studied greige nettle fibre fabric, which also exhibits blue staining (figure 8). However, as is obvious from figure 8, bleached samples, in comparison to greige fibre, are evenly dyed with methylene blue, leading to bluer appearance. As can be seen in figure 8, hydrogen peroxide bleaching led to a darker blue colour in comparison to ozone bleaching, which means that there was higher oxycellulose formation in the case of the hydrogen peroxide bleaching. This is actually in line with the results on tensile strength (figure 7). As is known, oxidative damage can decrease strength and change other physical properties of fibres [12]. Here, higher oxycellulose formation resulted in higher strength loss in the case of hydrogen peroxide bleaching than it did for ozone bleaching.

Chemical Oxygen Demand (COD) evaluation

The COD measurement results on the bleaching bath solutions after the ozonation and hydrogen peroxide bleaching processes are shown in table 3.

On the one hand, the COD of the bath after bleaching with ozonation was less than 300; on the other hand, the COD of the bath after hydrogen peroxide bleaching was 1,152 (table 3). It is clearly visible that the ozone bleaching bath has significantly less chemical oxygen demand than hydrogen peroxide bleaching. Therefore, ozone bleaching is more ecologic than hydrogen peroxide bleaching in respect to chemical oxygen demand.
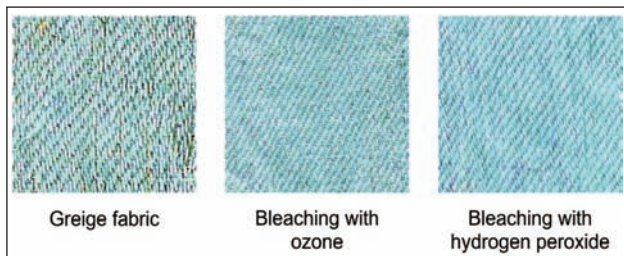
CONCLUSIONS

Ozonation resulted in the improvement of the whiteness of nettle fibre fabric. Duration of 30 minutes of ozonation was selected as an optimum ozonation time for nettle fibre bleaching, leads to an 8.9% whiteness improvement, to 68.59 Stensby units, without significant strength loss. Ozonation + UH caused a slightly higher whiteness value of 69.24 Stensby units, leading to a 10% whiteness improvement in comparison to greige nettle fibre fabric. It seems that the effect of ozone was slightly, but not to a great extent, intensified with the help of ultrasonic energy created by a UH probe.

Among all the process types applied, the highest improvement on the whiteness values of nettle fibres was achieved with the hydrogen peroxide and ozone bleaching processes. On the one hand, 90 minutes of conventional hydrogen peroxide bleaching process at 95 °C resulted in a whiteness value of 69.58 Stensby units; on the other hand, a comparably close whiteness value of 68.59 Stensby units can be obtained via ozonation, but with just 30 minutes of application at room temperature. This suggests that ozone bleaching could be effective with much shorter treatment times than is normally needed for hydrogen peroxide with, potentially, substantial cost savings.

Although whiteness improvements were not quite as impressive, ozonation as a second step bleaching process after conventional bleaching processes led to a slight improvement on the whiteness values of bleached nettle fibre. Therefore, one-step bleaching processes can be preferred over two-step bleaching processes which have ozonation as a second process step, due to less process complexity, less processing time, and lower cost need to achieve comparable whiteness values.

Greige nettle fibre fabric was already hydrophilic, with a time of 5.63 seconds until submersion. The ozonation bleaching process did not cause a significant improvement in hydrophilicity, whereas conventional hydrogen peroxide bleaching led to 3.71 seconds until submersion. Ozone bleaching led to less strength loss in comparison to hydrogen peroxide bleaching. Higher oxycellulose formation resulted in higher strength loss in the case of hydrogen peroxide bleaching in comparison to ozone bleaching. The zone bleaching bath had significantly less chemical oxygen demand than it did for hydrogen peroxide bleaching, indicating more ecologic bleaching process. In conclusion, it is believed that the ozonation of nettle fibre fabrics could be used as a viable alternative to hydrogen peroxide, not only due to its effectiveness, but also because of its lower application temperature, lower application time, and less environmentally harmful nature.

ACKNOWLEDGMENT

BIBLIOGRAPHY

[1] Vogl, C.R., Hartl, A., *Production and processing of organically grown fiber nettle (Urtica dioica L.) and its potential use in the natural textiles industry: a review.* In: American Journal for Alternative Agriculture, 2003, vol.18, issue 3, p. 119

[2] Ayan, A.K., Çalışkan, Ö., Çırak, C., *Isırgan otu(Urtica spp.)'nun Ekonomik Önemi ve Tarımı,* In: OMÜ Ziraat Fakültesi Dergisi, 2006, vol. 21, issue 3, p. 357

[3] Mıtıch, L.W. (1992). *The Nettles*, In: *Weed Technology*, vol. 6, p.1039

[4] Hartl, A., Vogl, C.R., *Dry matter and fiber yields, and the fiber characteristics of five nettle clones (Urtica dioica L.) organically grown in Austria forpotential textile use*, In: American Journal of Alternative Agriculture, 2002, vol. 17, issue 4, p.195

[5] Bodros, E., Baley, C., *Study of the tensile properties of stinging nettle fibres (Urtica dioica)*, In: Materials Letters, 2008, vol. 62, p. 2143

[6] Bacci L., Baronti S., Predieri S., Virgilio N. Di March, *Fiber yield and quality of fiber nettle (Urtica dioica L.), cultivated in Italy*, In: Industrial Crops and Products, 2009, vol. 29, issue 2–3, pp.480

[7] Taj, S., Ali Munawar, M., Khan S.U., *Natural fiber-reinforced polymer composites,* In: Proceedings Pakistan Academic Science, 2007, vol. 44, issue 2, p.129

[8] Nebel K., Reutlingen Research Institute, Niutex, Aufschlussverfahren für Bastfasern, Verfahren des Faseraufschlusses für Bastfasern am Beispiel von Hanf und Nessel, http://niutex.ch/wp-content/uploads/2010/05/100416_N_Ref_Nebel.pdf, Accessed on 2014.

[9] Huang, G., *Nettle (Urtica cannabina L) fibre, properties and spinning practice*, In: Journal of the Textile Institute, 2005, vol. 96, issue 1, p.11

[10] Cook, J.G., *Handbook of textile fibres 1: natural fibres*, England: Merrow Publishing, 1984, 5th Edition.

[11] Kurban, M., *Isırgan Otu Lifinden Üretilen Kumaşların Ön Terbiye İşlemlerinin Araştırılması*, Yüksek Lisans Tezi, 2011, Turkey.

[12] Perkins W.S., *Textile coloration and finishing*, 1996, Durham North Carolina: Carolina Academic Press.

[13] Karmakar S.R., *Chemical technology in the pre-treatment processes of textiles*, Textile Science and Technology 12, 1999, Amsterdam: Elsevier.

[14] Choudhury A.K. Roy., *Textile preparation and dyeing*, 2006, New Hampshire: Science Publishers.

[15] Anis, P., Davulcu, A., Eren, H.A., *Enzymatic pre-treatment of cotton Part I. Desizing and glucose generation in dezising liquor*, In: Fiber & Textile in Eastern in Eastern Europe, 2008, vol. 16, issue 4, p.100

[16] Anis, P., Davulcu, A., Eren, H.A., *Enzymatic pre-treatment of cotton. Part II. Peroxide generation in dezising liquor and bleaching*, In: Fiber & Textile in Eastern in Eastern Europe, 2009, vol. 17, issue 4, p. 87

[17] Eren, H.A. Anis, P., Davulcu, A., *Enzymatic one-bath dezising-bleaching-dyeing process for cotton fabrics*, In: Textile Research Journal, 2009, vol. 79, issue 12, p.1091

[18] Hashem, M., El-Bisi, M., Sharaf, S., Refaie, R. (2010). *Pre-cationization of cotton fabrics: An effective alternative tool for activation of hydrogen peroxide bleaching process*, In: Carbohydrate Polymers, 2009, vol. 79, p. 533

[19] Topalovic, T., Nierstrasz, V. A., Bautista L., Jocic, D., Navarro, A., Marijn, M. C., Warmoeskerken G. (2007). *Analysis of the effects of catalytic bleaching on cotton*, In: Cellulose, vol. 14, p. 385

[20] Lee, J.J., Hinks, D., Lim S.H., Hauser, P., *Hydrolytic stability of a series of lactam-based cationic bleach activators and their impact on cellulose peroxide bleaching*, In: Cellulose, 2010, vol. 17, p. 671

[21] Brooks R. E., Moore. S. B., *Alkaline hydrogen peroxide bleaching of cellulose,* 2000, In: Cellulose, vol. 7, p. 263.

[22] Zeronian, S.H., Inglesby, M. K., *Bleaching of cellulose by hydrogen peroxide*, In: Cellulose, 1995, vol. 2, issue 4, p. 265

[23] Ichimura, H., Umehara, R., Karakawa, T., Oshima, K., Nakase, K., Animal *fiber superior in shrink proofing and method for preparation thereof*, 2005, US Patent 6969409.

[24] Sando, Y., Nakano, E., Ishidosfiro, H., Sando, K., *Method and apparatus for the pretreatment of a cloth*, 1995, *US Patent 5407446.*

[25] Prabaharan, M., Venkata R. J., *Application of ozone on textile materials – A review*, In: Colourage, 2001, vol.48, issue 11, p. 25

[26] Avinc, O., Eren, H. A., Uysal, P., *Ozone applications for after-clearing of disperse-dyed poly(lactic acid) fibres*, In: Coloration Technology, 2012, vol. 128, p. 479

[27] Eren, H.A., Avinc, O., Erismis, B., *Comparison of different ultrasound support methods during colour and chemical oxygen demand removal of disperse and reactive dyebath solutions by ozonation*, In: Coloration Technology, 2012, vol. 128, p. 446

[28] Avinc, O., Eren, H. A., Uysal, P., Wilding, M., *The effects of ozone treatment on soybean fibres*, In: Ozone: Science and Engineering, 2012, vol. 34, p. 143

[29] Eren, H. A., *Afterclearing by ozonation: a novel approach for disperse dyeing of polyester,* In: Coloration Technology, 2006, vol. 122, issue 6, p. 329

[30] Eren, H.A., Anis, P., *Surface trimer removal of polyester fibers by ozone treatment, In:* Textile Research Journal, 2009, vol. 79, issue 7, p. 652

[31] Vigo, T.L., *Textile processing and properties*, Textile Science and Technology 11, 1994, Elsevier, Amsterdam.

[32] Fan, Q., *Chemical testing of textiles*, 2005, England: Woodhead Publishing Ltd.

[33] He, Z., Song, S., Xia, M., Qiu, J., Ying, H., Lü, B., Jiang, Y., Chen, J. , *Mineralization of C.I. reactive yellow 84 in aqueous solution by sonolytic ozonation*, In: Chemosphere, 2007, vol. 692, p. 191

[34] Houck Max M., *Identification of textile fibers,* 2009, England: Woodhead Publishing Ltd.

[35] Tarakçıoğlu, I., *Kimyasal tekstil muayeneleri*, 1979, Izmir, Turkey.

Authors:

MUTLU KURBAN[1]
ARZU YAVAŞ[2]
OZAN AVİNÇ[2]
HÜSEYİN AKSEL EREN[3]

[1]Vocational School of Technical Sciences
Çukurova University, Adana, Turkey

[2]Textile Engineering Department
Pamukkale University, 20070 Denizli, Turkey

[3]Textile Engineering Department
Uludağ University, Bursa, Turkey

e-mail: mkurban@cu.edu.tr; aozerdem@pau.edu.tr;
oavinc@pau.edu.tr; aksel@uludag.edu.tr

Corresponding author:

ARZU YAVAŞ
aozerdem@pau.edu.tr

Treatment of cotton with a laccase enzyme and ultrasound

OZAN AVINC
HÜSEYIN AKSEL EREN

BURCU ERIŞMIŞ
SEMIHA EREN

REZUMAT – ABSTRACT

Tratamentul bumbacului cu enzima tip lacază și ultrasunete

În acest studiu, au fost investigate efectele ultrasunetelor asupra tratamentului enzimatic cu lacază al țesăturilor din bumbac. Tratamentul enzimatic cu lacază al mostrelor de țesături de bumbac a fost efectuat cu ajutorul unui omogenizator cu ultrasunete (UH) și al unei băi cu ultrasunete (UB). Au fost determinate, în primul rând, concentrația enzimatică optimă, timpul și condițiile de temperatură pentru aplicarea enzimatică. Tratamentele cu ultrasunete au fost efectuate pe baza condițiilor optime obținute. Gradul de alb, gradul de galben, pierderea în greutate, grosimea materialului, rezistența la tracțiune, spectroscopia în infraroșu cu transformată Fourier (FTIR) și microscopia electronică de baleiaj (analiza SEM), precum și măsurarea COD a efluenților de proces, au fost efectuate. Gradul de alb al bumbacului a crescut ușor după tratamentul enzimatic cu lacază. Efectul enzimei a fost intensificat cu ajutorul energiei ultrasonice care a condus la o îmbunătățire a gradului de alb de până la 9,2%. Rezultatele au indicat că procesele din cadrul tratamentului enzimatic cu lacază nu au provocat nicio deteriorare semnificativă sau vreun efect și/sau nu au condus la nicio schimbare drastică negativă asupra morfologiei suprafeței fibrei de bumbac.

Cuvinte-cheie: lacază, bumbac, ultrasunete, omogenizator cu ultrasunete, enzimă

Treatment of cotton with a laccase enzyme and ultrasound

In this study, the effects of ultrasound on the enzymatic treatment of cotton fabrics with laccase were investigated. The laccase enzyme treatment of cotton fabric samples was carried out with the support of an ultrasonic homogeniser (UH) and an ultrasonic bath (UB). Optimum enzyme concentration, application time, and enzyme application temperature conditions were first determined. The ultrasound-supported treatments were performed with the obtained optimum conditions. Whiteness, yellowness, weight loss, fabric thickness, tensile strength, Fourier transform infrared spectroscopy (FTIR), and scanning electron microscopy (SEM) analysis, as well as COD measurement of the process effluents, were carried out. The whiteness of the cotton fabric slightly increased after the laccase enzyme treatment. The effect of the enzyme was intensified with the help of ultrasonic energy leading to up to a 9.2% whiteness improvement. Results indicated that the laccase enzyme treatment processes had no significant degradative damage or effect and/or did not lead to any drastic detrimental change to the surface morphology of the cotton fibre.

Keywords: laccase, cotton, ultrasound, ultrasonic homogenizer, enzyme

INTRODUCTION

High levels of water and chemicals are consumed during conventional textile finishing. Therefore, research on novel processes to decrease water and chemical consumption continues. The use of enzymes for textile finishing treatments such as scouring and bleaching has become an accepted strategy for overcoming these issues [1–3]. Untreated cotton fibres exhibit a natural yellowish/brownish colour and a bleaching process is usually applied with hydrogen peroxide [4–11].

Research on enzymatic treatment with laccases and glucose oxidases (GOx) has been reported for the bleaching of cotton. Laccase treatment enhances the whiteness of cotton fabrics. GOx enzymes also improve the whiteness of cotton by converting glucose into hydrogen peroxide in the desizing bath and utilising the generated hydrogen peroxide for bleaching [12–17].

Ultrasound is acoustic energy in the form of waves with a frequency above the hearing range of humans.

The shockwaves generated by cavitation bubbles during ultrasound treatment create an ideal stirring mechanism at the solid–liquid interface, leading to an increase in the overall reaction rate [18–21]. Basto et al. applied a laccase and ultrasound pre-treatment prior to hydrogen peroxide bleaching and reported that the laccase pre-treatment alone did not improve the fabric's whiteness, although a whiteness improvement of 1.67 Berger units was achieved after conventional oxidative bleaching of the enzymatically pre-treated samples [19]. Moreover, they reported a further 0.56 unit increase with the application of a combined ultrasound–enzyme pre-treatment [19]. Gonçalves et al. also reported a combined laccase–hydrogen peroxide process assisted by ultrasound. Similar to the study of Basto et al., a laccase assisted by ultrasound was applied as an enzymatic pre-treatment of cotton samples prior to hydrogen peroxide bleaching [19].

In this study, the effects of ultrasound on the laccase treatment of cotton fibre fabric were investigated. The

laccase treatment of cotton fabric samples was carried out with the support of an ultrasonic homogeniser (UH) and an ultrasonic bath (UB).

EXPERIMENTAL WORK

Materials and method

In this study, a desized and scoured plain-woven cotton fibre fabric with 25 warps/cm, 23 wefts/cm, and a weight of 164 g/m^2 was used in the experiments. The laccase enzyme was based on *Trametes versicolor* and supplied by Sigma Aldrich (USA).

Enzyme treatment

In order to make the enzyme process efficient, suitable enzyme concentration, application time and enzyme application temperature conditions were first determined.

Different concentrations of the laccase enzyme (0.01 g/L, 0.04 g/L, 0.08 g/L, 0.16 g/L, and 1 g/L) were applied to the cotton fabric at various temperatures (40, 50, and 60°C) at pH 5 (via an acetic acid–sodium acetate buffer) with a 1:20 liquor ratio for 30 minutes. After these enzyme treatments, each cotton fabric was after-treated by washing at 90°C for 10 minutes, rinsing at 70°C for 10 minutes, and then cold rinsing under tap water for 3 minutes.

After screening the enzyme concentrations and enzyme application temperatures, the most appropriate enzyme concentration and enzyme treatment temperature, according to the whiteness and yellowness results from Stage I, were chosen for the second stage of the study (Stage II). Therefore, in Stage II, 0.04 g/L of the laccase enzyme was applied at 40°C and pH 5 in varying periods of time (10, 20, and 30 minutes) on its own (Enzyme), with a UB (Enzyme + UB), and with a UH (Enzyme + UH). Cotton fabrics were washed at 90°C for 10 minutes following rinsing at 70°C for 10 minutes and cold rinsed under tap water for 3 minutes.

Combined use of laccase enzyme and ultrasound (Enzyme + UB and Enzyme + UH)

Two kinds of different ultrasound sources, UH and UB, were used in this study. A Bandelin Sonopuls HD2200 (20 kHz, probe type: VS70, 13 mm in diameter, 200 W HF-power, the pulsation and amplitude controls of the device were adjusted to 100% during the experiments, Germany) and Bandelin Sonorex RK103H (35 kHz, 140 W HF-power, Germany) were used for the UH and UB, respectively.

Whiteness and yellowness determination: The whiteness (Stensby index) and yellowness [ASTM D1925 yellowness index (YI)] of the samples were determined with a Konica Minolta CM3600d spectrophotometer (Japan).

Fabric weight measurements: Fabric weights after the respective ozonation processes were determined using a 1/1000 precision electronic balance, RADWAG PS 600/C/2 (Poland).

Fabric thickness determination: Fabric thickness properties were measured using an R&B Cloth Thickness Tester.

Fabrics' tensile strength measurements: Tensile strength testing was carried out in accordance with the ISO 13934 standard using an Instron Model 4301 tensile tester (USA).

Fourier transform infrared spectroscopy (FTIR): The infrared analysis was performed using a Thermo Nicolet 6700 FTIR microscope (USA) in attenuated total reflectance (ATR) mode, employing a diamond crystal at a resolution of 8 cm^{-1}.

Surface examination via scanning electron microscopy (SEM): A Carl Zeiss Evo 40 instrument (Germany), operating at an accelerating voltage of 5kV, was used for this purpose. In order to avoid problems due to charge build-up, the samples were sputter-coated with gold–palladium (%80Au–%20Pd) for two minutes in a BAL-TEC SCD 005 sputter-coating unit prior to examination.

Chemical oxygen demand (COD) evaluation: The COD values of the bath solutions were measured according to the standard titrimetric method (Standard Methods 5220C, APHA).

RESULTS

Effect of the laccase enzyme treatment conditions on whiteness and yellowness

The whiteness and yellowness values of the enzyme-treated cotton samples are given in table 1. The whiteness and yellowness values of the greige cotton fabric were 58.6 Stensby units and 23.5 YI, respectively. The whiteness of the cotton fabric distinctly increased after each laccase enzyme treatment (table 1). Simultaneously to the increases in whiteness, yellowness values decreased due to the enzymatic treatment. The whiteness value reached following the enzymatic process which was carried out with the lowest enzyme concentration (0.01 g/L) at the lowest temperature (40°C) was 62.1 Stensby units.

The whiteness and yellowness values reached following these enzymatic processes in the varying conditions were in the ranges of 62.0–62.7 Stensby units and 18.5–19.2 YI, respectively. The highest whiteness value (62.7 Stensby units) and lowest yellowness value (18.5 YI) were reached following enzyme treatment carried out at 40°C with 0.04 g/L enzyme (table 1). As the results obtained demonstrate, processing at high temperatures with high enzyme concentrations did not lead to a significant effect on whiteness. The enzymatic process carried out at lower treatment temperatures with lower enzyme concentrations leads to a more efficient and less energy-intensive enzymatic process.

Therefore, the best enzymatic process treatment conditions for the highest whiteness and the lowest yellowness were determined as 0.04 g/L of the laccase enzyme concentration and 40°C for the enzyme application temperature. A 7% improvement in whiteness was observed with these best process condi-

Table 1

EFFECT OF LACCASE TREATMENT ON COLOR AND WEIGHT LOSS OF THE SAMPLES					
Alternative	**Temperature (°C)**	**Enzyme Concentration (g/l)**	**Whiteness (Stensby)**	**Yellowness (ASTM D1925)**	**Weight Loss (%)**
No treatment	-	-	58.6	23.5	Reference
Enzyme treated samples	60	0.01	62.4	18.9	0.94
	60	0.04	62.5	18.8	0.83
	60	0.08	62.0	19.2	0.73
	60	0.16	62.1	19.1	0.85
	50	0.01	62.3	18.9	0.69
	50	0.04	62.5	18.9	0.76
	50	0.08	62.6	18.8	0.67
	50	0.16	62.2	19.1	0.87
	40	0.01	62.1	18.5	0.60
	40	0.04	62.7	18.5	0.63
	40	0.08	62.5	19.2	0.66
	40	0.16	62.5	18.9	0.73
	40	1	62.6	18.7	1.35

tions in comparison to the desized/scoured cotton fibre fabric.

Effect of the laccase enzyme treatment conditions on weight loss

Table 1 also shows the weight loss of the cotton fabrics after different enzyme treatments with varied temperature severities and enzyme concentrations. Each applied enzymatic treatment led to a weight loss of cotton fibre. Enzymatic processes carried out at 40, 50, and 60°C with 0.01, 0.04, 0.08, and 0.16 g/L enzyme concentrations led to weight loss in the range of 0.60–0.94%. Among these variant processes, no significant difference was observed with regard to weight loss. On the other hand, weight loss measured as a result of enzyme treatment carried out for control at 40°C with an extreme enzyme concentration of 1g/L of enzyme was 1.35%. The highest weight loss emerged as a result of this extreme enzyme concentration. The enzymatic process (0.04 g/L of enzyme at 40°C for 30 minutes) that gave the highest whiteness value did not lead to a significant weight loss of cotton fabric (0.63%).

Upon analysing the variant enzyme concentrations and temperature values, it was observed that the enzymatic treatment processed via 0.04 g/L of enzyme at 40°C led to a better whiteness value and a lower yellowness value without significant weight loss.

Whiteness, yellowness, and weight loss of cotton fabrics after different enzyme treatments

Table 2 displays the whiteness and yellowness values of cotton fabrics after different enzyme treatment types. Compared to greige fabric, only the Enzyme process increased the whiteness of the cotton up to 7.2%. The duration of the Enzyme process did not significantly affect the whiteness and yellowness

degree of cotton fibre. For instance, 10 minutes of enzyme treatment alone exhibited a whiteness of 62.6 Stensby units and a yellowness of 18.4 YI, whereas 30 minutes resulted in a whiteness of 62.7 Stensby units and a yellowness of 18.5 YI (table 2).

On the other hand, the effect of the enzyme was slightly intensified with the help of ultrasonic energy. Indeed, it is known that high-power ultrasound produces cavitation which facilitates particle disintegration or reactions. In this case, the effect of the enzyme strengthens with the application of the ultrasound energy. This enhanced whitening could be associated with improved diffusion of the enzyme from the liquid phase to the fibres' surface and throughout the textile fabric [19].

For example, 30 minutes of the Enzyme + UB process resulted in a whiteness value of 63.1 Stensby units and a 7.7% whiteness improvement. The Enzyme + UH process was more effective than the Enzyme and Enzyme + UB processes for the same application period due to the higher vibration activation of the UH probe. For instance, only 10 minutes of the Enzyme + UH process led to a whiteness value of 63.1 Stensby units and a 7.7% whiteness improvement.

This whitening improvement in the Enzyme + UH process could be explained by the expedited heterogeneous enzyme–cotton fibre reaction and the formation of reactive transient species because of the cavitation phenomenon during sonication [19].

The best whiteness and yellowness results were obtained from the Enzyme + UH. 30 minutes of the Enzyme + UH process led to a 9.2% improvement in whiteness (from 58.6 to 64.0 Stensby units).

The weight losses of the cotton fabrics after different enzyme treatments are shown in table 2. Each applied enzymatic treatment led to weight loss in the cotton fibre. Three different enzyme processes

Table 2

EFFECT OF ULTRASOUND SUPPORTON LACCASE TREATMENT RESULTS						
Alternative	Time (minutes)	Whiteness (Stensby)	Yellowness (ASTM D1925)	Thickness (mm)	Breaking Load (kN)	Elongation (%)
No treatment	-	58.6	23.5	0.630	0.37	26.0
Enzyme treated samples	10	62.6	18.4	0.640	0.40	27.5
	20	62.8	18.6	0.640	0.38	27.4
	30	62.7	18.5	0.640	0.39	28.4
Enzyme + UB	10	62.7	18.7	0.645	0.39	28.7
	20	63.2	18.4	0.645	0.38	29.1
	30	63.1	18.5	0.645	0.38	28.6
Enzyme + UH	10	63.1	18.5	0.645	0.38	27.8
	20	63.2	18.5	0.640	0.40	28.3
	30	64.0	17.6	0.645	0.40	29.0

(Enzyme, Enzyme + UB, and Enzyme + UH) applied for different durations (10, 20, and 30 minutes) led to weight loss in the range of 0.41–0.63%. No significant difference in weight loss was observed among these different processes. The Enzyme + UH process for 30 minutes, which created the highest whiteness value (64.0), did not lead to major weight loss (0.63%) in the cotton fabric.

Enzyme treatment with extreme enzyme concentration (1 g/L)

Enzyme treatments carried out at 40°C for 30 minutes with 1 g/L of enzyme (extreme enzyme concentration for pure enzyme usage) were included in the study for control. Processing with the variant enzyme combinations (Enzyme, Enzyme + UB and Enzyme + UH) and extreme enzyme concentrations did not lead to a significant effect on whiteness. On the other hand, weight loss values measured following the enzyme treatments carried out under extreme enzyme concentrations were considerably higher than those measured after enzyme treatments carried out with 0.04 g/L enzyme concentrations. The whiteness values were 62.6, 62.3, and 62.6 Stensby units and the weight loss values were 1.35%, 1.59%, and 1.48% for the Enzyme, Enzyme + UB, and Enzyme + UH treatments, respectively.

Fabric thickness of the cotton fabrics after different enzyme treatment types

The fabric thickness of the enzyme-treated (Enzyme, Enzyme + UB, and Enzyme + UH) cotton fabrics is shown in table 2. The fabric thickness of the greige cotton fabric was measured as 0.630 mm (table 2). All enzymatic processes at 40°C (Enzyme, Enzyme + UB, and Enzyme + UH) resulted in shrinkage of the cotton fabric, which led to an increase in the thickness of the fabric. Overall, fabric thicknesses of treated samples were very close to each other and varied between approximately 0.640 and 0.645 mm.

Tensile strength of the cotton fabrics after different enzyme treatments

The tensile strength of the enzyme-treated (Enzyme, Enzyme + UB, Enzyme + UH) cotton fabrics is shown in table 2. The tensile strength and elongation values of the greige cotton fabric were 0.37 kN and 26.0%, respectively. As expected, enzymatic processes with a laccase did not result in any negative effect or strength loss in the tensile properties (tensile strength and elongation) of the cotton fabric when it was compared with the greige fabric, as laccase enzyme treatment was carried out under mild pH conditions (pH 5) at a low temperature (40°C). Contrary to a decrease, all studied enzymatic processes (Enzyme, Enzyme + UB, and Enzyme + UH) resulted in slightly higher tensile strength results in comparison to greige fabric (table 2). This tensile strength increase can be explained by the fabric shrinkage. As mentioned earlier in the fabric thickness section, enzymatic processes at 40°C (Enzyme, Enzyme + UB, and Enzyme + UH) led to thicker fabrics due to fabric shrinkage (table 2). Moreover, the weft counts of the fabrics were 25,25.5–26,25.5–26, and 25.5–26 for the greige, Enzyme, Enzyme + UB, and Enzyme + UH samples, respectively.

Fourier transform infrared spectroscopy (FTIR)

The ATR-FTIR spectra of the laccase enzyme-treated cotton fabric samples (Enzyme, Enzyme + UB, Enzyme + UH) were investigated (figure 1). The constancy of the ATR-FTIR spectra (figure 1) displays that the respective laccase enzyme treatment processing types had no significant detrimental effect on the surface morphology of the cotton fibre. This agrees with the results on the tensile strength of the laccase-treated cotton fabrics (table 2), where no significant and/or drastic strength differences were noted between the respective samples.

SEM examination of fabrics

SEM micrographs of the laccase enzyme-treated cotton fabric samples (Enzyme, Enzyme + UB, Enzyme
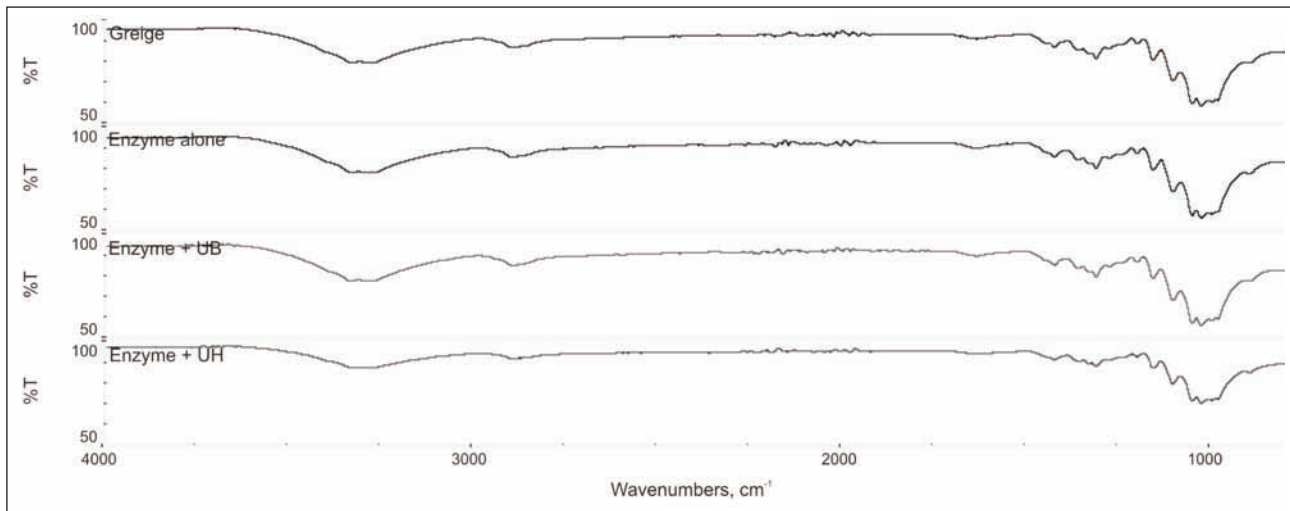
Fig. 1. FTIR (ATR) spectra of cotton fabrics after different laccase enzyme treatments
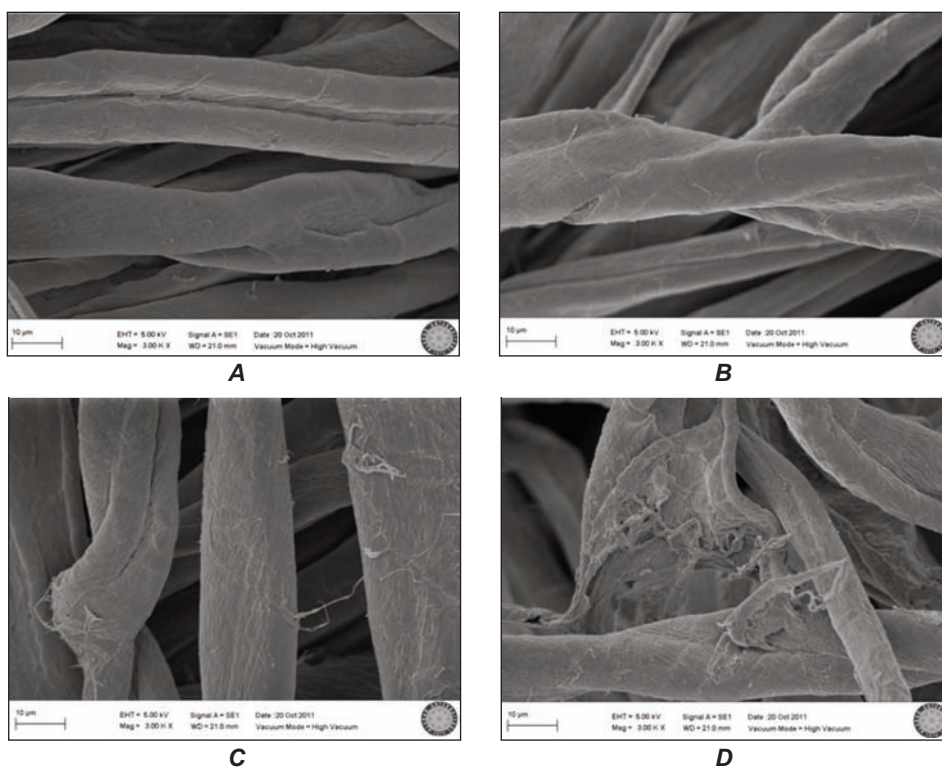
Fig. 2. Scanning electron micrographs of treated cotton fabrics with laccase
A – Greige cotton, B – Enzyme (*treated with only laccase enzyme with 0.04 g/l concentration at pH 5 and 40°C for 30 minutes*), C – Enzyme + UB (*Laccase enzyme with 0.04 g/l concentration at pH 5 and 40°C in Ultrasonic Bath for 30 minutes*), D – Enzyme + UH (*Laccase enzyme with 0.04 g/l concentration at pH 5 and 40°C with Ultrasonic Homogenizer for 30 minutes*)

+ UH) are shown in figure 2. The SEM micrograph of the greige cotton fabric (figure 2, A) exhibits smooth fibre surfaces. However, though the fibre shape and the fibre integrity did not alter following the different laccase enzyme treatments, there was some slight occurrence of fibrillation on the surface of the laccase enzyme-treated cotton fabrics after the Enzyme + UB and Enzyme + UH processes (figure 2, C and D). This slight surface topography alteration could be attributed to the oxidation/removal of the natural colouring matter, such as yellow/'creamy' chromophores, from the surface of the cotton fibre [22]. Nonetheless, this did not lead to any detrimental effect on the tensile strength values (table 2) or on the ATR-FTIR spectra (figure 1), although it did cause an improvement in the whiteness values (table 2). It is worth remarking that signs of pitting, cracking, or similar features, which would normally be associated with degradative damage, were not observed in any case.

Chemical oxygen demand (COD)

Chemical oxygen demand (COD) values of the laccase enzyme treatment effluent baths (Enzyme, Enzyme + UB, Enzyme + UH) are shown in table 3. There is no significant difference between the COD levels of the baths of Enzyme process and studied Enzyme + UB, Enzyme + UH processes.

Table 3

CHEMICAL OXYGEN DEMAND (COD) VALUES OF RESPECTIVE TREATMENT BATHS			
Alternative	**Time (minutes)**	**Temperature (°C)**	**COD (mg/l)**
Enzyme treated	30	40	1211
Enzyme + UB	30	40	1277
Enzyme + UH	30	40	1217

CONCLUSIONS

The whiteness of the cotton fabric increased after the laccase enzyme treatment. An increase in enzyme concentration did not lead to a significant increase in whiteness value. The best conditions for the Enzyme process in terms of the highest whiteness and the lowest yellowness were determined as a 0.04 g/L laccase enzyme concentration and 40°C enzyme application temperature, leading to a 7% improvement in whiteness.

The effect of the enzyme was slightly intensified with the help of ultrasonic energy. The Enzyme + UH process was more effective than the Enzyme and Enzyme + UB processes for the same application period due to the higher vibration activation of the UH probe.

The best whiteness and yellowness results were obtained with the Enzyme + UH process for 30 minutes, leading to a 9.2% whiteness improvement and again without significant weight loss in the cotton fabric.

None of the Enzyme, Enzyme + UB, or Enzyme + UH processes caused significant, drastic fabric thickness changes; nor did they result in a negative effect on or strength loss in the tensile properties (tensile strength and elongation) of the cotton fibre fabric, since laccase enzyme treatment was carried out under mild pH conditions (*p*H 5) at a low application temperature (40°C).

In line with the strength results, the constancy of the ATR-FTIR spectra and the visual examination of the SEM micrographs of treated cotton fabrics displayed that the respective laccase enzyme treatment processes had no significant degradative damage or effect and did not lead to any drastic detrimental change to the surface morphology of the cotton fibre.

BIBLIOGRAPHY

[1] Gonçalves, I., Herrero-Yniesta, V., Arce, I.P., Castañeda, M.E., Cavaco-Paulo, A. and Silva, C., *Ultrasonic pilot-scale reactor for enzymatic bleaching of cotton fabrics,* In: Ultrason. Sonochem., 2014, vol. 21, Issue: 4, pp. 1535–1543.

[2] Anis, P. and Eren, H.A., *Comparison of alkaline scouring of cotton vs. alkaline pectinase preparation,* In: AATCC Review, 2002, vol. 2, Issue: 12, pp. 22–26.

[3] Eren, H.A., Aniş, P. and Davulcu, A., *Enzymatic one-bath desizing – bleaching – dyeing process for cotton fabrics,* In: Text. Res. J.,2009, vol. 79, Issue: 12, 1091–1098.

[4] Karmakar, S. R., *Chemical technology in the pre-treatment processes of textiles*, Textile Science and Technology 12, Elsevier, Amsterdam, 1999.

[5] Shore, J., *Colorants and auxiliaries. Vol. 2 – Auxiliaries,* Society of Dyers and Colourists, West Yorkshire, England, 1990.

[6] Choudhury, A. K. R., *Textile preparation and dyeing*, Science Publishers, India, 2006.

[7] Lee, J.J., Hinks, D., Lim, S.H. and Hauser, P., *Hydrolytic stability of a series of lactam based cationic bleach activators and their impact on cellulose peroxide bleaching,* In: Cellulose, 2010, vol. 17, Issue: 3, pp. 671–678.

[8] Topalovic, T., Nierstrasz, V. A., Bautista, L., Jocic, D., Navarro, A., Warmoeskerken, M. C. G., *Analysis of the effects of catalytic bleaching on cotton,* In: Cellulose, 2007, vol. 14, Issue: 4, pp. 385–400.

[9] Brooks, R.E. and Moore, S.B., *Alkaline hydrogen peroxide bleaching of cellulose,* In: Cellulose, 2000, vol. 7, Issue: 3, pp. 263–286.

[10] Zeronian, S.H. and Inglesby, M.K., *Bleaching of cellulose by hydrogen peroxide,* In: Cellulose, 1995, vol. 2, Issue: 4, pp. 265–272.

[11] Perkins, W.S., *Textile coloration and finishing,* Carolina Academic Press, Durham North Carolina, 1996.

[12] Pereira, L., Bastos, C., Tzanov, T., Cavaco-Paulo, A. and Guebitz, G. M., *Environmentally friendly bleaching of cotton using laccases,* In: Environ. Chem. Lett., 2005, vol. 3, pp. 66–69.

[13] Tzanov, T., Costa, S.A., Gübitz, G.M. and Cavaco-Paulo, A., *Laccases to improve the whiteness in a conventional bleaching of cotton,* In: Macromol. Mater. Eng., 2003, vol. 288, pp. 807–810.

[14] Tzanov, T., Costa, S.A., Gübitz, G.M. and Cavaco-Paulo, A., *Bio-preparation of cotton fabrics,* In: Enzyme Microb. Tech., 2001, vol. 29, Issue: 6, pp. 357–362.

[15] Buschle-Diller, G. and Xiang, D.Y., *Enzymatic bleaching of cotton fabrics with glucose oxidase,* In: Text. Res. J., 2004, vol. 71, pp. 388–394.

[16] Eren, H.A., Aniş, P., Yılmaz, D., Kirişçi, Ş. and Inkaya, T., *Combined use of laccase, ozone and hydrogen peroxide for cotton bleaching,* In: Tekst. Konfeksiyon, 2009, vol. 19, Issue: 4, p. 299.

[17] Davulcu, A., Eren, H.A., Avinc, O. and Erişmiş, B., *Ultrasound assisted biobleaching of cotton,* In: Cellulose, vol. 21, Issue: 4, pp. 2973–2981.

[18] Capelo-Martínez, J. L., *Ultrasound in chemistry: analytical applications.* Wiley-VCH Verlag GmbH & Co. KGaA, Weinheim, 2009.

[19] Basto, C., Tzankov, T. and Cavaco-Paulo, A., *Combined ultrasound-laccase assisted bleaching of cotton,* In:Ultrason. Sonochem., 2007, vol. 14, Issue: 3, pp. 350–354.

[20] Yachmanev, G.V., Blanchard, E. J. and Lambert, A.H., *Use of ultrasonic energy for intensification of the bio-preparation of greige cotton,* In: Ultrasonics, 2004, vol. 42, pp. 87–91.

[21] Yachmanev, G.V., Bettoniere, N.R. and Blanchard, E.J., *Intensification of the bio-processing of cotton textiles by combined enzyme/ultrasound treatment,* In: J. Chem. Technol. Biot., 2002, vol. 77, Issue: 5, pp. 559–567.

[22] Mitchell, R., Carr, C.M., Parfitt, M., Vickerman, J.C. and Jones, C., *Surface chemical analysis of raw cotton fibres and associated materials,* In: Cellulose, 2005, vol: 12, Issue: 6, pp. 629–639.

Authors:

OZAN AVINC[1]
HÜSEYIN AKSEL EREN[2]
BURCU ERIŞMIŞ[2]
SEMIHA EREN[2]

[1]Pamukkale University, Textile Engineering Department, Denizli, TURKEY
[2]Uludag University, Textile Engineering Department, Bursa, TURKEY
e-mail: ozanavinc@yahoo.com; aksel@uludag.edu.tr;
buycu_22@hotmail.com; semihaeren@uludag.edu.tr

Corresponding author:

HÜSEYIN AKSEL EREN
aksel@uludag.edu.tr

Characterization and modeling of compression behaviors of biodegradable polydioxanone biliary stent for human body

YANHUI LIU   PEIHUA ZHANG

REZUMAT – ABSTRACT

Caracterizarea și modelarea comportamentului la compresie al stentului biliar biodegradabil din polidioxanonă pentru corpul uman

Această lucrare prezintă un studiu al comportamentului la compresie al stenturilor biliare biodegradabile din poli-dioxanonă, pentru corpul uman. Pentru a investiga efectul numărului de pori (ochiuri) asupra proprietăților de compresie ale stentului,au fost realizate patru tipuri de stenturi biliare din polidioxanonă cu număr diferit de pori pe baza structurii tip rețea de împletire manuală. Stenturile biliare finite din polidioxanonă au fost investigate în ceea ce privește răs-punsurile la compresie. Rezultatele obținute au evidențiat comportamentul la compresie al stenturilor, care se intensifică pe măsură ce numărul de pori crește. Răspunsurile la compresie și caracteristicile de forță compresie-deplasare la compresie ale stenturilor au fost, de asemenea, examinate prin metoda elementelor finite. Modelele elementelor finite ale stenturilor create de Abaqus au fost dezvoltate cu scopul de a simula experimente realizate pe stenturi biliare din polidioxanonă. Modelul numeric dezvoltat pe baza răspunsurilor forță compresie-deplasare la compresie a stenturilor este prezentat pentru a arăta o imagine adecvată a comportamentului experimental la compresie.

Cuvinte-cheie: stenturi biliare biodegradabile din polidioxanonă, comportament la compresie, metoda elementelor finite

Characterization and modeling of compression behaviors of biodegradable polydioxanone biliary stent for human body

This paper presents a study of the compression behaviors of biodegradable polydioxanone biliary stents developed for human body. To investigate the effect of braid-pin number on the compression properties of the stent, four types of polydioxanone biliary stents having different braid-pin number were fabricated based on the hand-braiding net structure. The finished polydioxanone biliary stents were characterized for the compression responses. The findings obtained indicate that the compression behaviors of the stents increase as the braid-pin number increases. The compression responses and compression force-compression displacement characteristics of the stents are also examined by the finite element method. The stents finite element models established by Abaqus were developed to simulate experiments performed on polydioxanone biliary stents. The numerical model based on compression force-compression displacement responses of the stents is shown to successfully capture the experimental compression behaviors.

Keywords: biodegradable polydioxanone biliary stents, compression behaviors; finite element method

INTRODUCTION

Benign biliary stricture (BBS) is the universal disease and complication in the biliary surgery field. The most common benign biliary strictures are iatrogenic stric-ture and stricture caused by chronic pancreatitis. Shanbhogue *et al*. pointed out that cholecystectomy and orthotopic liver transplantation were the common iatrogenic causes of benign biliary stricture, a spec-trum of diseases such as pancreatitis, autoimmune cholangitis, PSC and Mirizzi syndrome can also result in biliary stricture [1]. Hiroshi Shimada *et al*. reported that BBS was treated by three options. The surgery, a traditional mainstay of treatment, is asso-ciated with significant morbidity and mortality rates of approximately 9.1–28% and 0–2.6%, respectively [2, 3, 5]. With the development of endoscopic technolo-gy, endoscopic treatment with balloon dilation obtained greater application due to the advantage of less damage for human body. Endoscopic stenting treatment, as the technology developed later, owned higher success rate as compared to the other treat-ments [6]. Pitt HA *et al.* revealed that the recurrence

of jaundice or cholangitis due to postoperative biliary stricture to be much less likely after endoscopic bal-loon dilation than surgery [7]. However, because of avoiding liver puncture and accessing non-dilated intrahepatic ducts, endoscopic stenting treatment was preferable. Recently, it is a tendency that the biliary stents which were applied to treat BBS were fabricated from biodegradable materials on account of good biocompatibility and dilation properties. Giovanni Mauri *et al.* have evaluated feasibility and safety of patients treated with biodegradable biliary stents [8].

Currently, the biodegradable materials used for bil-iary stents include polyglycolic acid (PGA), polylactic acid (PLA), polycaprolactone (PCL), polydioxanone (PDO) etc. PDO material, as the more widely used biodegradable material, is degraded with low-toxicity to CO_2 and H_2O, and has good biocompatibility and safety [9–10]. The monofilament with smooth surface and good mechanical property can be obtained by melt spinning processes [11]. PDO monofilament used

DETAILED PARAMETERS OF PDO MONOFILAMENT					
Material	Diameter (mm)	Linear density (Tex)	Crystallinity (%)	Tensile Strength (N)	Modulus (N·Tex^{-1})
PDO	0.36	145.38	70.67	45.92	1.23

for human body had further obtained the certification of FDA (U.S. Food and Drug Administration) [12]. Many finite element method (FEM) works have studied different mechanical properties of stainless steel stents such as expansion, flexibility, fatigue and stent–tissue interactions, etc. [13–16]. Wei Wu *et al.* optimized the safety properties of biodegradable magnesium alloy stents (decreased the maximum principal stress after recoil with tissue by 29%, and decreased the maximum principal strain during expansion by 14%) and scaffolding ability (increased by 24%) by finite element analysis [17]. However, a few papers studied mechanical properties of biodegradable polymer stents by FEM, Zhiwen Que *et al.* evaluated theoretical value of the radial force of PDO coronary stent by FEA, but don't verify the simulation by the experimenting [18].

In the abovementioned literatures, few researchers were focused on compression behaviors of the biodegradable polydioxanone biliary stent with rhombic mesh structure. Moreover, there is still lack of the biodegradable polydioxanone biliary stent model with rhombic mesh structure to accurately simulate compression behaviors of biliary stent by FEA method.

In this paper, the biodegradable biliary stent with rhombic mesh structure was fabricated with PDO monofilament. To investigate the effect of braid-pin number on the compression properties of the Stent, four types of polydioxanone biliary stents having different braid-pin number were prepared based on the hand-braiding with rhombic mesh structure. At last, the finite element analysis, a classical method to analyze mechanical properties of the stents, was applied to simulate experiment results.

EXPERIMENT

Biliary stent design and fabrication

In this paper, PDO monofilament with 0.36 mm in diameter was involved for biliary stent. The detailed parameters of the PDO monofilament are shown in table 1.

The biliary stents with net structure were fabricated with PDO monofilament using a self-made cylinder of copper pipe mould. After finishing the braiding processes of the biliary stent, the heat setting process was carried out for the mould and biliary stent in an environment of 75°C for about 15 min. The structure of biliary stent was provided in figure 1. MTN-DA metallic stent with same net structure (Micro-Tech Nanjing CO., Ltd.) and the different braiding parameters involved for the evaluation are listed in the table 2.

STRUCTURE PARAMETERS OF PDO BILIARY STENTS				
Stent type	Braid–pin number	Axial length (mm)	External diameter (mm)	Internal diameter (mm)
1	6	44	9.43	8
2	8	44	9.52	8
3	10	44	9.56	8
4	12	44	9.67	8
MTN–DA metallic stent	8	70	9.3	8

Compression tests

In this paper, the compression tests were conducted by using YG601 radial compression instrument (Laizhou Electronic Instrument Co., Ltd) in our laboratory as
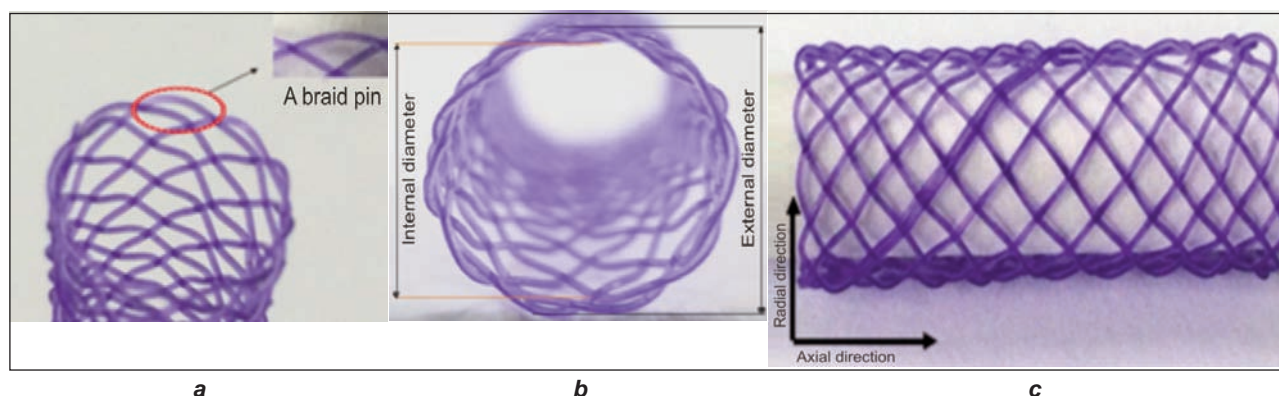

Fig. 1. The surface structure of PDO biliary stent: (a) a braid pin; (b) the cross section; (c) the axial structure
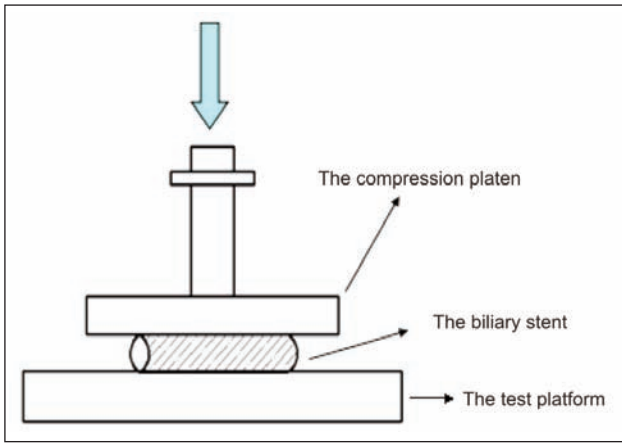
Fig. 2. Schematic representation for the radial compression performance test

biliary stents. When compression displacement reaches 50% of the initial biliary stent diameter, the compression platen was stopped, and the force value at this time is defined as the radial force. After staying 5 seconds, the compression platen was back to original position at a speed of 20 mm/min, and three repeats were carried out for each specimen.
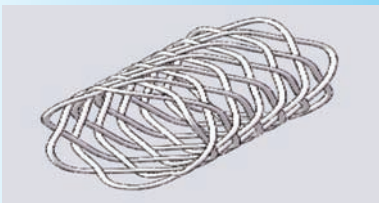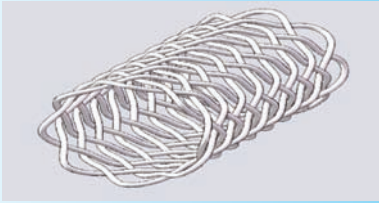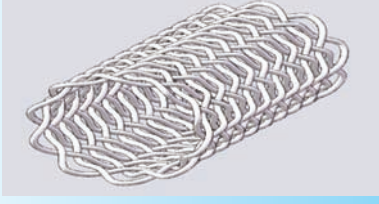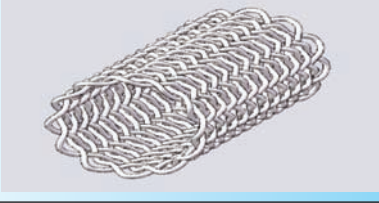
The finite element simulation for Compression tests

According to experimental results, the effect of the braid-pin number on the radial force can be obviously found. In order to have a better understanding of the relationship between the braid-pin number and compression force, the finite element method was applied to simulate the experimental results.

The design of the stent model

Based on actual biliary stents, with the internal diameter of 8 mm, four stent models were established with 44 mm in length by Solidworks software. All the stent models have the same structural parameters except the braid-pin number, which are 6, 8, 10 and 12, respectively. The detailed parameters involved for evaluation are illustrated in table 3.

shown in figure 2. The stent specimens were pressed to a deformation within 50% of the initial biliary stent diameter which is the internal diameter of biliary stent at a load speed of 20 mm/min [19]. The size of the compression platen is 60 mm in length and 24.5 mm in width. In the compression process, the compressions' initial height is defined as the position in which the compression platen just makes contact with the

Table 3

THE MODEL OF THE BILIARY STENTS			
Stent type	**Structural parameter**		**The models of biliary stent**
	internal diameter (mm)	**axial length (mm)**	
6 braid–pins biliary stent	8	44	
8 braid–pins biliary stent	8	44	
10 braid–pins biliary stent	8	44	
12 braid–pins biliary stent	8	44	
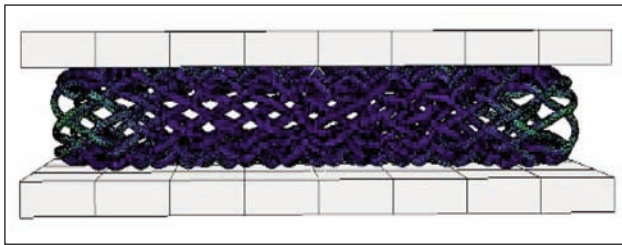
1
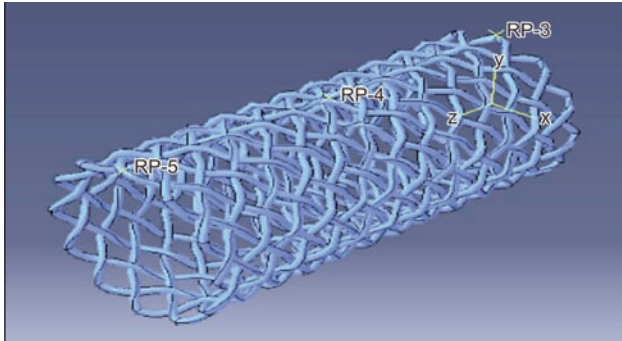
2

Fig. 3. The compression model and the compressed stent:
1 – The compression model; *2* – The compressed stent

Compression simulation tests

The compression model was built by ABAQUS/ Explicit 6.10.1 software (Dassault systems simulia Corp., Providence, RI, USA). The plate compression method was applied for simulation of the stent, two top and bottom plates having the size of 45 mm × × 10 mm × 2 mm were developed, as shown in the figure 3 (1). In the simulation process, the two plates were defined as the rigid body. The top platen would be compressed downward at the speed of 1 mm/min and the bottom plate was constrained in ALL DOF during the whole compression process, while the compression displacement was set as 5 mm. The parameters which were defined in the simulation are shown in table 4.

The relationship between the compression force and the stress value can be given as follow:

$$\sigma = \frac{F}{S} \qquad (1)$$

where *F* is the compression force, *S* – the compression contact area. Based on Eq. (1), the stress value increases with the increasing of compression force.

RESULTS AND DISCUSSION

The analysis of compression-recovery curve of PDO biliary stents

The average compression-recovery curve of three experimental results for PDO biliary stents are shown in the figure 4.

Referring to the figure 4, it is clear that the compression-recovery curve can be divided into four stages according to the slope of curve. In the initial phase of compression process (stage A), the compression force increased linearly with rising of compression distance. This is due to the fact that the PDO monofilament begins to be compressed when the compression platen touched the biliary stent. With further increasing of compression distance, the slope of compression curve becomes moderate, as shown in stage B in figure 4. The PDO monofilaments in the
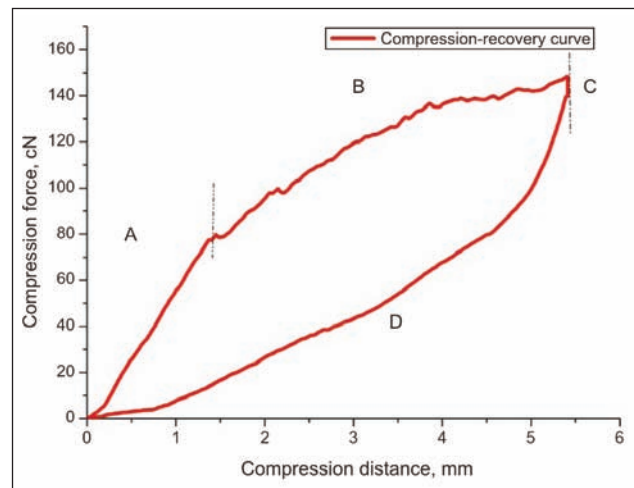
Fig. 4. Compression-recovery curve of PDO biliary stents

Table 4

THE PARAMETERS IN THE SIMULATION	
Parameter	**Extent**
The yarn property	The yarn property was defined as the elastic material. Young, s modulus: 1.5Gpa; Poisson's ratio: 0.35; Density: 1.45 g·mm^{-3}.
The top and bottom plates property	The yarn property was defined as the stainless steel material. Young, s modulus: 210 Gpa; Poisson's ratio: 0.25; Density: 7.80 g·mm^{-3}.
Step	One step was defined in the simulation, namely Step–1. The solver of the step is ABAQUS⁄Explicit.
Meshing scheme	The top and bottom plates were meshed with an 8–node linear brick, reduced integration, hourglass control; The biliary stent was meshed with a 10–node modified quadratic tetrahedron.
Boundary condition	The boundary condition of the top plate: U1 = U3 = UR1 = UR2 = UR3 = 0, U2 = –5 mm; The boundary condition of the bottom plate: U1 = U2 = U3 = UR1 = UR2 = UR3 = 0.
Contact algorithms	The contact definition in the FE model between the plates and biliary stent model was 'GENERALCONTACT'

Table 5

THE RELATIONSHIP BETWEEN THE NUMBER OF INTERLACING POINTS AND BRAID–PIN NUMBER				
Stent types	6 braid–pins biliary stent	8 braid–pins biliary stent	10 braid–pins biliary stent	12 braid–pins biliary stent
The number of interlacing points	66	120	190	276

stent having net structure intertwine to each other, so the slippage emerged among the PDO monofilaments after overcoming their friction. In the stage C, the compression force adds up to the maximum value when compression distance reached the pre-set compression distance, and then there is a stress relaxation phenomenon in the staying period of 5 second. Obviously, in the initial phase of stage D, the slope of curve is larger as compared to the end phase of the stage D due to the elastic recovery of PDO monofilaments. However, the compression force in stage D decreases with the decreasing of compression distance.

The effect of the structural parameter on compression behaviors

Based on the relationship between the number of interlacing points and biliary stent with different braid-pin number provided in the table 5, the number of braid pin can be defined the independent variables 'x', while the number of interlacing points was defined the dependent variables 'y'. The quadratic function can be given as follows:

$$y = ax^2 + bx + c \quad (a \neq 0, c \text{ constant}) \quad (2)$$

According to the coordinates (6, 66), (8, 120) and (10, 190), the constant factors 'a', 'b' and 'c' in the quadratic function can be obtained respectively. Thus, the quadratic function transforms into:

$$y = 2x^2 - x, x \in (6,8,10,12) \quad (3)$$

Where 'y' is the interlacing points in the biliary stent, 'x' is the braid-pin number.

When the independent variables 'x' is 12, the dependent variables 'y' is equal to 276 obtained by equation 3, thus, the relationship (as shown in equation 3) between the number of interlacing points and biliary stent with different braid-pin number can be established. The quadratic function curve is plotted as shown in figure 5.

As depicted in figure 5, the interlacing points increase with the increasing number of braid pins. The biliary stents were fabricated by different number of braid-pin, as shown in table 2. With same internal diameter of
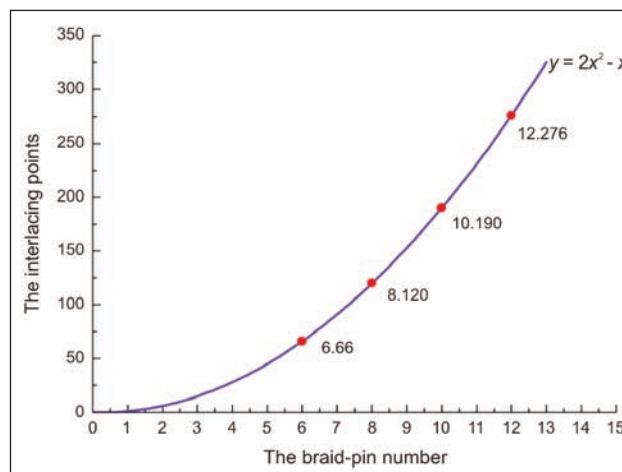
Fig. 5. The quadratic function curve

biliary stent, PDO monofilament diameter and axial length of biliary stent, the surface structure of different braid-pin number of biliary stents are shown in figure 6 to better understand increasing density of the interlacing points in the biliary stents with increasing braid-pin number.

The biliary stents with different number of braid-pin were characterized for compression responses. Because of different interlacing point number caused by different braid-pin number in four kinds of biliary stents, the results show that whereas the 12 braid-pin and 6 braid-pin biliary stents exhibits the highest and lowest values, respectively, the 10 braid-pin and 8 braid-pin biliary stents have middle values between the highest and lowest values as shown in figure 7.

As shown in the table 6, the elastic recovery rate of four types biodegradable biliary stents are close to that of MTN-DA metallic stent, so the biodegradable biliary stent designed by us meets absolutely the elasticity requirement.

The effect of the structural parameter on radial force

The compression force value at the position that compression distance reaches 50% of the stent diameter

Table 6

THE ELASTIC RECOVERY RATE OF BILIARY STENTS					MTN–DA Metallic stent
The biodegradable biliary stent					
The braid–pin number	6	8	10	12	91
The elastic recovery rate	86.2	91	89.1	92	
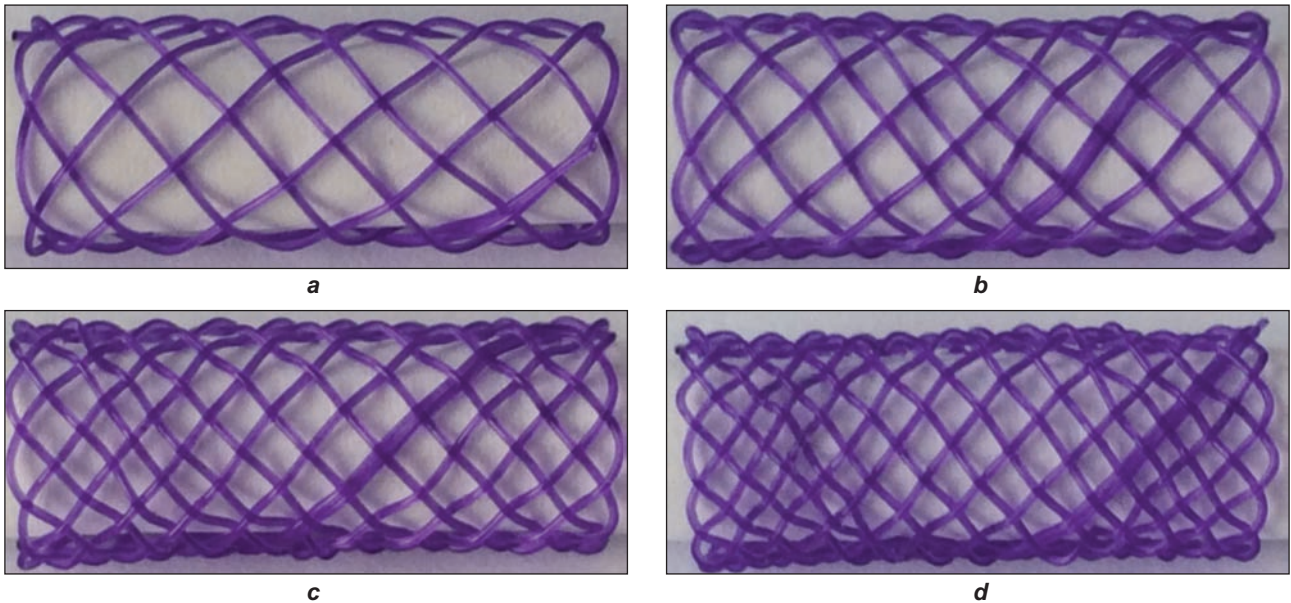
Fig. 6. The surface structure of different braid-pin number of biliary stents:
a – 6 braid-pins biliary stent; *b* – 8 braid-pins biliary stent;
c – 10 braid-pins biliary stent; *d* – 12 braid-pins biliary stent
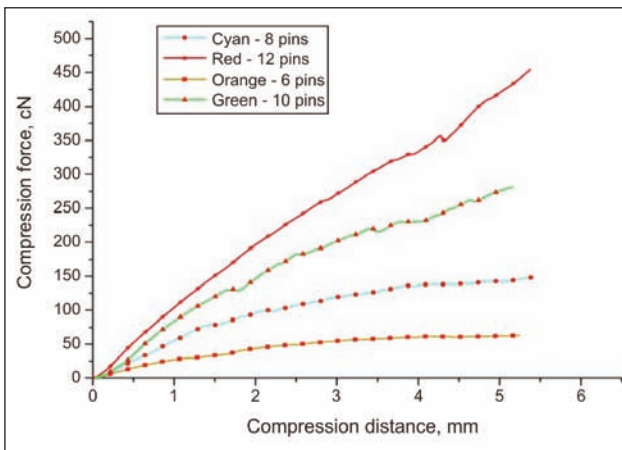
Fig. 7. The curve of different braid-pin number of the biliary stents
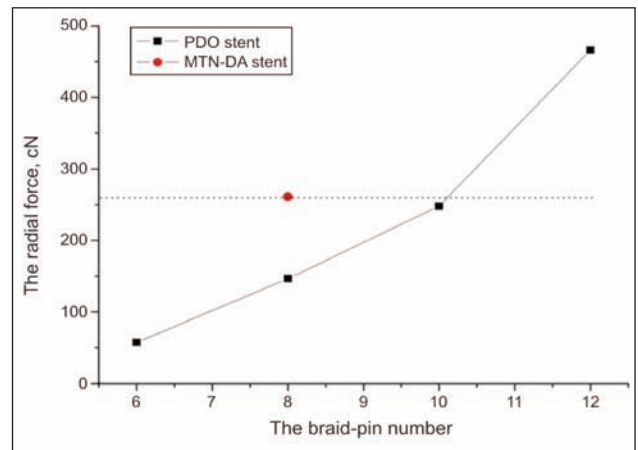
Fig. 8. The effect of braid-pin number on the radial force

is defined as radial force. The findings obtained from the compression tests conducted on the stents with different braid-pin numbers reveals that the radial force value increases with the increasing of braid-pin number, the radial force value of the 10 braid-pins biliary stent is close to MTN-DA metallic stent, and the radial force value of 12 braid-pins biliary stent is higher than MTN-DA metallic stent as shown in figure 8,

so the biodegradable biliary stent designed by us meets absolutely the mechanical requirement.

Analysis of the simulation results

According to compression simulation, when the compression distance reaches a displacement of 50% of the stent diameter as shown in table 7, the relationship between the compression force and the compression displacement in the compression process

Table 7

THE COMPRESSION DISPLACEMENT IN EXPERIMENT AN SIMULATION				
Stent types	6 braid–pin stent/mm	8 braid–pin stent/mm	10 braid–pin stent/mm	12 braid–pin stent/mm
Displacement in experiment	4.715	4.76	4.78	4.835
Displacement in simulation	5	5	5	5
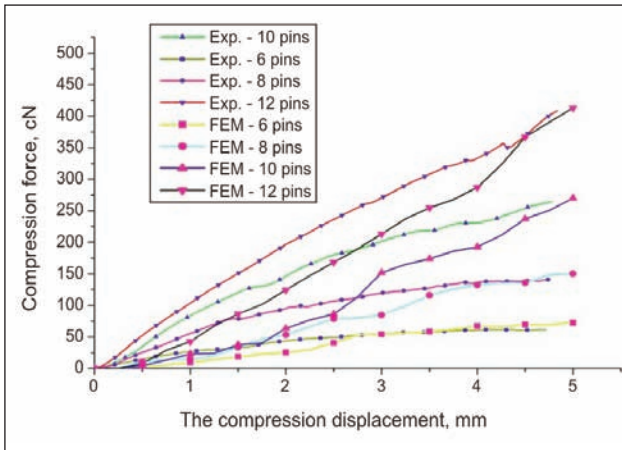
Fig. 9. The comparison between FEM curve and experimental curve
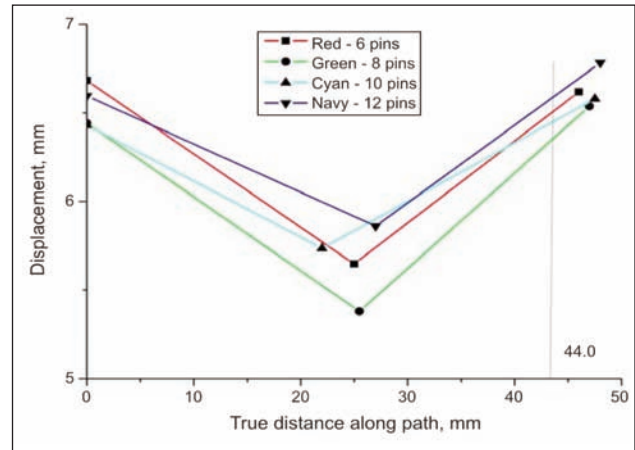
Fig. 10. The displacement curve of three points in biliary stent
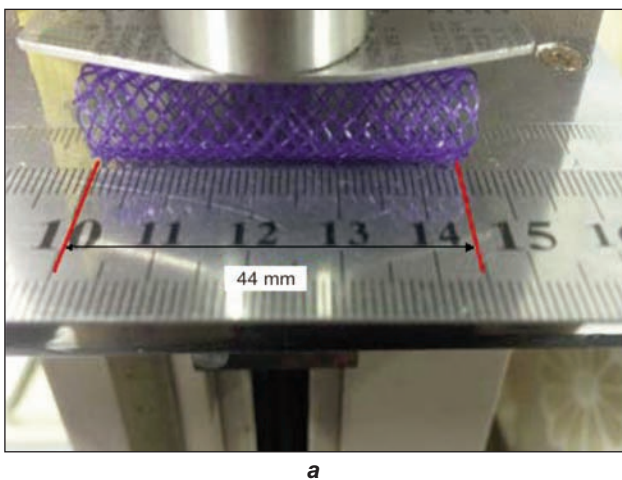
a
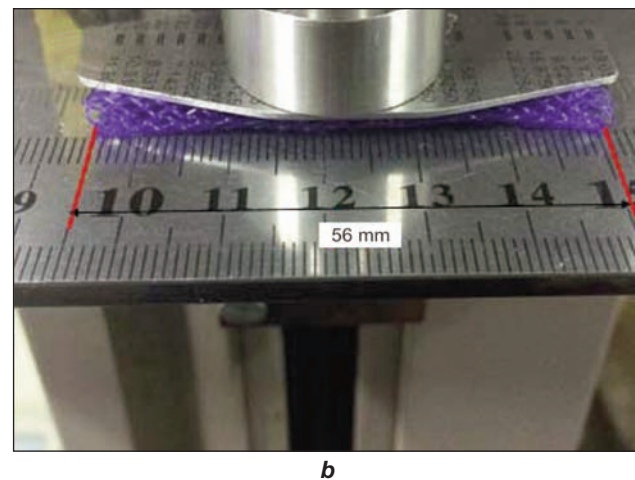
b

Fig. 11. The axial extension of biliary stent in the compression process:
a – the original length of biliary stent; *b* – the length of biliary stent after compression

can also be obtained from the simulation. The force-displacement curve based on the simulation results is provided in figure 9. At the same time, the experimental results are compared in the same figure. From the comparison results, it is clear that the simulation and experimental results have good agreement with each other, indicating that the simulation results can be given a reference to the investigation of biliary stents. However, it also can be found that the force value of each simulation curve in a big chunk of the whole compression process is lower than that in the corresponding experimental curve respectively, but the force value of end part in each simulation curve is higher than that in the corresponding experimental curve. Because of that the PDO monofilaments are simplified as homogeneous continuum and isotropy in the finite element simulation, while, the PDO monofilaments in the biliary stent will undergo complicated non-simultaneous slippage in experimental.

The points in the figure 3 (2) were defined as the path (RP-3 → RP-4 → RP-5). The displacements of three points in each biliary stent during the compression process are shown in figure 10. According to dis-

placements of these three points, the different displacements of three points in the same biliary stent reveal that the slippage between PDO monofilaments has appeared during compression process. The different displacements of three points in the different biliary stent illustrate that the deformation degrees of each stent is different. It is evident that true distance along the path is longer than 44 mm length of biliary stent as a result of the extension phenomenon during the compression process. The result of simulation has a good agreement with the experimental test as shown in figure 11.

According to above studies of good agreement between experiment and simulation, the actual stress variation of biliary stents is accurately projected by the simulation. Based on the compression simulation tests, the stress contours of biliary stent with different braid-pin number are depicted in the figure 12. It can be seen that the maximum stress value is occurred at the interlaced position between PDO monofilaments and the ends of biliary stent as shown in figure 12 (1), which is same with stress contour of other stents. According to the comparison results for the biliary stents with different braid-pin number, the emerging
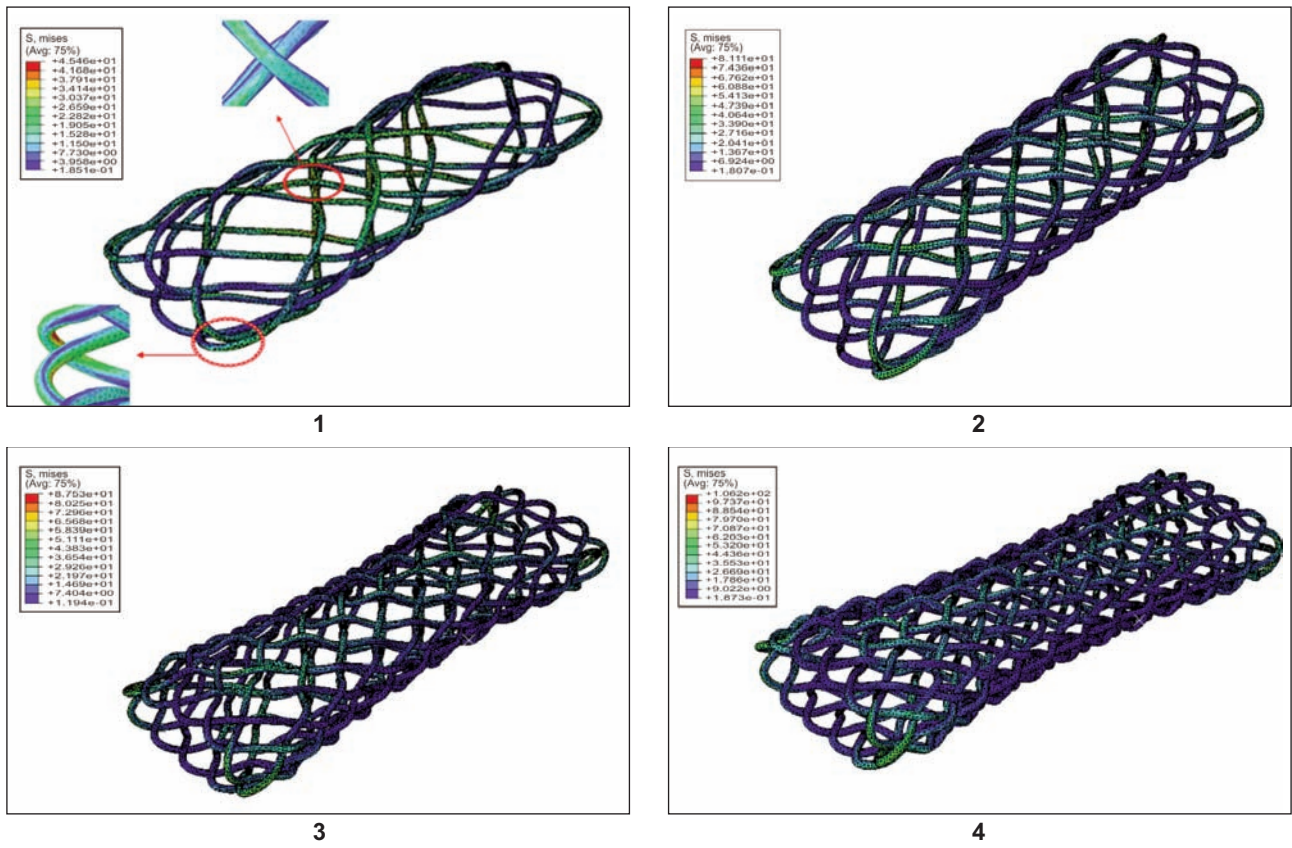
Fig. 12. The stress contour of biliary stent with different braid-pin:
1 – The 6 braid-pins biliary stent; *2* – The 8 braid-pins biliary stent;
*3* – The 10 braid-pins biliary stent; *4* – The 12 braid-pins biliary stent
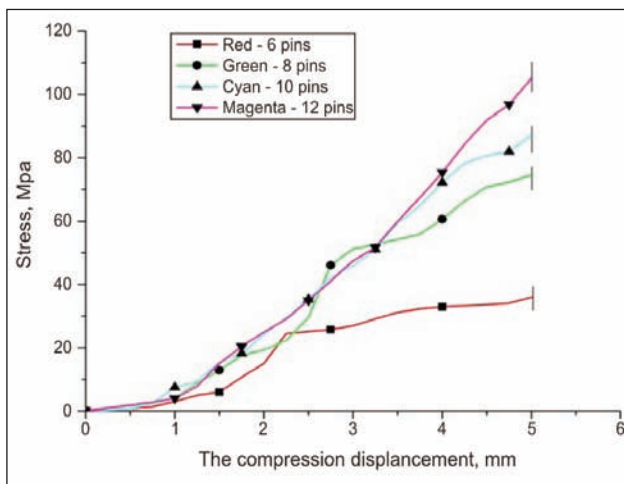

Fig. 13. The stress curves of biliary stent

stress has a tendency that the stress value increases as the braid-pin number involved in fabrication increases.

The stress-displacement curves during the compression process are obtained as well, as shown in the figure 13. According to stress- displacement curves, the variation trend of stress value for four kinds of biliary stents is the same, revealing that the stress value for all the biliary stents increases with the increasing of compression time, and the maximum value of stress increases as the braid-pin number increases.

CONCLUSION

In this paper, the compression behaviors of biodegradable polydioxanone biliary stent for human body, have been investigated. The following conclusions were established through this work:

Based on the compression results of biliary stents with different braid-pin numbers the compression force increases as the braid-pin number increases.

According to the experimental simulation by using the finite element method, the simulation and experimental results exhibit good agreement with each other, indicating that the finite element model is feasible and the simulation results can be seen as the guidance for the further study of the biodegradable polydioxanone biliary stents to optimize biliary structure. It is clearly seen that the maximum stress value is occurred at the interlaced position between PDO monofilaments and the ends of biliary stent. By comparing the biliary stents with different braid-pin number, it is revealed that the emerging stress increases with the increasing of braid-pin number. So, the conclusion is that the structure parameter, namely the braid-pin number, strongly affects the compression force and stress of the biliary stent whose value increases with increasing braid-pin number.

BIBLIOGRAPHY

[1] Shanbhogue A.K.P., Alampady K.P., Tirumani, S.H. *Benign Biliary Stricture: A Current Comprehensive Clinical and Imaging Review*, In: American Journal of Roentgenology, 2011, vol. 197, no. 2, pp. W295–W306

[2] Hiroshi S., Itaru E. *The current diagnosis and treatment of benign biliary stricture*, In: Surgery Today, 2012, vol. 42, no. 12, pp. 1143–1153

[3] Raute M., Podlech P., Jaschke W., Manegold B.C., Trede M. *Management of bile duct injuries and strictures following cholecystectomy*, In: World Journal of Surgery, 1993, vol.17, no. 4, pp. 553–562

[4] Frattaroli F.M., Reggio D., Guadalaxara A., Illomei G., Pappalardo G. *Benign biliary strictures: a review of 21 years of experience*, In: Journal of the American College of Surgeons,1996, vol.183, no. 5, pp. 506–513

[5] Tocchi A., Mazzoni G., Liotta G., Costa G., Lepre L., Miccini M. *Management of benign biliary strictures: biliary enteric anastomosis vs. endoscopic stenting*, In: Archives of Surgery, 2000, vol. 135, no. 2, pp. 153–157

[6] Isayama H., Nakai Y., Togawa O., Kogure H., Ito Y., Sasaki T. *Covered metallic stents in the management of malignant and benign pancreatobiliary strictures*, In: Journal of Hepato-Biliary-Pancreatic Surgery, 2009, vol. 16, no. 5, pp. 624–627

[7] Pitt H.A., Kaufman S.L., Coleman J. *Benign postoperative biliary strictures – Operate or dilate*, In: Annals of Surgery, 1989, vol. 210, no. 4, pp. 417–425

[8] Giovanni M., Caterina M. *Biodegradable biliary stent implantation in the treatment of benign bilioplastic-refractory biliary strictures: preliminary experience,* In: Journal European Radiology, 2013, vol. 23, no. 12, pp. 3304–3310

[9] Zhai W.Q., Zhen H.Y., Xing H.C. *The in vitro degradation study of two degradable intravascular stents materials*, In: Proceedings of 2011 International Forum Biomedical Textile Materials, vol. 1, Shanghai, China, 29 May 2011

[10] Zhai W.Q., Zhen H.Y., Xing H.C. *The in vitro degradation study of biodegradable intravascular stents of two different materials,* In: Proceedings of 2012 International Forum Biomedical Textile Materials, vol. 1, Shanghai, China, 29 May 2012

[11] Wang Y.H., Dou H.J. *Dynamic mechanical properties of biodegradable stents*, In: Journal of Shanghai Jiao Tong University, 2010, vol. 44, no. 11, pp. 1605–1609

[12] Docob D.F., Sacristan P.C., Flor C.B. *Randomized clinical study of polydioxanone and nylon sutures for Laparotomy closure in high-risk patients,* In: Cirugia Espanola, 2006, vol. 79, no. 5, pp. 305–309

[13] Houman Z., Daniel J.K., Houman Z., Caitriona L. *Simulation of a balloon expandable stent in a realistic coronary artery-Determination of the optimum modeling strategy,* In: Journal of Biomechanics, 2010, vol. 43, no. 11, pp. 2126–2132

[14] Wei W. *An FEA method to study flexibility of expanded coronary stents,* In: Journal of Materials Processing Technology, 2007, vol. 184, no. 2, pp. 447-450

[15] Li J.J., Qi Y.L., Xie Z.Y., Zeng Y.J. *Fatigue life analysis and experimental verification of coronary stent,* In: Heart and Vessels, 2010, vol. 25, no. 4, pp. 333–337

[16] Claudio C., Francesca G., Lorenza P., Gabridle D., Francesco M. *Assessment of tissue prolapse after ballon-expandable stenting: Influence of stent cell geometry,* In: Medical Engineering&Physics, 2009, vol. 31, no. 4, pp. 41–447

[17] Wei W., Petrini L., Gastaldi D. *Finite element shape optimization for biodegradable magnesium alloy stents.* In: Annals of Biomedical Engineering, 2010, vol.38, no. 9, pp. 2829–2840

[18] Que Z.W., Zhang P.H. *Radial force analysis of polydioxanone coronary stent by finite element method*, In: Journal of Donghua University, 2013, vol. 30, no. 5, pp. 373–377

[19] Xu H.J., Zhang P.H. *Preparation and radial compression performance of PDO intravascular stent*, In: Journal of Donghua University, 2014, vol. 40, no. 4, pp. 418–423

Authors:

YANHUI LIU[1,2]
PEIHUA ZHANG[1,2]

Donghua University
[1]College of Textile
[2]Key of Laboratory of Textile Science &Technology, Ministry of Education, China Technology,
2999 North Renmin Road,Shanghai,201620
P.R. China
e-mail: chainliuyanhui1@163.com, phzh@dhu.edu.cn

Corresponding author:

PEIHUA ZHANG
phzh@dhu.edu.cn

Optimizing the functionality of the willowing machine regarding recoverable materials

IOAN FILIP
DANIELA FARIMA
GEORGIOS PRINIOTAKIS

MIHAI CIOCOIU
RALUCA MARIA AILENI

REZUMAT – ABSTRACT

Optimizarea funcţionării maşinii de destrămat pentru materiale textile recuperabile

Industria de tapiţerie este una dintre marii consumatori de materiale textile recuperabile. Fibrele obţinute din prelucrarea prin destrămare a acestor materiale constituie o sursă de materii prime de calitate şi preţ acceptabile. Fibrele recuperate, rezultat al procesului de destrămare, constituie una dintre cele trei componente ale procesului de destrămare, alături de capetele de fire şi material recuperat nedestrămat. Pentru optimizarea randamentului, s-a realizat modelul matematic al procesului de destrămare. Parametrii tehnologici ai maşinii de destrămat, viteza de alimentare şi viteza de destrămare, constituie variabile de intrare ale modelului matematic, iar procentul de fibre recuperate, procentul de capete de fire şi procentul de material recuperat nedestrămat sunt cele trei rezultante ale modelului matematic. Modelele matematice se analizează din punct de vedere tehnologic şi grafic. Rezultatele acestor analize, sunt valorile optime ale parametrilor de intrare cu care se realizează cele mai bune randamente ale procesului de destrămare.

Cuvinte-cheie: destrămare, modelare matematica, optimizare, recuperare, tehnologie, textile

Optimizing the functionality of the willowing machine regarding recoverable materials

Upholstery industry is one of the biggest consumers of recoverable textiles. The fibers obtained by tearing process of these materials, are a source of raw material with quality and acceptable price. The fibers recovered from tearing process are one of the three components of tearing process, together with ends yarns and remains unprocessed material. To optimize the tearing process, a mathematical model was performed. Parameters of tearing machine, feed rate and speed of teasing, are input variables of the mathematical models and the percentage of recovered fiber, percentage of ends yarns and the percentage of recovered material, are the three resultants of mathematical model. Mathematical models are analyzed in terms of technology and graphics. The results of these analyzes, are the optimal values of input parameters, with the best yields achieved in the process of willowing.

Keywords: willowing, mathematical modeling, optimization, recoverable, technology, textile

INTRODUCTION

One of the sources not nearly insignificant of raw material for the industry of upholstery is represented by the scraps of material resulted after cutting tricots from polyacrylonitrile yarn in the clothing manufactory. These recovered materials are supplied to an aggregate for their processing, which in the first stage cuts the waste, thereafter they are passed through a thread opener. The result of this processing consists of oakum of graded wool, a quantity of non-teased yarns and a quantity of unprocessed remained knit. This teased fiber is the fiber recovered by processing on a willowing machine of waste knit from the knitting industry polyacrylonitrile yarns. These recovered fibers are used in the production of bulky nonwoven textiles under the denomination of upholstery cotton. The type of operation of the opening aggregate is very important for the economy of the society, and that is why a research was conducted in respect of performances of this aggregate "Margasa", respectively of its performance.

EXPERIMETAL PART

In order to analyze the performance of the aggregate of recoverable processing, mathematical models were achieved for the operation of this "Margasa" willowing machine. It was used the software application Optex, using a central, compound, rotatable program of the second order, based on a work matrix with 13 experiments [1, 2]. Each experiment which consists of the result of the processing of a weight of 100 kg waste was repeated 5 times, the average of these results being used as value measured in obtaining the 3 mathematical models. These mathematical models are y_1 – percentage of teased fibers, y_2 – percentage of non-teased yarns and y_3 – percentage of remained knit. In table 1 are presented the natural and coded values of entry variables, namely x_1 – rate of feed [m/min] of the willowing machine and x_2 – rate of feed of the willowing machine [m/min] [4, 6, 7]. With these values we compiled the work matrix in table 2.

The general equation 1 suggested is of the type, according to [3, 5, 6].

$$Y_1 = b_0 + b_1x_1 + b_2x_2 + b_{12}x_1x_2 + b_{11}x_1^2 + b_{22}x_2^2 \quad (1)$$

NATURAL AND CODED VALUES OF ENTRY VARIABLES						
Denomination of the entry variable	UM	Coded values				
		−1.414	−1	0	1	1.414
		Real values				
Rate of feed (x_1)	[m/min]	7.172	8.000	10.000	12.000	12.828
Rate of opening (x_2)	[m/min]	3.586	4.000	5.000	6.000	6.414

No.	X_{1cod}	X_{1real}	X_{2cod}	X_{2real}	Y_{meas}	Y_{calc}	D [%]
				WORK AND EXPERIMENTAL MATRIX			
1	+1	12.000	+1	6.000	61.500	62.008	0.8
2	−1	8.000	+1	6.000	48.000	50.336	4.9
3	+1	12.000	−1	4.000	54.500	52.526	3.6
4	−1	8.000	−1	4.000	49.800	49.654	0.3
5	−1.414	7.172	0	5.000	50.300	48.638	3.3
6	+1.414	12.828	0	5.000	58.000	58.921	1.6
7	0	10.000	−1.414	3.586	48.500	49.886	2.9
8	0	10.000	+1.414	6.414	59.200	57.073	3.6
9	0	10.000	0	5.000	48.600	48.773	0.4
10	0	10.000	0	5.000	52.100	48.773	6.4
11	0	10.000	0	5.000	47.900	48.773	1.8
12	0	10.000	0	5.000	48.300	48.773	1.0
13	0	10.000	0	5.000	46.900	48.773	4.0

RESULTS AND DISCUSSIONS

1. Optimizing the functionality of the willowing machine

The run of the software application OPTEX with the values, measured results in the work matrix allowed to obtain the mathematical models analyzed hereinafter.

1.1. Mathematical model of the percentage of teased fibers y_1

In the work matrix from table 2 the measured values of y resulted from experiments, the calculated values of the resulting y_1 and the value of the Adler test are presented.

The application OPTEX displays the control of significance of coefficients and the final form of the mathematical model as it is noticed in table 3.

The answer equation is of the type 2.

$$Y_1 = 48.773 + 3.661x_1 + 2.566x_2 + 2.150x_1x_2 +$$
$$+ 2.491x_1^2 + 2.341x_2^2 \qquad (2)$$

Testing the adequacy of the model with the Fisher-Snedecor test, automatically run by the software application OPTEX shows that the model is adequate [3, 6].

$$F_{calc} = 1.683$$
$$F_{tab} = 6.590$$

$F_{calc} < F_{tab}$ – the model is adequate.

SIGNIFICANCE ANALYSIS OF REGRESSION COEFFICIENTS		
Value of the coefficient	Value of the Student test	Decision
b_0 = 48.773	db0 = ± 1.766	b_0 – significant
b_1 = 3.661	db1 = ± 1.396	b_1 – significant
b_2 = 2.566	db2 = ± 1.396	b_2 – significant
b_{12} = 2.150	db12 = ± 1.974	b_{12} – significant
b_{11} = 2.491	db11 = ± 1.497	b_{11} – significant
b_{22} = 2.341	db22 = ± 1.497	b_{22} – significant

The coordinates of the new center S:
$$x_{1s} = -0.621$$
$$x_{2s} = -0.263$$

The rotation angle of axles x_1 and x_2: α = 43.005°.

As all coefficients are significant, the regression equation is 2.

The analysis of model's coefficients shows that in view of positive signs of numerical coefficients, both of the linear and square part, the variation towards the superior limits of values of variables x_1 and x_2 shall ensure the increase of the percentage of teased
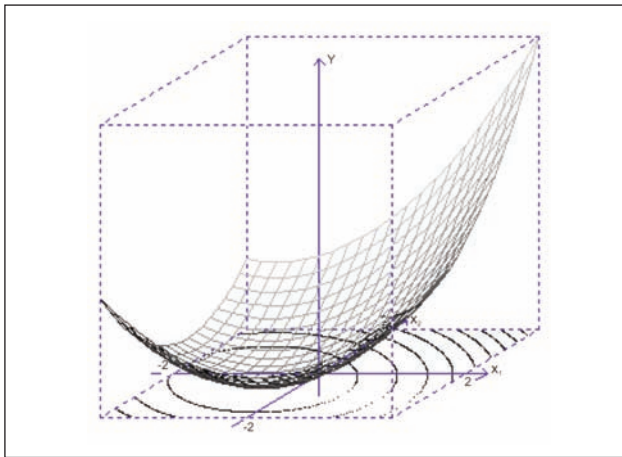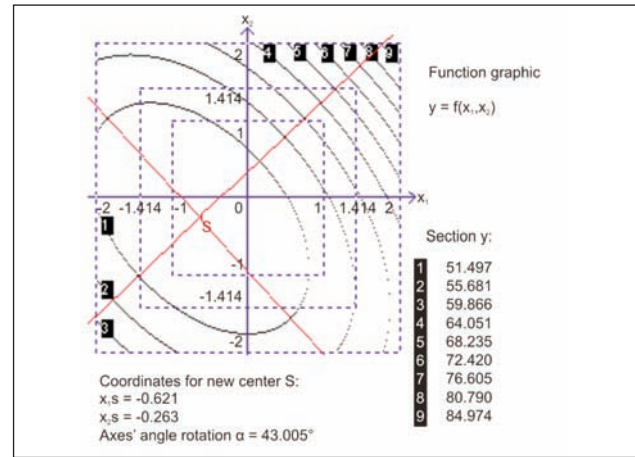
Fig. 1. 3D Graphic $y_1 = f(x_1,x_2)$

Function graphic
$y = f(x_1,x_2)$

Section y:

1	51.497
2	55.681
3	59.866
4	64.051
5	68.235
6	72.420
7	76.605
8	80.790
9	84.974

Coordinates for new center S:
$x_1s = -0.621$
$x_2s = -0.263$
Axes' angle rotation $\alpha = 43.005°$

Fig. 2. 2D Graphic $y_1 = f(x_1,x_2)$

Table 4

THE EXPERIMENTAL AND WORK MATRIX

No.	X_{1cod}	X_{1real}	X_{2cod}	X_{2real}	Y_{meas}	Y_{calc}	D [%]
1	+1	12.000	+1	6.000	35.750	34.466	3.6
2	−1	8.000	+1	6.000	47.664	51.000	6.5
3	+1	12.000	−1	4.000	44.240	45.620	3.1
4	−1	8.000	−1	4.000	47.660	46.989	1.4
5	−1.414	7.172	0	5.000	46.280	48.556	4.9
6	+1.414	12.828	0	5.000	38.880	38.257	1.6
7	0	10.000	−1.414	3.586	48.730	47.671	2.2
8	0	10.000	+1.414	6.414	37.550	40.262	7.2
9	0	10.000	0	5.000	49.670	49.394	0.6
10	0	10.000	0	5.000	46.050	49.394	7.3
11	0	10.000	0	5.000	50.370	49.394	1.9
12	0	10.000	0	5.000	49.820	49.394	0.9
13	0	10.000	0	5.000	51.010	49.394	3.2

fibers. The 3D graphical representation from figure 1 of the regression equation is a well-contoured surface represented by a parabolic. This has the accessional side of the surface oriented towards the positive area of variables x_1 and x_2, which suggests that the use of a pair of values x_1, x_2 in this quadrant shall allow the increase of the percentage of teased fibers correspondingly achieved.

The assertion is also confirmed by the analysis of the 2D representation of the equation. Consistent level curves from figure 2, resulted from the intersection of the 3D surface (figure 1) with plans y_1 constant, of which results that the constant level curve that represent high values of the resultant are placed in the area of the first quadrant.

For example, in order to obtain a percentage of oakum of graded wool of about 59%, the pair of variables x_1 x_2 must be placed within the range {+1,414 and +1,414}.

1.2. The mathematical model of the percentage of non-teased threads

In the work matrix from table 4 the measured values of the exit variable y_2 resulted from experiments, the

Table 5

TESTING THE SIGNIFICANCE OF REGRESSION COEFFICIENTS

Value of the coefficient	Value of the Student test	Decision
$b_0 = 49.394$	$db_0 = + 1.732$	b_0 – significant
$b_1 = -3.642$	$db_1 = - 1.369$	b_1 – significant
$b_2 = -2.620$	$db_2 = - 1.369$	b_2 – significant
$b_{12} = -2.958$	$db_{12} = - 1.937$	b_{12} – significant
$b_{11} = -2.995$	$db_{11} = - 1.469$	b_{11} – significant
$b_{22} = -2.715$	$db_{22} = - 1.469$	b_{22} – significant

calculated values of the resultant y_2 and the value of the Adler test are presented. The result of data processing is presented in table 5.

The adequacy of the model is also tested with the Fischer Snedecor, finding that the model ensures the representation of the real technological process, with 95% probability. In the table 2 the additional testing with the Adler test (column D) highlights the adequate character of the mathematical model y_2.
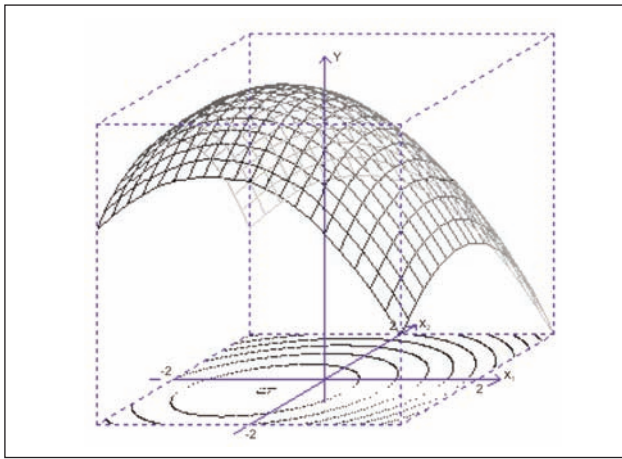
Fig. 3. Graphic 3D $y_2 = f(x_1, x_2)$

Function graphic

$y = f(x_1, x_2)$

Section y:

1	18.580
2	22.163
3	25.746
4	29.329
5	32.912
6	36.494
7	40.077
8	43.660
9	47.243
10	50.825

Coordinates for new center S:
$x_1s = -0.528$
$x_2s = -0.483$
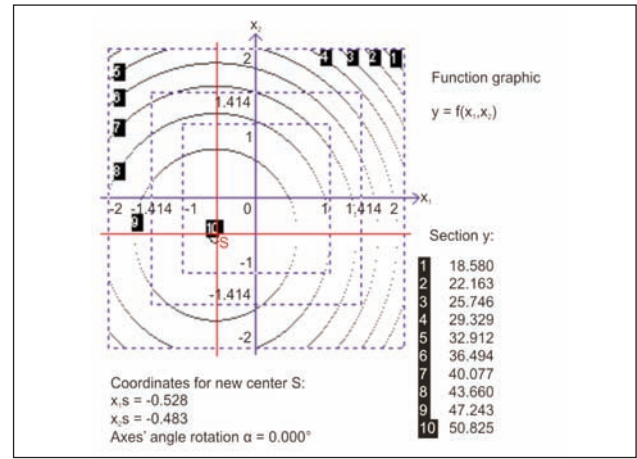Axes' angle rotation $\alpha = 0.000°$

Fig. 4. 2D Graphic $y_2 = f(x_1, x_2)$

As all coefficients are significant, the regression equation is the one mentioned above, finding that the model is adequate.

Equation 3 is the answer equation.

$$Y_2 = 49.394 - 3.642x_1 - 2.620x_2 - 2.958x_1x_2 - 2.995x_1^2 - 2.715x_2^2 \qquad (3)$$

Testing the adequacy of the model:

$$F_{calc} = 2.593$$

$$F_{tab} = 6.590$$

$F_{calc} < F_{tab}$ – the model is adequate.

The coordinates of the new center S are:

$$x_{1s} = -0.506$$

$$x_{2s} = -0.207$$

The rotation angle of axles x_1 and x_2: $\alpha = 42.297°$

Analyzing the regression equation, it is noticed that all numerical coefficients are negative, which suggests that the variation towards the superior limits of the experimental region for the entry variables x_1 and x_2, shall result in the corresponding reduction of

non-teased yarns. This consideration is corroborated with the observation from the interpretation of the mathematical model y_1. The 3D graphic of y_2 from figure 4 which represents a parabolic with maximal point shows that the variation of pairs of values x_1x_2 in the first quadrant ensures the reduction of the percentage of non-teased yarns.

The situation is also confirmed by the analysis of the 2D chart from figure 3 where constant level curves that represent the reduced values of the percentage of non-teased yarns is placed in the area of the first quadrant.

For example, in order to get a quantity of 30–32% non-teased material, the variables x_1 and x_2 must get values as in the previous case in the area {+1,414 and +1,414}.

1.3. The mathematical model of the percentage of remained knit, y_3

In the work matrix from table 6 the measured values of y_3 resulted from experiments, the calculated values of the resultant y_3 and the value of the Adler test

Table 6

No.	X_{1cod}	X_{1real}	X_{2cod}	X_{2real}	Y_{meas}	Y_{calc}	D [%]
				THE EXPERIMENTAL AND WORK MATRIX			
1	+1	12.000	+1	6.000	2.750	3.001	9.1
2	−1	8.000	+1	6.000	3.100	3.224	4.0
3	+1	12.000	−1	4.000	1.960	1.978	9.2
4	−1	8.000	−1	4.000	2.540	2.832	11.5
5	−1.414	7.172	0	5.000	3.420	3.228	5.6
6	+1.414	12.828	0	5.000	3.120	2.749	11.9
7	0	10.000	−1.414	3.586	2.770	2.370	14.4
8	0	10.000	+1.414	6.414	3.250	3.087	5.0
9	0	10.000	0	5.000	1.730	1.857	7.3
10	0	10.000	0	5.000	1.850	1.857	0.4
11	0	10.000	0	5.000	1.730	1.857	7.3
12	0	10.000	0	5.000	1.880	1.857	1.2
13	0	10.000	0	5.000	2.090	1.857	11.1

Fig. 5. 3D Graphic $y_3 = (x_1, x_2)$

Coordinates for new center S:
$x_1 s = -0.367$
$x_2 s = -0.543$
Axes' angle rotation α = 30.398°

Section y:
1	2.208
2	2.697
3	3.187
4	3.677
5	4.166
6	4.656
7	5.145
8	5.635
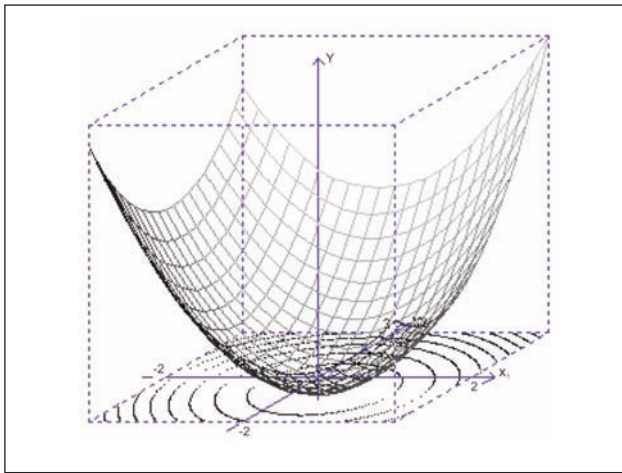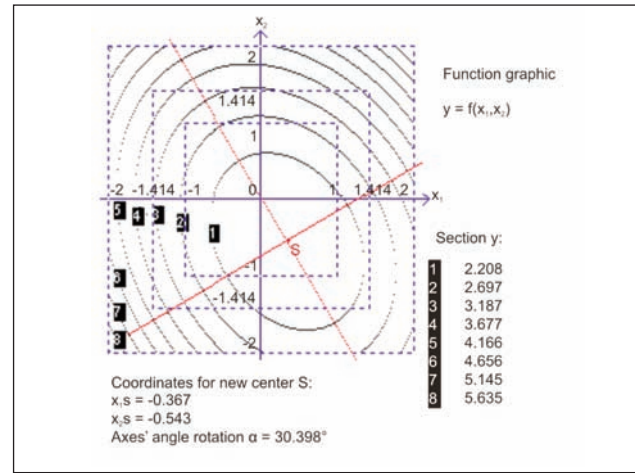
Fig. 6. Chart $y_3 = (x_1, x_2)$

Table 7

TESTING THE SIGNIFICANCE OF REGRESSION COEFFICIENTS		
Value of the coefficient	Value of the Student test	Decision
$b_0 = 1.857$	$db_0 = +0.132$	b_0 – significant
$b_1 = -0.169$	$db_1 = -0.104$	b_1 – significant
$b_2 = 0.254$	$db_2 = -0.104$	b_2 – significant
$b_{12} = 0.058$	$db_{12} = +0.148$	b_{12} – significant
$b_{11} = 0.566$	$db_{11} = -0.112$	b_{11} – significant
$b_{22} = 0.436$	$db_{22} = -0.112$	b_{22} – significant

are presented. The table 7 presents the results of the test of significance of numerical coefficients.

The answer equation is equation 4.

$$y_3 = 1.857 - 0.169x_1 + 0.254x_2 +$$
$$+ 0.566x_1^2 + 0.436x_2^2 \quad (4)$$

Testing the adequacy of the model:

$$F_{calc} = 10.707$$
$$F_{tab} = 6.590$$

$F_{calc} > F_{tab}$ – the model is not adequate!
The coordinates of the new center S:

$$x_{1s} = 0.150$$
$$x_{2s} = -0.291$$

The rotation angle of axles x_1 and x_2: α = 0.000°
The adequacy of the model is tested with the Fischer-Snedecor test, finding that the model ensures the correct representation of the real technological process, with 95% probability. In table 6 the additional testing with the Adler test (column D%) shows that this test has values which correspond to the references and sustains the character of adequacy of the mathematical model y_3 [3].

The numerical coefficient b_1 is negative, which shows that the variation between the superior limits of x_1 shall contribute to the reduction of percentage of remained knit. Its influence is of about 12% on the free term, when the variable x_1 varies with the unit and is 15% smaller than the value of the coefficient b_2.

The reduction of the percentage of remained knit is also highlighted by finding out the fact that coefficient b_{12} is insignificant, as it results from table 7, figure 5. Testing the adequacy, one may find that the value of the calculated Fischer test is a little bit higher than the value of the tabled Fischer test, but the difference being small, the model was considered adequate. From the values of the percentage column of the work matrix, it is noticed that 3 of the experiments give higher values than the accepted ones [3, 5]. But considering the reduced difference of values in both tests, as well as the corroboration of conclusions for the 3 models, it was considered necessary to accept the model in the purpose of analyzing the activity of the willowing machine.

From the 3D graphic of the model y_3 which represents a parabolic with a minimum, it is confirmed the above observation related to the evolution of value of the pair $x_1 x_2$, and which is strengthened by the analysis of the 2D chart (figure 6) of constant level curves y_3.

For example, in order to get a percentage of 3% of remained knit, the pair of values $x_1 x_2$ must get values in the range {+1,414 and +1,414}.

1.4. Testing the correctness of mathematical models of the opening process

For the practical testing of correctness of achievement of the mathematical model of the opening process, as well as its degree of adequacy, based on the above assertions, a pair of values $x_1 x_2$ was chosen, registering the values of the exit variables on the respective constant level curves from charts and which shall be considered the calculated values of the resultant variable, y_{calc} [8]. With these values, in their natural variant, namely $x_1 = 10$ m/min, $x_2 = 4{,}8$ m/min the willowing machine was adjusted; thereafter the measurement of the 3 components of the product of the opening process was performed, these representing the measured value y_{meas} of the

Table 8

Mathematical model	X₁		X₂ [m/min]		y [%]		D [%]
	code	natural [m/min]	code	natural[m/min]	y_{calc}	$y_{meas.}$	
y_1	+1	10	+1,2	4,8	63,955	64,05	+0,15
y_2	+1	10	+1,2	4,8	32,126	34,49	−7,3
y_3	+1	10	+1,2	4,8	3,181	3,28	−3,18

TESTING THE CORRECTNESS OF MATHEMATICAL MODELS OF THE OPENING PROCESS FOR THE QUANTITY OF OAKUM OF GRADED WOOL

Table 9

TESTING THE CORRECTNESS OF THE THREE MATHEMATICAL MODELS

No. exp.	Y_{1calc}	Y_{2calc}	Y_{3calc}	Sum of calc. val.
1	62.008	34.466	3.001	100.267
2	50.336	47.664	3.224	101.224
3	52.526	45.620	1.978	100.124
4	49.654	46.989	2.832	99.475
5	48.638	48.556	3.228	99.943
6	58.921	38.257	2.749	99.927
7	49.886	47.671	2.370	99.927
8	57.073	40.262	3.087	100.422
9	48.773	49.394	1.857	100.024
10	48.773	49.394	1.857	100.024
11	48.773	49.394	1.857	100.024
12	48.773	49.394	1.857	100.024
13	48.773	49.394	1.857	100.024

resulting variable. Results are centralized in table 8. Comparing the two values of the resulting variable, one may find the quality of the mathematical model, by the fact that the measured value and the value calculated for all the 3 models, differences are minimal [4].

The research of the functionality of the willowing machine, using the mathematical modeling was achieved by weighting a quantity, always the same, of recoverable material, which means that the entire quantity was also measured at the end of the willowing process, which means 100%. It is normal that the calculated results of exit variables to give 100% too by summation. As we speak of a technological process statistically examined, through the three mathematical models of performances of teased fibers, non-teased yarns and remained knit, it was compiled the table where three columns represent the measured values of the exit variables and the last column is their sum.

Analyzing the data in table 9 and especially in the last column, one may notice the correctness of the model of achievement of the mathematical modeling of the analyzed process [8, 9]. In all cases, namely in any of the 13 experiments of the work matrix, the sum of calculated values of the three exit variables is practically 100%, the existent differences are totally insignificant from a statistical point of view. Consequently, one may clearly ascertain that the research was well done and the mathematical models of the functionality of the opening aggregate correctly represent the modeled process.

CONCLUSIONS

Mathematical models were achieved for the results of functionality of the willowing machine [7, 9].

The technological and graphical analysis of models allowed determining the optimal values of the pair of entry variables for each of the three models.

The "in situ" testing of the reliability of these optimal values confirmed the functional correctness of these mathematical models.

BIBLIOGRAPHY

[1] Irovan, M. *Aspecte teoretice şi experimentale privind optimizarea proceselor de proiectare constructivă a produselor de îmbrăcăminte exterioară pentru bărbaţi,* Teza de doctorat, Iaşi, 2002

[2] Filip, I., Sava, C., Ciocoiu, M. *The optimization densities of the technical fabric for upholstery,* The 15-th Romanian Textile and Leather Conference International, Poiana Brasov, Romania, 2014

[3] Adler P. I. *Planirovanie Ekperimenta pri poiske optimalnie uslovii,* Izd. „Nauka", Moskva 1971

[4] Filip I. *Contribuţii teoretice şi experimentale la diversificarea producţiei de articole tehnice destinate industriei de tapiţerie*, Teză de doctorat, Iaşi, 2014

[5] Ciocoiu M. *Strategia cercetării,* vol. 2, Iasi, Ed. Performantica, 2002

[6] Mihail R. *Introducere în strategia experimentării cu aplicaţii în tehnologia chimică*, Ed S. E. Bucureşti, 1976

[7] Aishwariya, S., Amsamani, S. *Recycling Textile Waste-Newer Dimensions*, India, 2010

[8] Sargent, R.G. *Verification and validation of simulation models*, WSC '05 Proceedings of the 37th conference on Winter simulation, US, 2005.

[9] Meerschaert, M.M. *Mathematical Modeling*, Elsevier, London, UK, 2007

Authors:

Chief of works Dr. Eng. FILIP IOAN[1]

Conf. Dr. Eng. FARIMA DANIELA[2]
Prof. Mat. Dr. Eng. CIOCOIU MIHAI[2]
Prof. Dr. Eng. GEORGIOS PRINIOTAKIS[3]
Dr. Eng. AILENI RALUCA MARIA[4]

[1]SC TAPARO S.R.L.

Targu Lapus, Romania

e-mail: ioan.filip@taparo.ro

[2]Faculty of Textile and Leather Engineering and Industrial Management,

Dimitrie Mangeron No. 29, 700050, Iasi, Romania

e-mail: d_farima@yahoo.com

mciocoiu@tex.tuiasi.ro

[3]Technological Educational Institute of Piraeus, Greece

e-mail: gprin@teipir.gr

[4]National Research & Development Institute for Textiles and Leather,

Lucretiu Patrascanu No.16, Bucharest, Romania

e-mail: raluca.aileni@certex.ro

INFORMATION FOR AUTHORS

Industria Textila magazine is an international peer-reviewed journal published by the National Research & Development Institute for Textiles and Leather – Bucharest, in print editions.

Aims and Scope: *Industria Textila* magazine welcomes papers concerning research and innovation, reflecting the professional interests of the Textile Institute in science, engineering, economics, management and design related to the textile industry and use of fibres in consumer and engineering applications. Papers may encompass anything in the range of textile activities, from fibre production through textile processes and machines, to the design, marketing and use of products. Papers may also report fundamental theoretical or experimental investigations, practical or commercial industrial studies and may relate to technical, economic, aesthetic, social or historical aspects of textiles and the textile industry.

Submission of Manuscripts

The paper submitted for publication shall concern problems associated with production and application of fibers and textiles.

Please include full postal address as well as telephone/fax/e-mail details for the corresponding author, and ensure that all correspondence addresses are included. Also include the scientific title of the authors.

Industria Textila magazine considers all manuscripts on the strict condition that they have been submitted only to the *Industria Textila* journal, on this occasion, and that they have not been published already, nor are they under consideration for publication or in press elsewhere. Authors who fail to adhere to this condition will be charged with all costs which *Industria Textila* magazine incurs and their papers will not be published.

Manuscripts

Manuscripts of the following types are accepted:
Research Papers – An original research document which reports results of major value to the Textile Community
Notes – see below
Book Reviews – A brief critical and unbiased evaluation of the current book, normally invited by the Editor
Correspondence – Communications based on previously published manuscripts

Manuscripts shall be submitted in English in double-spaced typing, A4 paper, size font 10, Arial, margins 2 cm on all sides, under electronic version in Word for Windows format.

The volume of the submitted papers shall not exceed 10 pages (including the bibliography, abstract and key words), typescript pages including tables, figures and photographs.

All articles received are reviewed by a reviewer, renowned scientist and considered expert in the subject the article concerns, which is appointed by the editorial board. After the article has been accepted, with the completions and the modifications required by the reviewer or by the editorial staff, it will be published.

The submission of the above-mentioned papers is by all means the proof that the manuscript has not been published previously and is not currently under consideration for publication elsewhere in the country or abroad.

There may also be published papers that have been presented at national or international scientific events, which have not been published in volume, including the specification related to the respective event.

The articles assessed as inappropriate by the reviewer or by the editorial staff, concerning the subject matter or level, shall not be published.

The manuscript shall be headed by a concise title, which should represent in an exact, definite and complete way the paper content. Authors should also supply a shortened version of the title, suitable for the running head, not exceeding 50 character spaces.

The manuscript shall also be headed by complete information about the author(s): titles, name and forename(s), the full name of their affiliation (university, institute, company), department, city and state, as well as the complete mailing address (street, number, postal code, city, country, e-mail, fax, telephone).

Tables and figures (diagrams, schemes, and photographs) shall be clear and color, where possible.

The photographs shall be sent in original format (their soft), or in JPEG or TIF format, having a resolution of at least **300 dpi**.

All tables and figures shall have a title and shall be numbered with Arabic numerals, consecutively and separately throughout the paper, and referred to by the number in the text.

Generally, symbols and abbreviations shall be used according to ISO 31: specifications for quantities, units and symbols. SI units must be used, or at least given comprehensive explanations or their equivalent.

Cited references shall be listed at the end of the paper in order of quotation and contain: **for a paper in a periodical** – the initials and surname of the author(s), title of journal and of the article, year and number of issue, number of volume and page numbers; **for a book** – the initial and surname of the author(s), full name of the book, publisher, issue, place and year of publishing, and the pages cited; **for patents** – the initial and surname of the author(s), the title, the country, patent number and year.

[1] Popescu, D., Popa, I., Cicea, C., Iordănescu, M. *The expansion potential of using sales promotion techniques in the Romanian garments industry*. In: Industria Textilă, 2013, vol. 64, issue 5, pp. 293-300

Authors are requested to send an abstract of the paper, preferably no longer than 100 words and a list of 5-6 key words (preferably simple, not compound words, in alphabetical order). Avoid abbreviations, diagrams and direct reference to the text.

All manuscripts with the material proposed for publication, shall be sent to:

 certex@certex.ro

Complimentary issue – The corresponding author will receive a complimentary print copy of the issue in which his/her article appears. It will be up to the corresponding author if he/she decides to share or route his/her copy to his/her co-author(s).